ALL-HYDROCARBON STAPLED PEPTIDES AS INTRACELLULAR PROTEIN-PROTEIN INTERACTION DISRUPTORS

by

AMEYA JITENDRA LIMAYE

(Under the Direction of Eileen Kennedy)

ABSTRACT

Protein-protein interactions (PPIs) are ubiquitous and play a vital role in regulating signal transduction as well as various other fundamental cellular processes. Their dysregulation is implicated in the development of several pathological conditions making them potentially attractive drug targets. However, PPIs have traditionally been dubbed "undruggable" due to their inherent nature making them incompatible with the traditional drug design strategies and approaches. Nonetheless, PPIs provide a novel avenue for the development of PPI disruptors and modulators, not only as potential therapeutics but as molecular tools to dissect and better elucidate the intricacies of cellular signaling.

Making mimetics for one of the interacting interfaces involved in mediating a PPI has long been considered a viable strategy for targeting such interactions. PPI interfaces often involve and are stabilized by defined, complementary secondary structures of the interacting proteins. Provided that the structural information is available for the PPI of interest, designing peptides, natural or synthetic, modeled after the structural template provided by the interacting protein interfaces serves as a logical step in developing a modulator. However, excising a peptide out of a parent protein results in the loss of its

defined secondary structure due to factors such as backbone solvation and side chain interactions. This increases the overall entropic penalty, making target engagement unfavorable while also making these peptides susceptible to proteolytic degradation. Such native peptides can then be synthetically modified to improve upon all aspects mentioned above. All-hydrocarbon stapling involves strategic placement of synthetic olefinic amino acid residues within the native peptide sequence followed by ring closing metathesis. This leads to macrocyclization of the peptide thus reinforcing its secondary structure, reducing entropic penalty while also making the peptide resistant to proteolytic cleavage.

The goal of this work was to explore the design and development of all-hydrocarbon stapled peptides to develop novel molecular tools to probe and disrupt various intracellular PPIs. This involves stapled peptides that modulate scaffolded, spatiotemporal signaling of Protein Kinase C as well as peptide disruptors designed to target the multiprotein WASF Regulatory Complex implicated in regulating actin cytoskeleton and driving breast cancer metastasis.

INDEX WORDS: Protein-protein interactions, Stapled peptide, Protein kinase C, A kinase anchoring proteins, Wiskott-Aldrich syndrome protein, Breast cancer, Metastasis

ALL-HYDROCARBON STAPLED PEPTIDES AS INTRACELLULAR PROTEIN-PROTEIN INTERACTION DISRUPTORS

by

AMEYA JITENDRA LIMAYE

B.Pharm + MBA, NMIMS India, 2016

A Dissertation Submitted to the Graduate Faculty of The University of Georgia in Partial Fulfillment of the Requirements for the Degree

DOCTOR OF PHILOSOPHY

ATHENS, GEORGIA

2022

© 2022

Ameya Jitendra Limaye

All Rights Reserved

ALL-HYDROCARBON STAPLED PEPTIDES AS INTRACELLULAR PROTEIN-PROTEIN INTERACTION DISRUPTORS

by

AMEYA JITENDRA LIMAYE

Major Professor:	Eileen Kennedy
Committee:	Brian Cummings
	Neil Grimsey
	Eugene Douglass

Electronic Version Approved:

Ron Walcott
Vice Provost for Graduate Education and Dean of the Graduate School
The University of Georgia
May 2022

DEDICATION

To my mom and dad, to my brother, to my wife and countless others among my family, friends, mentors, and colleagues who have played a part, knowingly-unknowingly into shaping me to be the person I am, to make this work possible.

ACKNOWLEDGEMENTS

To begin with, I would like to thank Dr. Eileen Kennedy, for enabling me and guiding me accomplish everything documented here. Thank you for trusting me with this opportunity to explore the world of peptides, challenging me to push myself into new directions. I am forever grateful for your mentorship.

To Dr. George Bendzunas and Dr. Leah Helton, my work brother and sister. I could not have possibly asked for better companions through grad school and through the hardships of scientific research. You two have taught me more about science and life than any college, any university ever could. I will forever cherish you both as fellow scientists and friends.

I would like to thank Dr. Wided Najahi Missaoui for showing confidence in my skills when I doubted them the most and pushing me to venture into the doctoral program. Thank you for your mentorship and your support.

I would like to thank all my friends, who have been a family away from home; Sohan Nipunage, Dnyanada Shirsat, Dr. Pragati Jain, Prathamesh Dhanawade, Dr. Farah Pathan, Ameya Sawadkar, Rajani Ravishankar and Gaurav Beejee. Life in Athens just would not be the same without you.

To my committee members, Dr. Brian Cummings, Dr. Neil Grimsey, and Dr. Eugene Douglass for providing guidance on my projects, for making me think more critically about my work and for making me a better scientist.

To Julie Simmons for always having a solution handy when it came to navigating administrative formalities and for always being on the students' side. I am forever thankful.

To my parents, my family and my best friends who have shaped me in ways I cannot count but have all contributed to get me to where I am today. And finally, my wife Apurva Phadke-Limaye, my vehement patron. The last mile is always the hardest and your love, your support and your companionship made it possible for me to keep my head above the water.

TABLE OF CONTENTS

Page

LIST OF FIGURES

Page

CHAPTER 1

INTRODUCTION AND LITERATURE REVIEW

1.1 Statement of Purpose

Protein-protein interactions (PPIs) make up for the majority of the human protein interactome, with the current estimates putting the number of PPIs encompassed by the human proteome in the neighborhood of 650,000 interactions [1]. More than 1700 multiprotein complexes, composed of over 2400 distinct gene products have been mapped, which make up for over 12% of the protein coding genes within the human genome [2]. Through their complexity and exquisite modes of regulation, PPIs exert control over fundamental biological processes, both extracellular and intracellular [3].

Dysregulation of PPIs has often been associated with the development of various pathological conditions, ranging from cardiovascular and neurodegenerative diseases to various cancers [3]. Thus, PPIs have long been considered attractive therapeutic targets. Aside from their role as potential therapeutic targets, PPIs and thereby, PPI modulators also represent a novel avenue for the design and development of molecular tools that can be applied to systematically modulate, disrupt, and dissect various PPIs of interest to better elucidate the biological functions they regulate. Given the current estimates, only 0.01% of the PPIs within the human interactome have been targeted; there exists a vast space of PPIs that are yet unexplored [4].

The goal of this work is to explore some of the previously unexplored PPIs through the design and synthesis of constrained, all-hydrocarbon stapled peptides as both, novel molecular tools as well as potential therapeutic agents.

1.2 Protein-Protein Interactions as Therapeutic Targets

With an estimated 130,000 to 650,000 interactions involving over 12% of the protein coding genes within the human genome, PPIs play an essential role in regulating fundamental cellular processes from cell growth and differentiation to death [5]. Dysregulation of PPIs is often associated with various pathologies and it has long made them attractive, yet daunting therapeutic targets [6]. Additionally, since PPIs carry out a major role in mediating protein functions, their targeted disruption or stabilization also provides a novel avenue of gaining deeper insights into their biological functions within the cellular environment. There still remains a major need for the design and development of novel molecular tools capable of targeted perturbation of specific PPIs to better elucidate the biological roles of individual proteins and protein complexes [7-9].

Structural analyses of various PPIs revealed that these interactions primarily occur over flat, often solvent exposed protein surfaces with an estimated area of interaction spanning between 1000 to 2000 $Å^2$ per side [10]. This is in stark contrast to the deep "pockets" that traditional small molecules rely on to interact with their target proteins. These pockets range between 300 to 500 $Å^2$ in terms of the overall surface area of interaction (Fig. 1.1A,B) [11]. This makes PPIs a particularly daunting target and seemingly incompatible with traditional approaches of drug design [12]. Lack of structural information is another major factor impeding the development of PPI modulators. There is

only enough structural information to explore the binding interfaces of about 300 multiprotein complexes [13].

Strides have been made over the decades to overcome the challenges involved in targeting PPIs. Approaches for designing PPI modulators have evolved from “hot spots” to “hot segments” to peptides and peptidomimetics [12]. With the improved availability of the structural information, peptides and peptidomimetics, modeled after one of the interacting interfaces provide a logical template for designing PPI modulators.

1.3 Constrained Peptides as Molecular Tools, Potential Therapeutics

Provided that the structural information is available for the interfaces involved in a PPI of interest, designing a peptide that mimics the secondary structure of one of the interacting interfaces affords a lucrative strategy for the development of a modulator. Peptides are additionally suited for such a mimicry as they already possess all of the functional groups within the protein structure, required for the interaction.

Although, attractive, peptides as PPI modulators present several challenges. Peptides, despite being modeled after parent proteins, often lose their secondary structure in solution, outside the stabilizing context of a protein domain owing to factors such as backbone solvation and side chain interactions [14]. This results in increased entropic penalty during target engagement and an overall reduction in target affinity [15]. This lack of structural stability also makes native peptides highly susceptible to proteolytic degradation by proteases and peptidases [16]. Peptides have also traditionally suffered from poor cellular uptake, limiting their utility for targeting intracellular PPIs [17].

Several strategies have been developed over time to tackle the challenges presented by peptides as potential molecular tools and therapeutics. Macrocyclization is one of the most widely adopted strategies that primarily aims to constrain a peptide in a conformation such that its side chains and functional groups are optimally oriented for target engagement, improving target affinity while also imparting other "drug-like" properties [18]. This includes macrocyclization via head to tail cyclization as well as several synthetic side chain modifications to introduce linkers that can then be cyclized to form constraints such as lactam bridge, disulfide bridge, bis-alkylation of cysteine residues, olefin metathesis of O-allylserine residues, all-hydrocarbon staple and various other click linkers [19].

Many of the synthetic strategies described above are aimed at stabilizing α helical peptides since α helical motifs have been identified in nearly 62% of the PPIs. Additionally, α helical peptides are able to disrupt much larger PPI interfaces of up to 2000 Å compared to traditional drug like molecules [20, 21]. All-hydrocarbon stapling is one such strategy employed to stabilize α helical peptides while also imparting additional "drug like" properties to them. All-hydrocarbon stapling involves strategic placement of synthetic olefinic amino acid resides within a peptide sequence during synthesis. The olefinic side chains are then cyclized using Ruthenium based Grubbs catalyst via ring closing metathesis. The α-methyl substitutions on these synthetic olefinic amino acid residues induce helicity that is then reinforced by the cyclization of the side chains (Fig. 1.2A) [22]. This added structural stability significantly improves the overall binding affinity of the peptide by optimally orienting the interacting side chains and reducing the backbone solvation (Fig. 1.2B) [23]. It also improves the proteolytic stability of the peptide due to the added structural rigidity as well as the occlusion of access to the peptide backbone by

the staple. Stapled peptides also enjoy improved cellular uptake compared to their native, unmodified counterparts through active uptake mechanisms [24-28].

Stapled peptides occupy a privileged position where they combine the cell permeability of traditional small molecules with the higher target specificity of antibodies, thus representing a novel toolset to address the "undruggable" and to explore previously unelucidated biological processes.

1.4 Modulation of Kinase Signaling by Stapled Peptides

A significant portion of the human proteome undergoes posttranslational modification via covalent transfer of phosphates to serine/threonine or tyrosine side chains as carried out by protein kinases [29]. Protein phosphorylation serves as an essential mode of structural and functional regulation of proteins and thereby a myriad of cellular processes [30]. Protein kinases represent a class of phosphotransferase responsible for catalyzing the transfer of γ-phosphate group from an ATP molecule to the side chain of a serine/threonine or a tyrosine residue. Currently, the human kinome encompasses over 500 distinct kinases and accounts for about 1.8% of the human genome making it one of the largest protein families [31].

The activity of these distinct kinases is tightly regulated through varied modes of activation, substrate specificity and subcellular localization. Dysregulation in the functional aspects of protein kinases has been identified in various pathological conditions [32]. This has made protein kinases an attractive therapeutic target, making them the second most targeted group of drug targets followed by the G-protein coupled receptors [33]. There are currently over 60 FDA approved kinase inhibitors with hundreds more in

clinical trials, aimed at pathologies ranging from various cancers to autoimmune conditions [34, 35]. Despite this success, many factors still confound the development of kinase inhibitors. Majority of the currently approved kinase inhibitors are small molecules that compete with ATP by interacting with the kinase binding pocket within the catalytic domain of protein kinases. The ATP binding pocket and its proximal regions represent some of the most conserved areas among proteins kinases, and with over 500 of them represented within the human genome, it is a daunting task to achieve specificity for a specific kinase while being beholden to the constraints of small molecule drug design [36]. Additionally, there exist a multitude of proteins apart from protein kinases that bind ATP making the promiscuity an ever-present challenge for small molecule kinase inhibitors.

These challenges have culminated into investigations of modalities that can enable modulation of protein kinases through domains beyond the ATP binding pocket and the catalytic domain. Receiving activating stimuli via second messengers and their activation in space and time is critical for tightly regulating the fidelity of signaling cascades mediated by protein kinases. Subcellular localization by scaffold proteins, as well as timely maturation plays a critical role in spatiotemporal regulation of protein kinase signaling [37]. Targeting these interactions, PPIs in nature represents a novel approach of fine-tuning kinase output without directly inhibiting its catalytic activity.

1.41 Protein Kinase C (PKC): Activation and Signaling

Protein Kinase C (PKC) is a subfamily of serine/threonine kinases and is a member of the AGC branch of the human kinome. It was discovered in the late 1907s by Yasutomi Nishizuka as a calcium and lipid activated protein kinase [38-40]. Since its initial discovery, PKC has evolved into a subfamily consisting of nine different isoforms, further

classified as conventional (α, β, γ), novel (δ, ε, θ, η) and atypical (ζ, ι) based on their second messenger responsiveness as well as domain architecture [41-44]. Additional splicing variants for certain isoforms (PKCβI, PKCβII and PKMζ, a brain specific variant of PKCζ) have also been reported [45, 46].

Combined, PKC is activated in response to generation of lipid second messengers such as diacylglycerol and phosphatidylserine, along with an elevation in the intracellular Ca^{2+} levels in combination with protein-protein interactions. Canonically, elevation in the intracellular Ca2+ levels triggers translocation of cytosolic, autoinhibited PKC towards the cell membrane, where it is fully activated by its engagement with membrane lipids. This leads to the release of the autoinhibitory pseudosubstrate, out of the catalytic domain of PKC, allowing substrate phosphorylation. Given its membrane vicinity, a lot of the currently known PKC substrates are membrane proteins including a myriad of G-protein coupled receptors, certain receptor tyrosine kinases and ABC transporters. PKC also phosphorylates substrates colocalized on protein scaffolds such as Par3 and Lgl. Through its nine isoforms PKC regulates a wide range of cellular processes such as cell growth, differentiation, metabolism, morphology, and apoptosis [47-51].

It is unsurprising given the complex, nodal location of PKC across various cellular signaling networks that the dysregulation of PKC activation and signaling is implicated in various disease states [52]. Various cancers, metabolic disorders such as diabetes, heart conditions, lung, and kidney disorders as well as many autoimmune conditions have been linked to PKC dysregulation [53-58]. Efforts have been made to therapeutically target PKC using various approaches, most of which have focused on the development of small molecule inhibitors aimed at PKC catalytic domain. Early generation compounds were

synthetic analogs of staurosporine, a natural product obtained from Streptomyces staurosporeus. These compounds, similar to staurosporine, suffered from lack of selectivity for PKC. Most notable are bisindolylmaleimide derived inhibitors, enzastaurin, ruboxistaurin and sotrastaurin which entered clinical trials for several cancers, diabetic retinopathy, and immunosuppression respectively. Despite early success, neither of the compounds were able to successfully meet their respective trial endpoints and there are no FDA approved PKC inhibitors currently in the market [59-61].

Given the complexity of PKC signaling, overlapping expression profiles and substrate specificities between its isoforms combined with their paradoxical roles in pathogenesis, it is evident that more nuanced approaches are required to subtly tune PKC's catalytic output and to gain a deeper understanding of its functioning before it can be targeted therapeutically. Subcellular localization of kinases is known to dictate their substrate access while also controlling their access to activating stimuli [37]. PPIs mediated scaffolding can compartmentalize different kinases to different cellular compartments thereby tightly regulating the fidelity of localized kinase signaling. PKC has long been known to be scaffolded by various partner proteins such as Receptor for Activated C Kinase (RACK) and A Kinase Anchoring Proteins (AKAPs) and systematically dissecting these scaffolding interactions may provide novel insights into the functional aspects of localized PKC signaling [47, 62, 63].

1.42 A Kinase Anchoring Proteins (AKAPs) and Kinase Scaffolding

A Kinase Anchoring Proteins are a group of diverse scaffold proteins that all share the commonality of scaffolding the regulatory (R) subunits of Protein Kinase A (PKA) thereby earning the name AKAPs [64, 65]. "At present, over 30 mammalian AKAPs have

been reported and experimentally verified [66]. Anchoring of PKA only denotes one aspect of AKAP family's scaffolding functions. AKAPs form multivalent protein assemblies with other signaling enzymes to integrate multiple second messenger signaling cascades along with their feedback loops and localize these signaling events to specific intracellular sites [64, 67]. Some notable examples of cellular proteins scaffolded by AKAPs to distinct subcellular locations are adenylate cyclase (AC), protein kinase C (PKC), protein phosphatase 1, 2A and 2B (PPl, PP2A, PP2B), calcineurin (CaN), phosphodiesterase 4D3 and 3A (PDE4D3, PDE3A), L-type calcium ion channels, actin cytoskeleton, and tubulin [68-70]. Vastly different cellular responses can be elicited from AKAP complexes based upon which other proteins are present in an AKAP complex at any given time." [1] (Fig. 1.3)

1.43 Stapled Peptides as PKC-AKAP Scaffolding Disruptors

"Given the extent of scaffolding and spatiotemporal control exerted by AKAPs on cellular functions, AKAP complexes have long been considered viable targets for disease intervention [69-71]. The majority of this work has focused on targeting PKA RI and RII domains and their anchoring by AKAPs, primarily due to the availability of high-resolution crystal structures, well-defined binding motifs, and conserved PKA-binding domain across multiple AKAPs [71]." [1]

"As an alternative approach, one could envision targeting the PPI mediated by a protein that only binds a small subset of AKAPs. One example of this is PKC. PKC, a major cellular kinase known for controlling a plethora of signaling cascades and diverse cellular processes, has been shown to directly interact with only a handful of AKAPs

---

[1] Helton L.G., Limaye A.J., Bendzunas G.N., Kennedy E.J. (2020) Novel Stabilized Peptide Inhibitors of Protein Kinases. In: Shapiro P. (eds) Next Generation Kinase Inhibitors. Springer, Cham. https://doi.org/10.1007/978-3-030-48283-1_7
Portions of this chapter are reproduced here with permission of the publisher.

including AKAP12, APAP79, AKAP1, AKAP7, AKAP9, AKAP13, and Ezrin [70]. Its interaction with discrete signaling complexes results in various cellular effects such as altered actin cytoskeleton dynamics and suppression of cell migration and invasiveness when bound to AKAP12 [72, 73] and altered neuronal plasticity when bound to AKAP79 [74, 75]. Targeting AKAP-mediated PKC scaffolding may provide invaluable information on the various roles of PKC signaling via AKAP complexes, the role of localized pools of calcium on PKC activity, and how different PKC isoforms may be differentially compartmentalized and regulated." [1]

Efforts have previously been made to develop allosteric peptide modulators that target PPIs involving PKC and its binding partners in order to better elucidate the localized, spatiotemporal dynamics of PKC signaling [76-81]. However, perhaps due to the lack of a conserved binding interface for AKAP-PKC binding combined with the selectivity of some AKAPs for certain PKC isoforms has hindered the development of PKC specific AKAP scaffolding disruptors. Our work to address this gap has resulted in the development of two novel all-hydrocarbon stapled, PKC specific AKAP scaffolding disruptor peptides named CSTAD5 and CSTAD6.

1.44 PKC Maturation and Dimerization

Maturation and priming of the majority of the human protein kinases involves phosphorylation of a key residue within the activation loop segment [82]. Similar to all other members of the AGC kinase family, the activation loop phosphorylation for PKC is carried out by phosphoinositide-dependent kinase-1 (PDK1) [83, 84]. Another hallmark of

---

[1] Helton L.G., Limaye A.J., Bendzunas G.N., Kennedy E.J. (2020) Novel Stabilized Peptide Inhibitors of Protein Kinases. In: Shapiro P. (eds) Next Generation Kinase Inhibitors. Springer, Cham. https://doi.org/10.1007/978-3-030-48283-1_7
Portions of this chapter are reproduced here with permission of the publisher.

AGC kinases, is their C-terminally extended kinase domain, commonly referred to as the C-tail. This C-tail harbors a "hydrophobic motif" that contains a conserved phosphorylation site, essential for regulating their maturation and activity [85-87]. The C-tail contains another phosphorylation site contained within the "turn motif". Traditional dogma proposes that both of these C-tail phosphorylation sites for PKC are regulated by the multiprotein kinase complex mTORC2 [88]. However, the exact mechanisms and chronology behind the mTORC2 mediated maturation of PKC has remained elusive. With the prevalence of mTOR inhibitors in drug development, research has gone into understanding how mTORC2 controls PKC maturation.

Recent research confirmed PDK1 as the regulator of the activation loop phosphorylation and mTORC2 as the prime regulator for the turn motif phosphorylation. Additionally, this research work identified a novel motif within the PKC C-tail, dubbed the TOR-interaction motif (TIM) which contains a previously unidentified mTORC2 dependent phosphorylation site conserved across all of the mTORC2 dependent PKC isoforms. The novel TIM was also found to mediate homodimerization of newly synthesized, nascent PKC, occluding mTORC2's access to the novel TIM phosphorylation site (Fig. 1.4). Finally, this research work also showed the hydrophobic motif to be an autophosphorylation site for PKC [89].

Combined, this new body of research proposed a new dogma for PKC maturation: newly synthesized, unprimed PKC exists in a homo-dimeric state mediated by the TIM. Binding of mTORC2 disrupts TIM dimer interface, followed by the phosphorylation of the novel TIM as well as the turn motif phosphorylation sites relieves PKC homodimers. This exposes the C-tail, allowing PDK1 recruitment and subsequent phosphorylation of the PKC

activation loop. This primes PKC for autophosphorylation of the hydrophobic motif completing its maturation [89].

1.45 Stapled Peptides as PKC Dimerization Disruptors

mTOR signaling works through two distinct multiprotein complexes; mTORC1, mTORC2 and is involved in a myriad of cellular signaling pathways that regulate growth, metabolism, and cell survival [90]. mTOR dysregulation has been identified in various pathological conditions, making it an attractive therapeutic target particularly in various cancers [91]. Several generations of mTOR inhibitors have been developed, with some achieving specificity for either of the two complexes formed by mTOR [92]. Clinical success for mTOR inhibitor monotherapy has often met with mixed results and development of resistance [92].

PKC was initially identified as a potential oncogene; however, recent studies have identified a potential tumor suppressor role for PKC in various cancer [93]. With recent research revealing its dependence on mTORC2 for maturation and priming, inhibition of mTORC1/2 may result in unwarranted and potentially detrimental consequences on PKC processing. Given that the nascent, homo-dimeric PKC serves as a rate liming step, its extraneous disruption may promote mTORC2's access to PKC, consequently upregulating its processing and potentiating mTOR inhibitors. Following that line, we designed and developed two all-hydrocarbon stapled peptides that serve as cell permeable, PKC dimerization disruptors. Both of these dimerization disruptor peptides could upregulate PKC processing as monitored by C-tail phosphorylation. These peptides serve as a proof-of-concept that PKC dimerization, mediated by TIM is actionable and its disruption can promote PKC maturation by mTORC2 [89].

1.5 Cancer metastasis and Lethality

The primary reason for the lethality of the vast majority of cancers is not the primary tumor but the metastatic spread resulting from the primary carcinoma [94]. Combined with the complexity of cancer metastasis, the overall lack of therapies designed to specifically target metastasis has resulted in a considerable amount of research into understanding the fundamental processes and molecular mechanisms that drive cancer cell motility and invasion.

Cancer cell metastasis occurs as the result of an evolutionary process where the cells hijack normal, physiological migratory pathways such as epithelial to mesenchymal transition (EMT) for their survival and growth, which consequently leads to invasion and metastasis to distant tissues. EMT is a highly complex process driven by various genetic and epigenetic processes wherein, epithelial cells lose their polarity and cell-cell adhesions to acquire migratory properties of mesenchymal cells. EMT is essential for various physiological functions such as embryogenesis and wound healing, however in cancer cells it is aberrantly deployed for the development of a metastatic phenotype which allows intravasation, evasion of anoikis and immune surveillance and extravasation at remote tissues [95].

The primary step in EMT is local invasion of surrounding stromal cell layers and neighboring tissue. This step is marked by the radical remodeling of the actin cytoskeleton and cell morphology as well as the loss of cell polarity and cell-cell junctions [96]. During local invasion, cancer cells deploy F-actin rich protrusions called invadopodia that are accompanied by the expression and secretion of matrix metalloproteinases (MMPs),

enzymes that can degrade extracellular matrix (ECM) further facilitating invasion and metastasis. [97-99].

The dynamic reorganization of the actin cytoskeleton is an essential step in the formation of Invadopodia and migration of metastatic cancer. Actin polymerization is mediated by actin related protein 2/3 (Arp2/3) and induced though interactions with nucleation factors such as the Wiskott-Aldrich syndrome protein (WASP). The WASP family of proteins consists of WASP and neuronal-WASP (N-WASP/WASL), WASP family protein members (WASF1/WAVE1/SCAR1, WASF2/WAVE2/SCAR2, WASF3/WAVE3/SCAR3), WASP homolog associated with actin, membranes, and microtubules (WHAMM), WASP and SCAR homolog (WASH/ WASHC1), and junction-mediating regulatory protein (JMY) [100-103]. They allow for the spatiotemporal regulation of F-actin nucleation and assembly in a variety of cellular processes including polarization, adhesion, vesicle trafficking, as well as migration and invasion [103].

1.51 Wiskott-Aldrich Syndrome Family (WASF) Proteins

The three WASF members of the WASP family share a high degree of homology marked by: a conserved WASF/SCAR homology domain (WHD/SHD) at the N-terminal end, followed by a basic region [104-106] followed by a proline-rich domain (PRD) which can bind proteins containing Src-homology (SH3) domains. At the C-terminal end, the WASF proteins possess a conserved verprolin-cofilin-homology acidic (VCA) domain which allows them to interact with actin related protein 2/3 (Arp2/3) to form pseudo-actin globule that stimulates actin nucleation [104-108].

Unlike their neuronal counterpart the N-WASP which contains an autoinhibitory domain, WASF1/2/3 are constitutively bound in a hetero-pentametric complex named the

WASF regulatory complex (WRC) [109]. This complex is comprised of CYFIP, NCKAP, ABI and BRK1 proteins. It maintains WASF1/2/3 in an inactive form by cooperatively sequestering its VCA domain within the complex [110-112]. All members of the WRC, with the exception of BRK1, have multiple isoforms: CYFIP1/2, NCKAP1/1L, ABI1/2/3, WASF1/2/3 [113]. The potential combinatorial complexity of the WRC allows for at least 36 different WRCs that can be deployed in various cell and tissue specific contexts to fine tune actin dynamics (Fig. 1.5A).

Cooperative binding of Rac1 GTPases and acidic phospholipids to the WRC, along with the phosphorylation of key tyrosine residues on WASF1/2/3, results in recruitment of the WRC to the cell membrane. At the leading edge of the cell, the WRC propagates the outward mechanical force exerted by the F-actin cytoskeleton to the cell membrane allowing for the formation of lamellipodia [109, 110, 114-117]. In migratory cancer cells, MMPs are secreted through these lamellipodia thus being dubbed invadopodia (Fig. 1.5B).

WASF3 has been demonstrated to be essential for motility and invasion [110, 118, 119] as well as the formation of Invadopodia in cancer cells [118, 120]. The WASF3 gene has been demonstrated to be a promoter of cell motility and invasion *in vitro* and metastasis *in vivo* [121]. In addition to its role in cytoskeletal reorganization, WASF3 acts via suppression of KISS1 which results in the upregulation of NFkB which then goes on to promote the expression of MMP9 and ZEB1, two proteins known to aid invasion and stemness [120, 122]. WASF3 is also found to be activated following cytokine and growth factor stimulation and is the only member of the WASF family that possesses a STAT consensus sequence in its promoter thus forming feed-forward loop via the IL6-JAK2/STAT3 pathway [123, 124]. Signaling pathways downstream of

Phosphatidylinositol-3 kinase (PI3K), transforming growth factor-β (TFG-β), and epidermal growth factor activate WASF3 and thereby cell motility and invasion [125]. WASF3 has been implicated in promoting TGF-β/Smad signaling to enable EMT and metastasis in triple negative breast cancer cells [126]. WASF3 suppresses E-cadherin expression and other members of the miR-200 target family that suppress EMT [122, 127].

1.52 Stapled Peptides as Modulators of WASF Function

The function of the WRC is regulated though interactions within two sub complexes comprised of the ABI-BRK1-WASF trimer and the NCKAP-CYFIP dimer. The ability to control and modulate the protein-protein interactions within and between these complexes has provided an opportunity to establish a novel approach for the development of potential therapeutics. Modulation of WRC activity and stability via mimicry of interfacial protein segments using stapled peptides provides just such an approach. Large portions of the protein-protein interactions comprising the WRC are mediated via interfaces involving α-helices which are tractable to inhibition via synthetically stabilized peptides.

The first class of stapled peptide inhibitors of the WRC targeted essential interactions between WASF3 and the ABI2-BRK1 helical bundle. These peptides were based on residues 21-46 of the WHD and were dubbed the WASF Helical Mimetics (WAHM) peptides [128]. WAHM peptide treatment leads to a loss of WASF3 phospho-activation which results in suppression of downstream signaling in MDA-MB-231 cells. Targeting the WASF3-WRC interaction led to a down regulation of invasion related signaling cascades which have been reported to be WASF3 dependent including regulation of KISS1 and MMP9. In the absence of phosphorylation and WRC activation WASF3

levels were found to be reduced below detectable levels indicating that WASF3 stability is contingent upon phosphorylation when the WRC is inactive. Upon WAHM treatment both Rac1 and Rac2 were absent from the WASF3 immunocomplex. Additionally, WAHM peptides were capable of suppressing invasion and metastasis *in vivo* as well as *in vitro* [129]. In contrast to non-constrained peptides, WAHM peptides were found to be stable and active even after three days in serum. The WAHM peptides provided a proof of principle for suppression of WASF3 mediated function though targeting specific PPI within the WRC.

Following the successful template established by the WAHM peptides, a second generation WASF mimetic peptide was developed which primarily aimed at increasing overall potency and improving *in vivo* pharmacokinetic properties. A combination of homology modeling, structure-based design and *in silico* alanine scans led to the identification of a stretch of amino acid residues on WASF3 which contribute the highest energy to the WASF3-ABI2-BRK1 binding interaction. This region mapped by residues 36-57 of WASF3 is C-terminal to the original WAHM sequence and has a partial overlap. Peptides based on these residues were named WAHM *In Silico* (WAHMIS). Of the four WAHMIS peptides, WAHMIS-2 was found to be significantly better at inhibiting invasion in MDA-MB-231 cells than WAHM1 at significantly lower dosage concentrations. It also demonstrated a significant reduction in ABI2 and WASF3 protein levels as well as MMP9 expression similar to its predecessor.

With the success of the WAHM1 and WAHMIS-2, peptides disrupting interactions within the NCKAP1-CYFIP1 dimer was next investigated. A series of peptides based on several α-helices at the interface between NCKAP1 and CYFIP1 were designed and

synthesized. Three regions of NCKAP1 encompassing residues 631-642, 933-944, and 1110-1121 were used as the basis for these peptides which were termed WASF3 NCKAP Targets (WANT) 1-3 respectively [130]. When MDA-MB-231 cells were treated with these peptides at 10 μM, only WANT3, based on residues 1110-1121, was effective at inhibiting invasion. As with the WAHM peptides, treatment with WANT3 peptides resulted in suppression of engagement with Rac, but in contrast to WAHM peptides, resulted in not only reduction of NCKAP1 protein levels but also WASF3 as well.

Taken together these two peptides targeting different aspects of the WRC provide two different approaches for modulation of WASF3 activity and suggest that other helical interfaces within the WRC may be amenable to similar strategies.

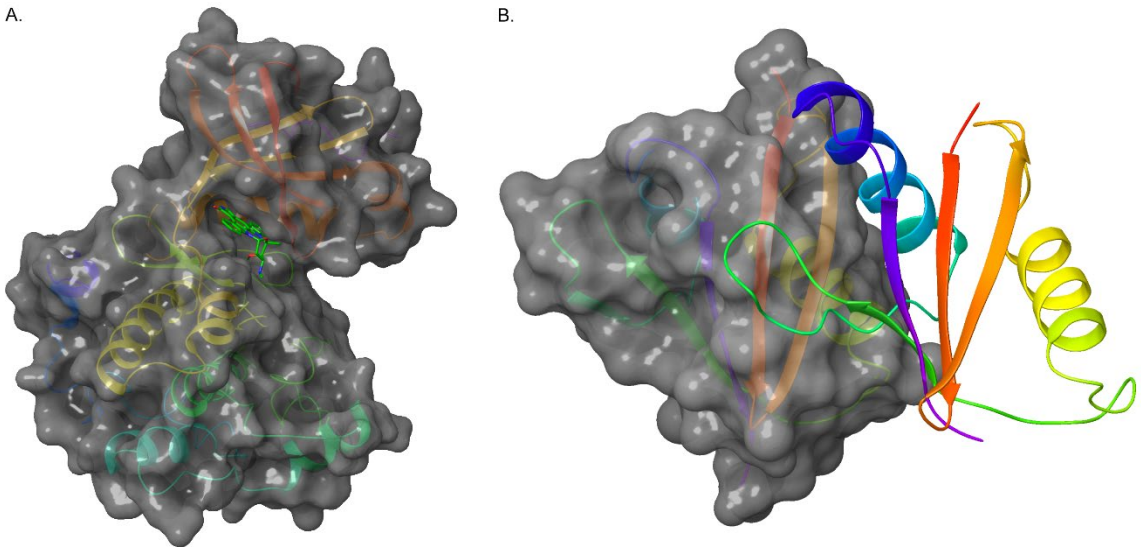

Figure 1.1 Surface area of engagement: small molecule versus PPI (A) Crystal structure of the catalytic domain of PKCθ (surface view) in complex with a small molecule inhibitor, Staurosporine (sticks), PDB ID:1XJD. (B) Crystal structure of PB1 domain of PKCι (surface view) interacting with PB1 domain of Par6α (cartoon view), PDB ID: 1WMH.

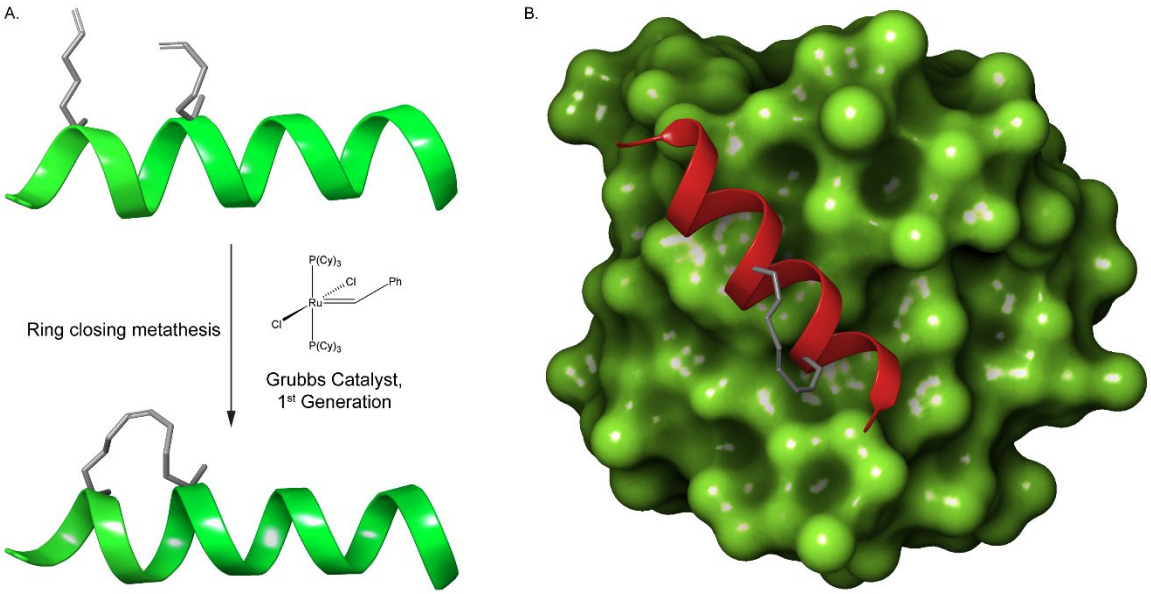

Figure 1.2 All-hydrocarbon stapled α helical peptide (A) Ring closing metathesis carried out on synthetic, olefinic amino acid side chains (grey sticks) using Grubbs catalyst creates all-hydrocarbon staple. (B) Conformational stability afforded by an all-hydrocarbon staple improves target binding.

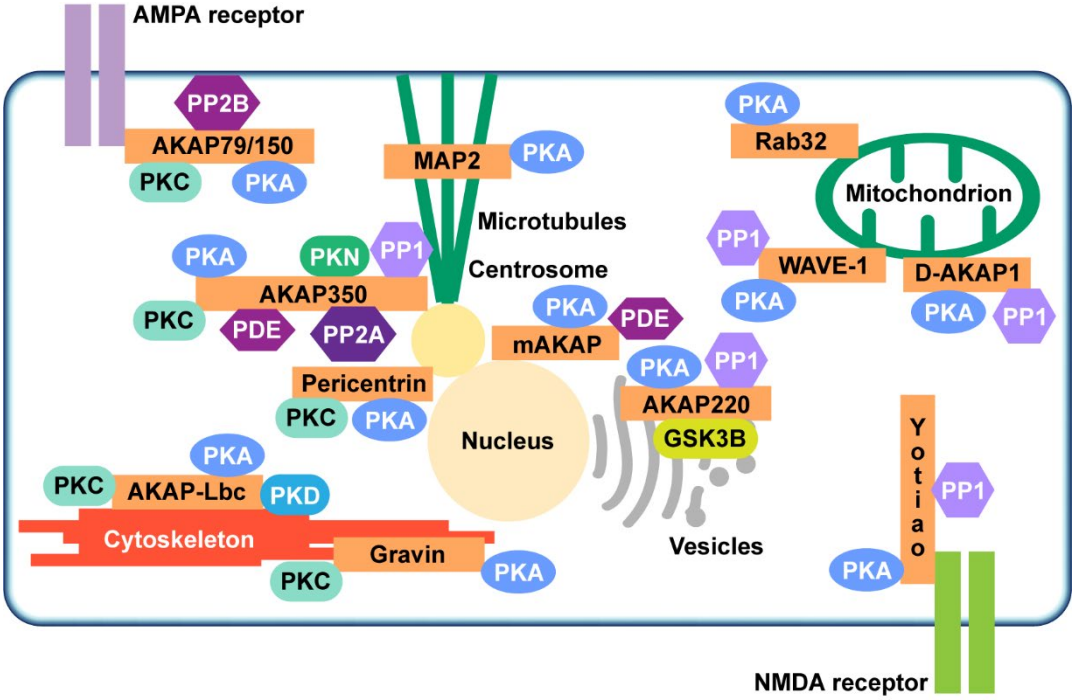

Figure 1.3 Scaffolding by A Kinase Anchoring Proteins (AKAPs) AKAPs form multi-protein signalosomes that include various protein kinases and phosphatases at various subcellular compartments.

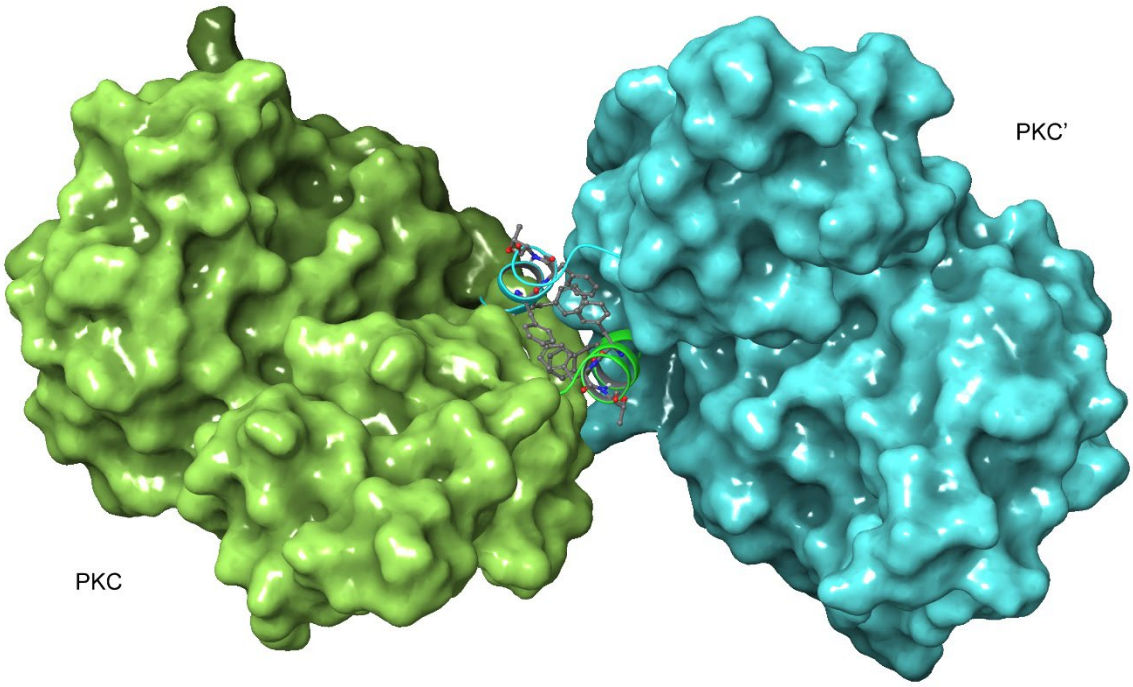

Figure 1.4 Nascent PKC homodimer Crystal structure (PDB ID: 2I0E) demonstrating homodimerization of two nascent PKC catalytic domains (surface view, green and cyan) coordinated by the novel TOR-interaction motif (cartoon representation and sticks).

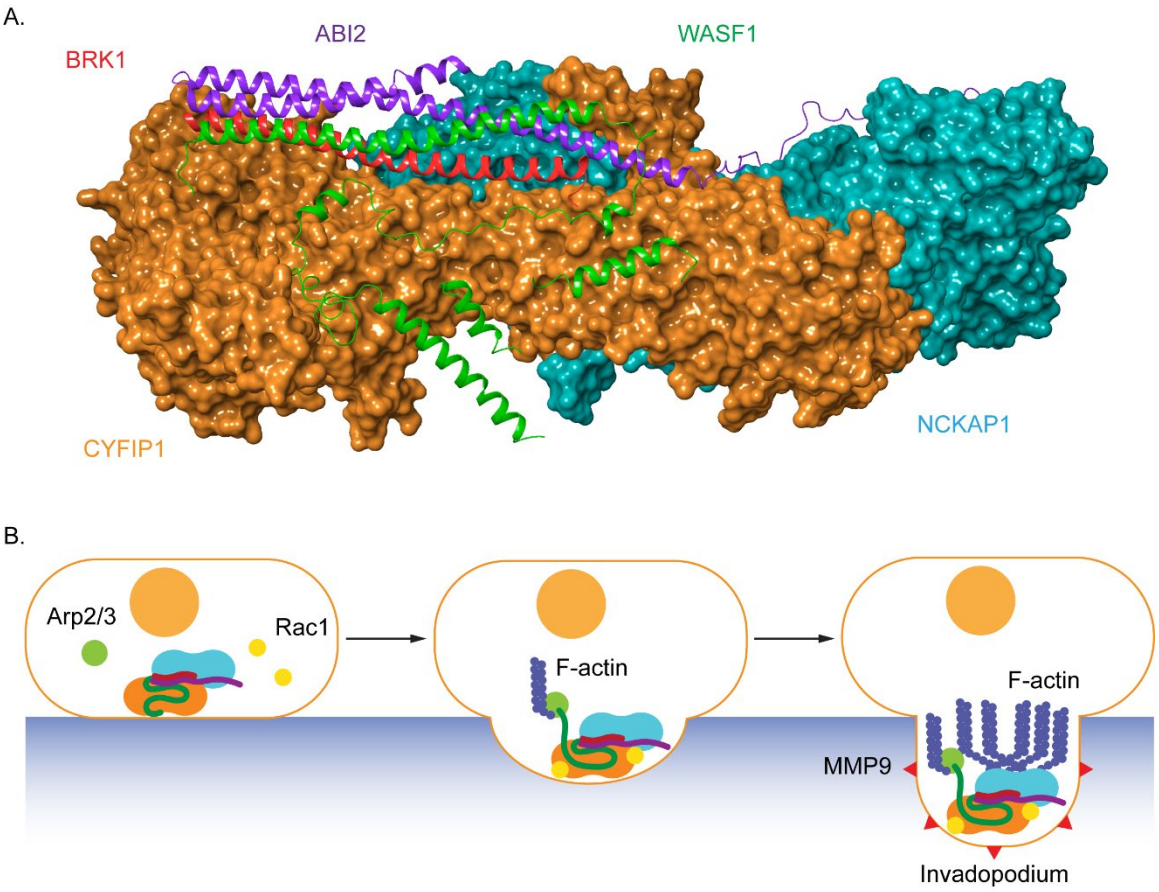

Figure 1.5 WASF Regulatory complex and its role in metastasis (A) Crystal structure of the WASF Regulatory Complex (WRC) with CYFIP1 (orange), NCKAP1 (cyan), ABI2 (purple), WASF1 (green) and BRK1 (red). (B) Schematic representation of the WRC in its inactive state, its activation by Rac1 binding, actin nucleation coordinated by Arp2/3 bound WASF VCA domain and formation of invadopodia coupled with MMP9 secretion.

CHAPTER 2

TARGETED DISRUPTION OF PKC FROM AKAP SIGNALING COMPLEXES [2]

[2] Limaye, A. J., Bendzunas, G. N., & Kennedy, E. J. (2021). Targeted disruption of PKC from AKAP signaling complexes. RSC chemical biology, 2(4), 1227–1231. https://doi.org/10.1039/d1cb00106j
Reprinted here with permission of the publisher.

2.1 Abstract

Protein Kinase C (PKC) is a member of the AGC subfamily of kinases and regulates a wide array of signaling pathways and physiological processes. Protein-protein interactions involving PKC and its scaffolding partners dictate the spatiotemporal dynamics of PKC activity, including its access to activating second messenger molecules and potential substrates. While the A Kinase Anchoring Protein (AKAP) family of scaffold proteins universally bind PKA, several were also found to scaffold PKC, thereby serving to tune its catalytic output. Targeting these scaffolding interactions can further shed light on the effect of subcellular compartmentalization on PKC signaling. Here we report the development of two hydrocarbon stapled peptides, CSTAD5 and CSTAD6, that are cell permeable and bind PKC to disrupt PKC-gravin complex formation in cells. Both constrained peptides downregulate PMA-induced cytoskeletal remodeling that is mediated by the PKC-gravin complex as measured by cell rounding. Further, these peptides downregulate PKC substrate phosphorylation and cell motility. To the best of our knowledge, no PKC-selective AKAP disruptors have previously been reported and thus CSTAD5 and CSTAD6 are novel disruptors of PKC scaffolding by AKAPs and may serve as powerful tools for dissecting AKAP-localized PKC signaling.

2.2 Introduction, Results and Discussion

Protein Kinase C (PKC) is a serine/threonine kinase that is involved in regulation of a multitude of fundamental cellular processes [131]. It plays a critical role in several signal transduction pathways that modulate cell growth, differentiation, proliferation, migration, gene expression and apoptosis [132]. PKC is activated by generation of lipid

second messengers and/or an increase in cytoplasmic calcium levels in response to stimuli such as hormones, growth factors and cytokines [133]. Given its ubiquitous expression across virtually all cell types and overlapping substrate specificities within the family, PKC activity is tightly regulated [49, 134]. Protein-protein interactions (PPIs) involving PKC play an important role in determining localization, activity and amplitude of PKC signaling as well as its accessibility to various substrates [48, 135, 136].

A Kinase Anchoring Proteins (AKAPs) serve as a class of scaffolding proteins that partly regulate PKC. AKAPs are a family of over 40 proteins that are diverse but share the commonality of binding to the regulatory (R) subunits of Protein Kinase A (PKA) through a conserved helical binding interface called the A Kinase Binding (AKB) domain [137, 138]. This anchoring interaction allows AKAPs to spatially confine PKA to specific subcellular compartments. This spatial confinement dictates the accessibility of PKA to a pool of activating second messenger molecules as well as potential substrates [138]. AKAPs form multivalent protein assemblies that involve several different kinases, phosphatases, and their substrates in order to integrate multiple second messenger signaling cascades as well as their feedback loops to create localized signalosomes for PKA [139-141].

However, PKA scaffolding only denotes one aspect of AKAP function. While all AKAPs can bind and anchor PKA, PKC can also be scaffolded by some AKAPs. Various members of the AKAP family have been reported to interact with PKC through binding regions that are distinct from that of PKA anchoring and with PKC isozyme specificities including AKAP79 (AKAP5), gravin (AKAP12, AKAP250), AKAP9 (AKAP350, yotiao), AKAP-Lbc (AKAP13), AKAP149 (AKAP1, D-AKAP-1), AKAP7 (AKAP15, AKAP18),

ezrin and pericentrin [64, 142-150]. PKC scaffolding by AKAPs can have a profound effect on PKC activity via altered substrate engagement and modulation of downstream signaling cascades [62, 150-152].

Disruption of PPI-mediated scaffolding and subcellular localization of PKC presents a unique avenue for tuning PKC output while avoiding outright inhibition of its catalytic activity. Given the importance of PKC localization and protein-protein interactions in a myriad of cellular functions, we sought to develop conformationally constrained peptide disruptors that target PKC scaffolding by AKAPs (Fig. 2.1 A). We focused on the PKC binding site on AKAP79 which is also one of the only well-characterized AKAP-PKC interactions which occurs through an N-terminal polybasic domain on AKAP79 (AKAP79 residues 31-52) [153]. Two arginine (R) residues at positions 39 and 40 were reported to be indispensable for binding [153]. This predicted helical binding site also contains a potential helix-disrupting proline (P) residue at position 49 [153-155]. A helical wheel projection of residues 31-48 reveals the amphipathic nature of the binding site with positively charged lysine (K) residues clustered onto the hydrophilic face while the two arginine (R) residues critical for binding are located on the opposite face (Fig. 2.1 B). Due to the lack of any structural information pertaining to this binding interaction, we proceeded to develop a small library of peptides corresponding to residues 31-48 of AKAP79 that were synthetically constrained with all-hydrocarbon staples to chemically reinforce the secondary structure of the peptide. The native sequence also contains a methionine residue at position 34. It was replaced with an isosteric norleucine in the library design so as to avoid possible oxidation of the methionine side chain. Peptides were synthesized using standard Fmoc chemistry on solid support and

synthetic olefinic amino acid residues ((S)-2-(4′-pentenyl)alanine, S_5) were placed at *i, i*+4 positions to allow for stabilization across a predicted single helical turn (Fig. 2.1 C). Ring closing metathesis was performed using Grubb's 1st generation catalyst (Fig. 2.1 D).

To first screen which peptides could disrupt PKC-AKAP docking, we used a cell morphology assay that was previously described [72]. It was shown that phorbol ester-induced remodeling of actin cytoskeleton and cell rounding in epithelial prostate cancer cells is dependent on a direct scaffolding interaction between PKC and the AKAP gravin. We used prostate derived PC-3 cells for cell-based experiments due to their native high expression of gravin and tested for Phorbol 12-myristate 13-acetate (PMA)-induced cytoskeletal remodeling and cell rounding as a function of PKC scaffolding by gravin in the presence and absence of our peptides. Following an initial screen of PKC-Stapled Anchoring Disruptors (CSTADs), CSTAD5 and CSTAD6 were chosen as the lead candidates due to their ability to downregulate cytoskeletal remodeling in PC-3 cells (Fig. S2.1).

Next, the two lead compounds were evaluated for cellular uptake and target binding. Cells were treated with 5 μM of 5(6)-carboxyfluorescein (FAM)-labeled CSTAD5 or CSTAD6 for four hours prior to imaging. Both CSTAD5 and CSTAD6 showed considerable permeation at the four-hour time point with diffuse distribution throughout the cytoplasm as well as some degree of nuclear localization (Fig. 2.2 A, S2.2). Notably, the non-modified native sequence demonstrated poor cell permeability and was thus not carried forward for cell-based experiments (Fig. S2.2-S2.4). We then analyzed whether the lead CSTAD peptides could bind PKC using pulldown assays. Cell lysates were treated with 5 μM biotin-labeled CSTAD5 and CSTAD6 peptides along with their corresponding

scrambled controls for four hours. Pulldowns were then performed using streptavidin-agarose beads followed by immunoblotting with a pan-PKC antibody (Fig. 2.2 B). Whole cell lysates were used as input controls and lysate treated with vehicle (DMSO) was used as a negative control. Both lead peptides were able to successfully pull-down PKC while their scrambled controls did not (Fig. 2.2 C).

After confirming cellular uptake and PKC binding, we next investigated whether these candidate peptides could successfully disrupt PKC binding to an AKAP scaffold. To evaluate this, we first performed pulldown assays using biotin labeled CSTAD5 and CSTAD6 peptides and immunoblotted for PKC and the AKAP gravin. Although PKC was present in both CSTAD5- and CSTAD6-treated pulldowns, no detectable levels of gravin were observed (Fig. 2.3 A). Next, we performed the reciprocal experiment where gravin was immunoprecipitated from cell lysates that were pretreated with either of the lead peptides, their respective scrambled controls or vehicle (DMSO) and immunoblotted for PKC. PKC levels observed with CSTAD5 and CSTAD6 treatment were nearly undetectable as compared to the scrambled controls or vehicle thus demonstrating the successful disruption of binding between gravin and PKC (Fig. 2.3 B, S2.5). We then utilized a previously established PMA-induced cytoskeletal remodeling assay which showed that a direct scaffolding interaction between gravin and PKC was required for PMA-induced remodeling of the actin cytoskeleton and cell morphology to assess cell rounding [72]. PC-3 cells were serum starved for 24 hours, followed by treatment with 5 μM of CSTAD5 or CSTAD6 for four hours. Cells were then stimulated with 500 nM PMA for 45 minutes followed by imaging to analyze altered morphology as defined by cell rounding (Fig. 2.3 C, S2.6). Cells pre-treated with CSTAD5 or CSTAD6 predominantly

maintained a flat, elongated morphology even after PMA stimulation, whereas cells pre-treated with scrambled controls or vehicle displayed radically altered morphology with collapse of flat cytoplasmic surfaces towards perinuclear regions (Fig. S2.7). The average percentage of rounded cells following PMA stimulation in CSTAD5 and CSTAD6 treated cells was ~30% and ~27%, respectively, as compared to over 60% rounding for vehicle treated cells (Fig. 2.3 D). Although these data do not directly measure the disruption of the scaffolding interaction, they support the hypothesis that CSTAD5 and CSTAD6 disrupt PKC scaffolding by gravin.

Additionally, we tested the effect of CSTAD5 and CSTAD6 peptides on PKC substrate phosphorylation since its localization by AKAPs is known to influence substrate access. Serum starved PC-3 cells were treated with increasing concentrations of CSTAD5 and CSTAD6, sotrastaurin (selective catalytic inhibitor of PKC) or vehicle (DMSO) for four hours. Cells were then stimulated with PMA and harvested. Western blots probed with an anti-PKC p-Serine substrate antibody revealed a dose dependent reduction in phosphorylated PKC substrates in cells treated with either CSTAD5 or CSTAD6. Intriguingly, cells treated with the highest concentrations (5 μM) of CSTAD5 and CSTAD6 showed lower levels of PKC p-Serine substrates as compared to the serum starved, untreated unstimulated control (Fig. 2.4 A).

Since gravin has been implicated in controlling cell migration and motility through its ability regulate PKC and PKA signaling [156-158], we assessed whether the lead CSTAD peptides would have an effect on cell motility. To measure this, wound healing assays were performed in the presence of 5 μM CSTAD5, CSTAD6 or vehicle (DMSO) in media supplemented with 5% fetal bovine serum. After 24 hours, both CSTAD5 and

CSTAD6 showed a statistically significant reduction in wound healing with only approximately 62% closure in the presence of either peptide as compared to vehicle-treated cells which achieved over 90% wound healing (Fig. 2.4 B, C).

In conclusion, here we describe the development of AKAP-derived stapled peptides that were designed to disrupt PKC scaffolding by AKAPs. Two peptides, CSTAD5 and CSTAD6, could permeate cells and bind PKC to disrupt the PKC-gravin complex. Notably, both peptides were able to downregulate cytoskeletal remodeling mediated by AKAP-scaffolded PKC as measured by cell rounding and could also downregulate PKC-mediated signaling and cell motility. To the best of our knowledge, no PKC-selective AKAP disruptors have previously been reported and thus this work establishes CSTAD5 and CSTAD6 as the first disruptors of PKC scaffolding by AKAPs.

Indeed, such an approach has been applied to develop disruptors for other PPIs involving PKC. Most notable are the peptide disruptors aimed at a scaffolding interaction between PKC and Receptor for Activated C Kinase (RACK) [79, 80]. With several AKAPs being identified as scaffolding partners that regulate the spatiotemporal dynamics of PKC, these AKAP-PKC scaffolds provide targets for the development of new disruptors that can aid in elucidating the intricacies of localized PKC signaling.

Multiple iterations of peptide disruptors for AKAP-PKA complexes have been developed and reported, however, no such disruptors have been designed to target AKAP-PKC complexes [71, 159-162]. The overall structural and functional conservation in the AKB domain across the AKAP family provides for a relatively streamlined development of peptide disruptors to target PKA anchoring by AKAPs [160, 162-164]. Conversely, no such conserved binding interface has been identified for AKAP-PKC binding and

selectivity of certain AKAPs for some PKC isoforms has further confounded the complexity of these interactions. Taken together, these results provide tantalizing hints at a complex role for scaffolding and subcellular localization in determining the PKC signaling output. It also demonstrates that extraneous disruption of spatiotemporal regulation of PKC can directly result in alteration of various cellular functions. This work provides two original stapled peptides that can disrupt AKAP scaffolding of PKC, thereby providing a powerful new tool for further exploration of the intricacies of intracellular PKC activity. Combining these peptides with previously established PKA anchoring disruptors can allow for systematic dissection of AKAP signalosomes to gain a deeper understanding of how they orchestrate specific cellular activities.

2.3 Methods

Peptide synthesis

Rink amide MBHA resin along with N-α-Fmoc protected amino acids were purchased from Novabiochem. (S)-NFmoc-2-(4'-pentenyl)alanine and Grubb's catalyst (1st Generation) were purchased from Sigma. All other reagents and organic solvents were purchased from Fisher Scientific unless specified. Solvents used in this synthesis were HPLC grade.

All peptides used in this study were synthesized using standard Fmoc (fluorenylmethoxycarbonyl) protected solid phase peptide synthesis. Rink amide MBHA resin was equilibrated in NMP (1-methyl-2-pyrrolidinone) for 15 minutes. Fmoc protection group was deprotected using 25% v/v solution of piperidine in NMP for 30 minutes. Deprotection step was followed by three washes with NMP. Amino acid coupling was

carried out by adding 10 equivalents of Fmoc-protected amino acid (0.25 M final concentration) in NMP to the deprotected resin along with HCTU [O-(1H-6-Chlorobenzotriazole-1-yl)-1,1,3,3-tetramethyluronium hexafluorophosphate] in NMP (0.24 M final concentration) followed by 8% v/v DIEA (N, N-Diisopropylethylamine). Amino acid coupling was carried out for 45 minutes followed by three washes with NMP. Deprotection and coupling steps were repeated for the addition of the remaining amino acid residues. Two residues of olefinic amino acid 'S5' [Fmoc-(S)-2-(4-pentenyl)alanine] were incorporated at suitable positions using standard coupling conditions. Olefin metathesis (ring closing metathesis) was performed on Fmoc-protected, resin bound peptide using 0.4 equivalents of Grubb's first-generation catalyst [Benzylidene-bis(tricyclohexylphosphine)dichlororuthenium] in 1,2-dichloroethane for 1 hour. This step was carried out twice to ensure completion of staple formation. Addition of β-Alanine (Fmoc-b-Ala-OH) as a flexible N-terminal linker was performed under standard coupling conditions. Peptides were labeled with either fluorescein or biotin at the N-terminal end. For fluorescein labeling, deprotected, resin bound peptides were agitated overnight with 2 equivalents of 5(6)-carboxyfluorescein, 0.046 M HCTU and 2% v/v DIEA in DMF (N, N-Dimethylformamide). Biotin labeling was performed overnight with 10 equivalents of D-biotin, 0.14 M HCTU and 4% v/v DIEA in a 1:1 mixture of DMF and DMSO (dimethyl sulfoxide). Peptides were cleaved from resin in a cleavage cocktail of 95% TFA (trifluoroacetic acid), 2.5% water and 2.5% TIS (triisopropylsilane) for four hours. Products were then precipitated in ice cold MTBE (methyl-tert-butyl ether) and allowed to air dry. Crude products were dissolved in equal parts water and methanol and purified using high performance liquid chromatography. Product peptides were verified with ESI

(electrospray ionization) mass spectroscopy. Fluorescein labeled peptides were quantified by measuring their absorbance at 495 nm. Biotin labeled peptides were quantified by measuring diminished absorbance of HABA [2-(4'-hydroxybenzeneazo)benzoic acid]-avidin complex at 500 nm. Pure, dry peptides were dissolved in DMSO to achieve 10 mM stocks and were stored at 4°C, protected from light.

Sequences for the peptides used in this study are as follows (red stars represent S_5 residues):

CSTAD1= (5/6 FAM) - β-Ala – K*S(Nle)L*FKRRKKAAKALK

CSTAD2= (5/6 FAM) - β-Ala – KA*(Nle)LC*KRRKKAAKALK

CSTAD3= (5/6 FAM) - β-Ala - KAS(Nle)LC*KRR*KAAKALK

CSTAD4= (5/6 FAM) - β-Ala - KAS(Nle)LCF*RRK*AAKALK

CSTAD5= (5/6 FAM) - β-Ala - KAS(Nle)LCFKRRK*AAK*LK

CSTAD5= Biotin - β-Ala - KAS(Nle)LCFKRRK*AAK*LK

CSTAD6= (5/6 FAM) - β-Ala - KAS(Nle)LCFKRRKK*AKA*K

CSTAD6= Biotin - β-Ala - KAS(Nle)LCFKRRKK*AKA*K

Scramble 5= (5/6 FAM) - β-Ala - LLSKAAFKAKK*RAR*(Nle)K

Scramble 5= Biotin - β-Ala - LLSKAAFKAKK*RAR*(Nle)K

Scramble 6= (5/6 FAM) - β-Ala - RLKAAFALKSKK*(Nle)KK*A

Scramble 6= Biotin - β-Ala - RLKAAFALKSKK*(Nle)KK*A

Molecular weights of purified peptides are as follows:

(5/6 FAM) - β-Ala - CSTAD1= 2564.4 (Expected mass= 2565.2)

(5/6 FAM) - β-Ala - CSTAD2= 2504.4 (Expected mass= 2505.1)

(5/6 FAM) - β-Ala - CSTAD3= 2464.2 (Expected mass= 2464.0)

(5/6 FAM) - β-Ala - CSTAD4= 2482.2 (Expected mass= 2483.0)

(5/6 FAM) - β-Ala - CSTAD5= 2539.2 (Expected mass= 2540.1)

Biotin - β-Ala - CSTAD5= 2407.5 (Expected mass= 2408.1)

(5/6 FAM) - β-Ala - CSTAD6= 2554.5 (Expected mass= 2555.1)

Biotin - β-Ala - CSTAD6= 2422.2 (Expected mass= 2423.1)

(5/6 FAM) - β-Ala - Scramble 5= 2508.0 (Expected mass= 2508.0)

Biotin - β-Ala - Scramble 5= 2376.0 (Expected mass= 2376.1)

(5/6 FAM) - β-Ala - Scramble 6= 2479.5 (Expected mass= 2480.1)

Biotin - β-Ala - Scramble 6= 2347.8 (Expected mass= 2348.0)

Cell culture

PC-3 and A549 cells were obtained from ATCC. Cell culture medium (RPMI-1640) and trypsin were purchased from Corning. Fetal bovine serum (FBS) was purchased from HyClone.

Cells were maintained in RPMI-1640 supplemented with 10% FBS and 1% Penicillin-Streptomycin at 37°C with 5% CO_2. Cells were passaged at least twice before being used in any experiment and all experiments were performed in at least triplicate at different passage numbers.

PMA induced cytoskeletal remodeling assay

$3x10^4$ cells were seeded per chamber on a chamber slide and allowed to adhere overnight. Cells were then briefly washed with PBS and serum starved for 24 hours. Following serum starvation, serum free media containing 5 mM CSTAD5, CSTAD6 or vehicle (DMSO) was introduced into respective chambers and slides were incubated for

four hours. Following incubation with the treatment, media containing peptides (or vehicle) was aspirated and cells were briefly washed with serum free medium. Fresh serum free medium containing 500 nM PMA (Phorbol 12-myristate 13-acetate) was introduced to each chamber. Cells were imaged following 45 minutes of incubation with PMA containing medium using Olympus IX71 inverted microscope. Cells were counted across three independent chambers for each treatment condition with at least 150 cells per image. Total quantification was performed with four independent experiments, statistical analysis was carried out with one-way ANOVA and Bonferroni's multiple comparisons test in GraphPad Prism.

Peptide uptake assay

$3x10^4$ cells were seeded per chamber on an 8-chamber slide (Nunc Lab-Tek II CC2) and allowed to adhere overnight. Cells were briefly washed with PBS and media containing 5 μM CSTAD5, CSTAD6 or vehicle (DMSO) was introduced to respective chambers. Cells were incubated with peptides (or vehicle) for four hours followed by three washes with PBS. Cells were then fixed using 2% paraformaldehyde solution for 10 minutes followed by three brief washes with PBS. Fixed cells were permeabilized using 0.1% Triton X-100 in PBS for 10 minutes. After permeabilization, cells were washed thrice with PBS. Nuclear staining was performed by adding 300 nM DAPI solution to each chamber followed by five minutes of incubation away from light. Cells were washed three times with PBS and slides were air dried. A coverslip was mounted overnight at 4°C using Permafluor aqueous mounting medium. Phase contrast and fluorescence imaging was

performed using Olympus IX71 microscope equipped with Exfo X-Cite 120Q light source. ImageJ was used to generate channel overlays for acquired images.

Biotin-Streptavidin pulldown assay

PC-3 cells were lysed in ice cold NP-40 lysis buffer (50 mM Tris pH 8.0, 150 mM NaCl, 1% Nonidet P-40 supplemented with 1X Halt Protease Inhibitor Cocktail). Cell lysates were treated with 5 μM biotin labeled peptides (CSTAD5 or CSTAD6), respective scrambled controls or vehicle (DMSO) and were agitated for four hours at 4°C. 25 mL of Streptavidin-Agarose resin (Millipore) was added to all samples and the samples were agitated overnight at 4°C. Resin was collected by centrifuging the lysate mixtures at 1000G for 5 minutes. Collected resin was washed at least three times with ice cold lysis buffer and boiled in Laemmli sample buffer (60 mM Tris-HCl pH 6.8, 2% SDS, 10% glycerol, 5% b-mercaptoethanol, 0.01% bromophenol blue) for 10 minutes at 95°C. SDS-PAGE was performed using 10% polyacrylamide gels (Tris-Glycine), followed by standard western blot on to PVDF (Immobilon-FL, Millipore) membranes. Pan-PKC antibody (1:1000, Rabbit mAb, Abcam) was used for primary immunodetection. Secondary antibody (1:15000, IRDye 800CW Goat anti-Rabbit, LI-COR) was used for fluorescence imaging. Membranes were imaged with Odyssey Fc imaging system (LI-COR). Densitometric quantifications were obtained using LI-LOR Image Studio. Statistical analysis was carried out with one-way ANOVA and Bonferroni's multiple comparisons test in GraphPad Prism. Alternatively, A549 cells were lysed using Triton X-100, Tween 20 lysis buffer (20 mM Tris-HCl, pH 7.4, 150 mM NaCl, 10 mM EDTA, 0.25 % Triton X-100, 0.05 % Tween-20 supplemented with 1X Halt Protease Inhibitor Cocktail). Pulldowns were performed as described previously followed by western blotting. Gravin antibody (1:1000, Mouse mAb,

MilliporeSigma) and Pan-PKC antibody (1:1000, Rabbit mAb, Abcam) were used for primary immunodetection of gravin and PKC, respectively. Secondary antibodies (1:15000, IRDye 680RD Goat anti-Rabbit and IRDye 800CW Goat anti-Mouse, LI-COR) were used for secondary immunodetection and fluorescence imaging. Membranes were imaged with Odyssey Fc imaging system (LI-COR).

Immunoprecipitation assay

A549 cells were seeded, allowed to attach overnight and serum starved for 24 hours. Serum starved cells were then treated with 5 mM CSTAD5, CSTAD6, respective scrambled controls and DMSO for four hours. Ice cold Triton X-100, Tween 20 lysis buffer (20 mM Tris-HCl, pH 7.4, 150 mM NaCl, 10 mM EDTA, 0.25 % Triton X-100, 0.05 % Tween-20 supplemented with 1X Halt Protease Inhibitor Cocktail) was used to lyse the pretreated cells. Resulting lysates were agitated overnight with pre-conjugated gravin antibody (Mouse mAb, MilliporeSigma) and protein A/G-agarose resin beads (Protein A/G PLUS-Agarose, Santa Cruz Biotechnology) at 4ºC. Resin was collected by centrifuging the lysate mixtures at 1000 G for 1 minute. Resin was washed three times with ice cold lysis buffer and boiled in Laemmli sample buffer (60 mM Tris-HCl pH 6.8, 2% SDS, 10% glycerol, 5% b-mercaptoethanol, 0.01% bromophenol blue) for 10 minutes at 95°C followed by SDS-PAGE and western blotting. Blots were probed with pan-PKC antibody (1:1000, Rabbit mAb, Abcam) for primary immunodetection followed by secondary immunodetection (1:15000, IRDye 680RD Goat anti-Rabbit). Membranes were imaged and densitometric quantifications were obtained using Odyssey Fc imaging system (LI-

COR). Statistical analysis was performed in GraphPad Prism with one-way ANOVA and Bonferroni's multiple comparisons test.

PKC substrate phosphorylation assay

PC-3 cells were seeded in 12 well plates and allowed to attach overnight. Cells were washed briefly with PBS and serum starved for 24 hours. Following serum starvation, cells were treated with various concentrations (1, 2.5, 5 mM) of peptides (CSTAD5 and CSTAD6), 500 nM Sotrastaurin or vehicle (DMSO) for four hours. Post treatment, cells were briefly washed with PBS and incubated with serum free cell medium containing 100 nM PMA for 5 minutes. Following stimulation, cell medium was aspirated and cells were harvested using 2X Laemmli sample buffer. Harvested samples were boiled at 95°C for 10 minutes and briefly centrifuged. SDS-PAGE was performed using 8% polyacrylamide gels, followed by standard western blot on to PVDF (Immobilon-FL, Millipore) membranes. Phospho-(Ser) PKC Substrate antibody (1:1000, Rabbit mAb, Cell Signaling Technology) was used to detect phosphorylated PKC substrates along with α-Tubulin (1:1000, Mouse mAb, DSHB, 12G10) antibody as loading control. Secondary antibodies (1:15000, IRDye 800CW Goat anti-Rabbit and IRDye 680RD Goat anti-Mouse, LI-COR) were used for secondary immunodetection and fluorescence imaging. All membranes were imaged with LI-COR Odyssey Fc imaging system.

Cell motility assay

PC-3 cells were seeded on to 24 well plates and allowed to form confluent monolayer. A vertical wound was introduced into each well using a pipette tip. Cells were

then briefly washed with PBS and serum free medium to remove any detached cells and cell debris. Media supplemented with 5% FBS along with 5 mM peptides (CSTAD5, CSTAD6) or vehicle (DMSO) was carefully introduced into respective wells. Cells were imaged for '0 hour' time point using Olympus IX71 inverted microscope before being incubated. Following 24 hours of incubation, cells were imaged once again at the 24-hour time point. Wound area calculation for all captured images was performed using MRI wound healing tool for ImageJ. Zero hour and 24-hour time point wound areas were used to calculate percentage wound healing for each individual well across three independent assays. Statistical analysis was carried out in GraphPad Prism with one-way ANOVA and Bonferroni's multiple comparisons test.

Proteomic mass spectrometry

A549 cells were lysed using Triton X-100, Tween 20 lysis buffer (20 mM Tris-HCl, pH 7.4, 150 mM NaCl, 10 mM EDTA, 0.25 % Triton X-100, 0.05 % Tween-20 supplemented with 1X Halt Protease Inhibitor Cocktail). Resulting lysate was treated with 5 μM biotin labeled peptides (CSTAD5 or CSTAD6) or their respective scrambled controls and were agitated for four hours at 4°C. 25 μL of Streptavidin-Agarose resin (Millipore) was added to all samples and the samples were agitated overnight at 4°C. Resin was collected by centrifuging the lysate mixtures at 1000 G for 5 minutes. Collected resin was washed at least four times with ice cold lysis buffer and boiled in Laemmli sample buffer (60 mM Tris-HCl pH 6.8, 2% SDS, 10% glycerol, 5% β-mercaptoethanol, 0.01% bromophenol blue) for 10 minutes at 95°C. SDS-PAGE was performed using 8% polyacrylamide gels (Tris-Glycine). Electrophoresis was stopped after the proteins had

travelled a nominal distance into the separating gel. Gel was thoroughly washed with deionized water followed by staining with colloidal Coomassie blue to visualize protein bands. Bands for each treatment were then excised. Trapped proteins were digested using mass spectrometry grade trypsin and the resultant peptides were extracted in 50% acetonitrile and 0.1% TFA. 1 µL of sample was injected and analyzed via LC-MS/MS on a ThermoScientific Orbitrap Velo Elite. Proteome Discoverer Version 1.4 was used to identify interacting proteins. A cut-off score of 125 was set for the Proteome Discoverer score and proteins above the cut-off were compared between the lead peptides and their respective scrambled controls. A list of proteins enriched by the lead peptides but not by their scrambled controls along with the common proteins enriched in both was compiled and sorted according to the scores.

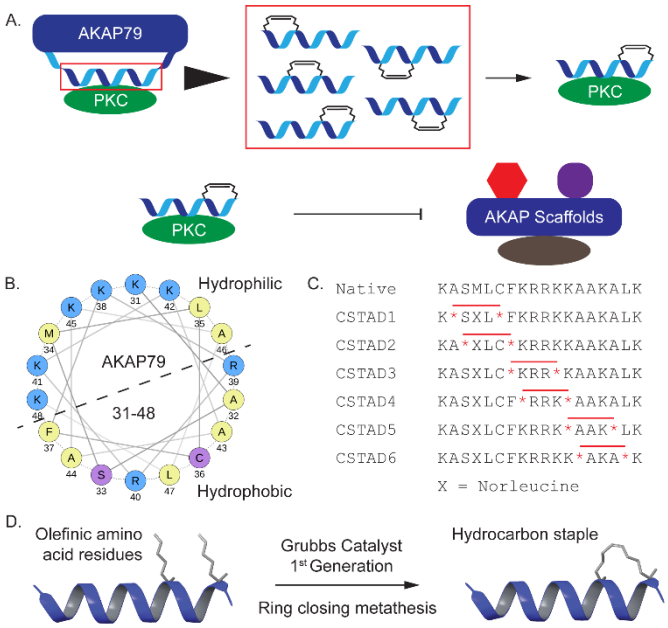

Figure 2.1 Design and synthesis of all-hydrocarbon stapled peptides to target PKC scaffolding by AKAPs (A) Schematic representation of the rationale behind the design of all-hydrocarbon stapled peptides derived from AKAP79 and designed to disrupt PKC scaffolding by AKAPs. (B) Helical wheel projection of the PKC binding site present on AKAP79 (residues 31-48) with basic residues in blue, polar residues in lilac and nonpolar residues in yellow. Helical wheel was generated using NetWheels. (C) The native AKAP79 PKC binding site sequence was used to design a library of stapled peptides where olefinic amino acids (*) were placed in various positions to place the staple on the non-binding peptide interface. The hydrocarbon staple is represented by a red line drawn across two olefinic amino acids (*). CSTAD stands for PKC-Stapled Anchoring Disruptor. (D) Ring closing metathesis of olefinic amino acid residues placed at i, i+4 positions was performed using Grubb's 1st generation catalyst to result in a hydrocarbon staple across individual helical turns.

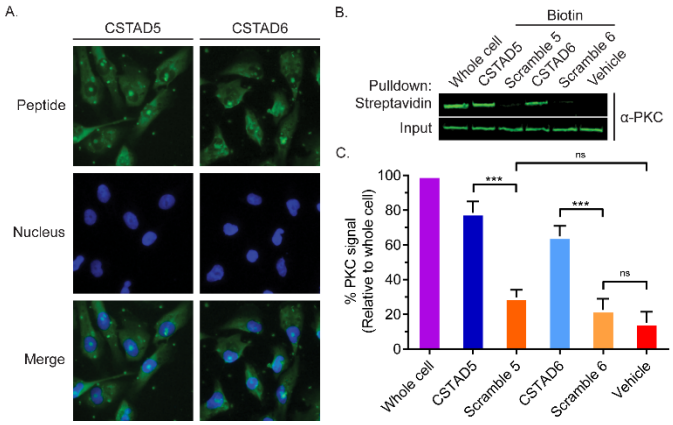

Figure 2.2 CSTAD5 and CSTAD6 permeate cells and bind PKC (A) Fluorescence microscopy of PC-3 cells following treatment with CSTAD5 or CSTAD6 (5 μM) for four hours. Both peptides show diffuse fluorescence throughout the cytoplasm along with detectable puncta in the nucleus. (B) Representative western blot (n=6) demonstrating that the CSTAD peptides, but not their scrambled controls, bind their intended target of PKC. PC-3 cell lysates were treated with biotin-labeled peptides for four hours. Pulldowns were performed using streptavidin-agarose resin. PKC was detected by immunoblotting. (C) Densitometric quantification of six independent streptavidin-biotin pulldown assays using LI-COR Image Studio shows that CSTAD5 and CSTAD6 bound to PKC but their scramble controls did not. *** $p < 0.01$; ns, not significant as assessed by one-way ANOVA and Bonferroni's multiple comparisons test. Error bars represent standard deviation.

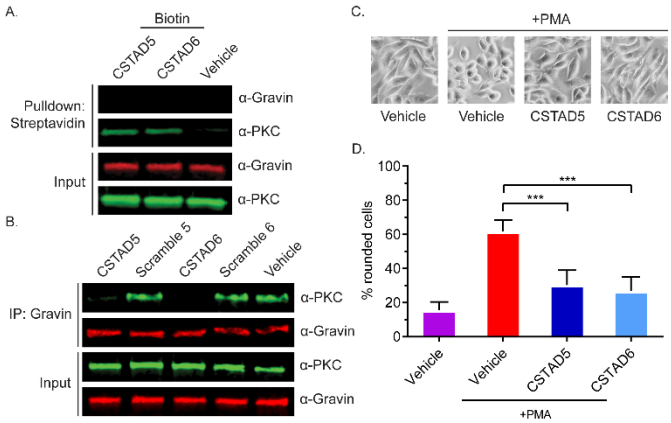

Figure 2.3 CSTAD5 and CSTAD6 disrupt the interaction between PKC and gravin and downregulate PMA-induced cytoskeletal remodeling in PC-3 cells (A) Representative western blot showing disruption of the PKC-gravin interaction by CSTAD5 and CSTAD6 peptides (n=3). A549 cell lysates were treated with biotin-labeled peptides for four hours. Pulldowns were performed using streptavidin-agarose resin. Gravin and PKC were probed by immunoblotting. CSTAD5 and CSTAD6 bound to PKC, but gravin was not detected in complex with PKC. (B) To probe complex formation, gravin was immunoprecipitated and PKC was probed by western blotting using A549 cell lysates (n=4). In the presence of CSTAD5 or CSTAD6, PKC levels were significantly reduced. The gravin-PKC complex was not affected by vehicle or scrambled control treatments. (C) Representative phase contrast images showing morphology of PC-3 cells treated with 5 μM CSTAD peptides or vehicle for four hours and stimulated with 500 nM PMA for 45 minutes. CSTAD5 and CSTAD6 downregulated PMA-induced cell rounding. (D) Quantification of PMA induced cytoskeletal remodeling in PC-3 cells treated with CSTAD5 or CSTAD6 peptides versus vehicle (n=4). Both peptides significantly inhibited rounding as compared to vehicle-treated cells. *** $p < 0.01$ by one-way ANOVA and Bonferroni's multiple comparisons test. Error bars represent standard deviation.

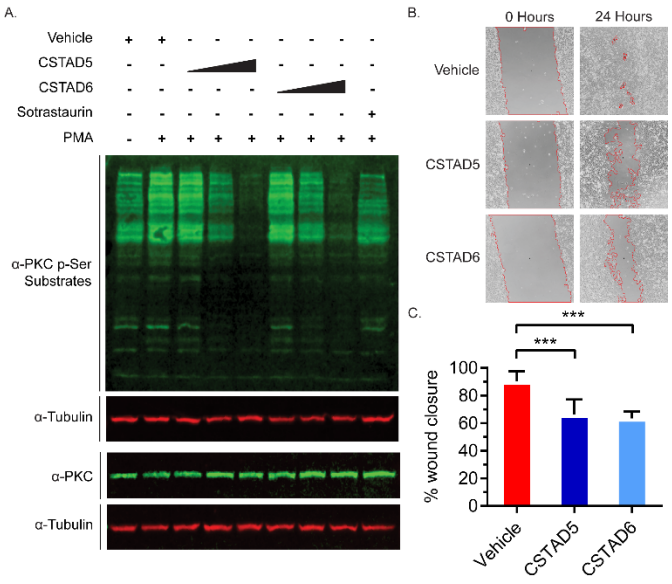

Figure 2.4 CSTAD5 and CSTAD6 downregulate PKC substrate phosphorylation and cell migration (A) Representative western blot from serum starved PC-3 cells treated with CSTAD5, CSTAD6 (either 1, 2.5, 5 μM, four hours) or vehicle (DMSO) along with a PKC specific catalytic inhibitor (sotrastaurin, 500 nM, 90 minutes) followed by PMA stimulation (500 nM) for five minutes (n=3). Both peptides caused a significant reduction in PKC signaling at 5 μM treatments. (B) Wound healing assays were performed using PC-3 cells treated with 5 μM CSTAD5, CSTAD6 or vehicle (DMSO) for 24 hours. The wound area is marked by red boundary lines generated using MRI Wound Healing Tool for ImageJ. Representative images (n=3) show CSTAD5 and CSTAD6 slowed wound healing over this time course. (C) Quantification of PC-3 cell motility as assessed by measuring percentage wound closure from 0 to 24 hours across three independent wound healing assays. Wound area was calculated using MRI Wound Healing Tool for ImageJ. *** $p < 0.01$ by one-way ANOVA and Bonferroni's multiple comparisons test. Error bars represent standard deviation.

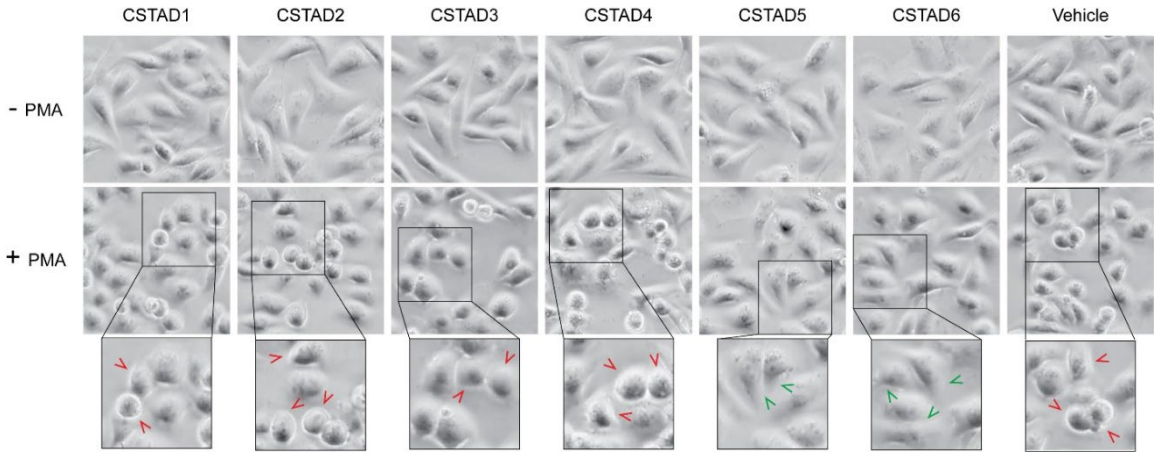

Figure S2.1 CSTAD5 and CSTAD6 peptides downregulate PMA induced cytoskeletal remodeling in PC-3 cells. Serum starved PC-3 cells were treated with 5 μM CSTAD peptides or vehicle (DMSO) for four hours, followed by 500 nM PMA for 45 minutes. Phase contrast images pre- and post-PMA stimulation displaying altered in morphology (cell rounding) for cells treated with CSTAD 1-4 whereas CSTAD 5 and CSTAD 6 treated cells preserve a more flattened morphology.

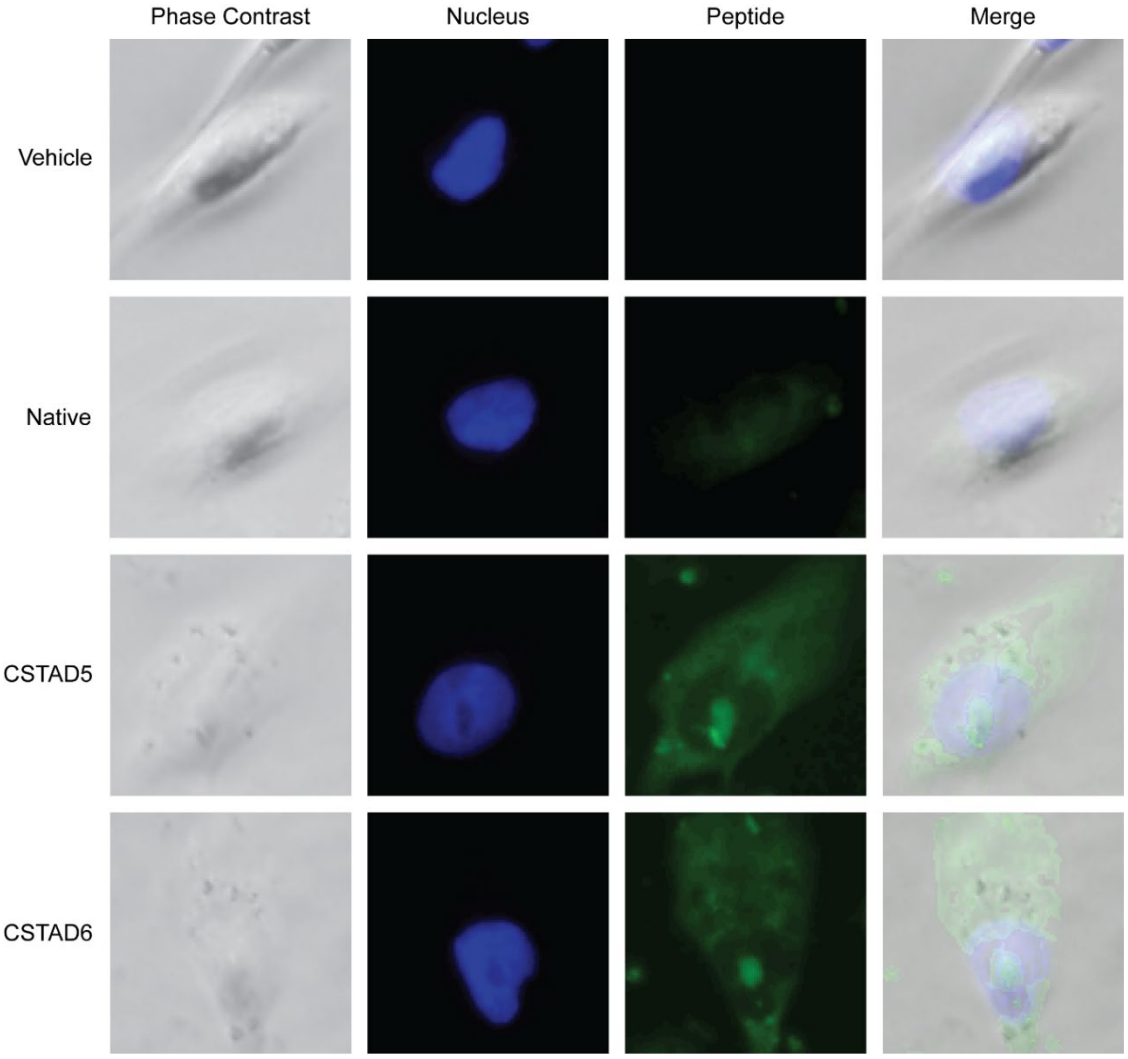

Figure S2.2 CSTAD peptides permeate cell membranes and display cytoplasmic localization. PC-3 cells were treated with 5 mM vehicle (DMSO), CSTAD5, CSTAD6 or native peptide for four hours. Cells were washed, fixed with paraformaldehyde, permeabilized with Triton X-100 followed by nuclear staining with DAPI. Fluorescence images along with their overlays demonstrate the primarily cytoplasmic localization of CSTAD peptides with some degree of presence within the nucleus.

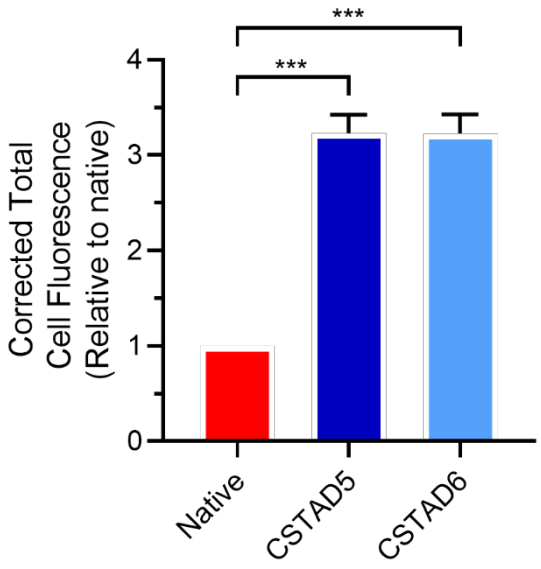

Figure S2.3 Addition of an all-hydrocarbon staple improves cellular uptake. PC-3 cells were treated with 5 mM CSTAD5, CSTAD6 or vehicle (DMSO) for four hours. Cells were washed, fixed with paraformaldehyde, permeabilized with Triton X-100 followed by nuclear staining with DAPI. Peptide uptake was quantified as Corrected Total Cell Fluorescence (CTCF) using ImageJ. *** $p<0.01$ by one-way ANOVA and Bonferroni's multiple comparisons test. Error bars SEM from n=100 cells.

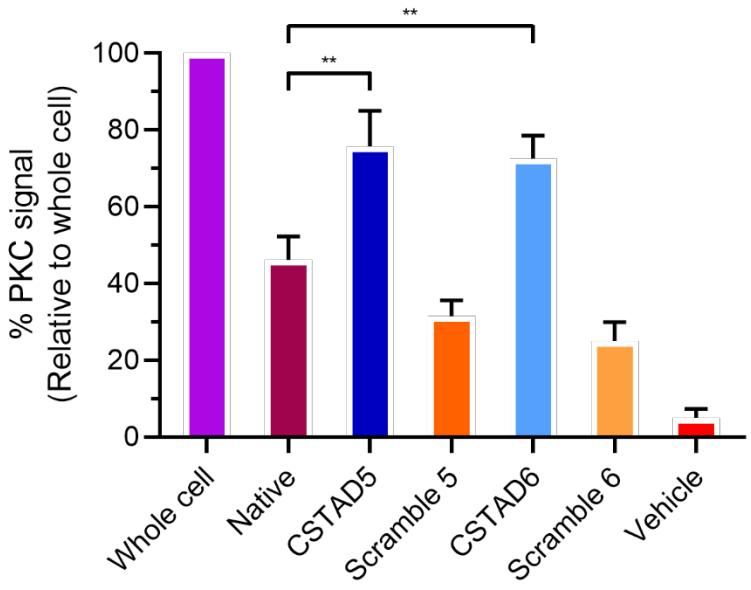

Figure S2.4 Addition of an all-hydrocarbon staple improves PKC binding. PC-3 cell lysates were treated with biotin-labeled peptides for four hours. Pulldowns were performed using streptavidin-agarose resin. PKC was detected by immunoblotting. Densitometric quantifications were performed using LI-LOR Image Studio. * $p<0.05$; ** $p<0.01$ by one-way ANOVA and Bonferroni's multiple comparisons test. Error bars represent standard deviation from n=5 experiments.

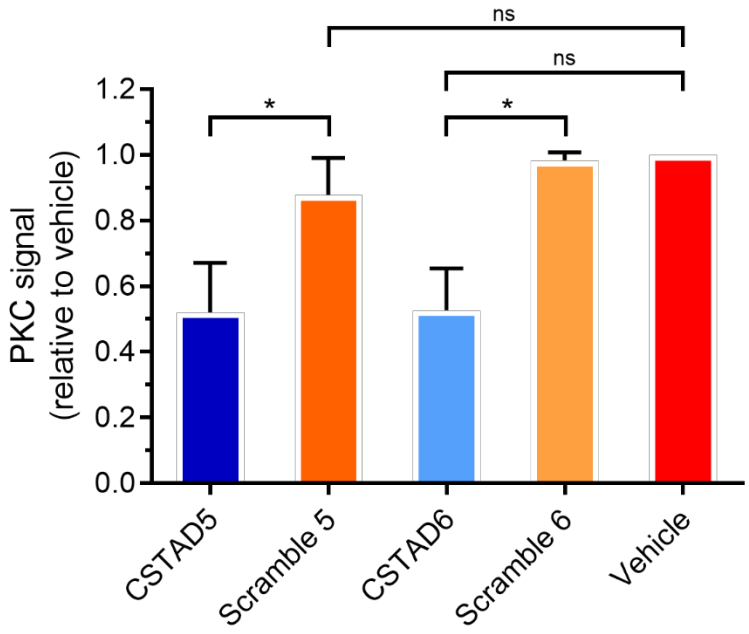

Figure S2.5 CSTAD5 and CSTAD6 reduce PKC scaffolding by gravin. Serum starved A549 cells were treated with 5 mM CSTAD5 or CSTAD6, their respective scrambled controls or DMSO for four hours. Treated cells were lysed and gravin was immunoprecipitated followed by SDS-PAGE and immunoblotting for PKC. Densitometric quantifications show reduced PKC coprecipitation with gravin in lysates from cells pretreated with CSTAD5 or CSTAD6 as compared to their scrambled controls. * $p<0.05$; ns, not significant by one-way ANOVA and Bonferroni's multiple comparisons test. Error bars represent standard deviation from n=4 experiments.

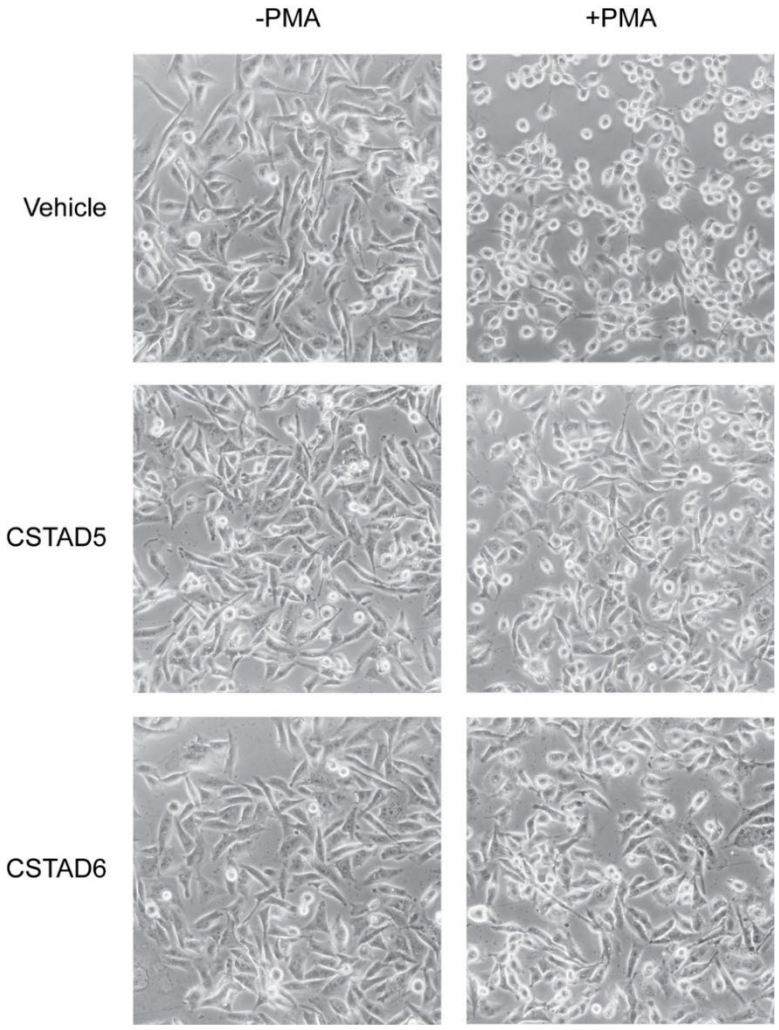

Figure S2.6 CSTAD peptides reduce PMA induced cytoskeletal remodeling in PC-3 cells. Serum starved (24 hours) PC-3 cells were treated with 5 μM CSTAD peptides or vehicle (DMSO) for four hours followed by 45 minutes with 500 nM PMA. Phase contrast images pre- and post-PMA stimulation show the preservation of non-rounded cell morphology in CSTAD5- or CSTAD6-treated cells as compared to vehicle-treated cells.

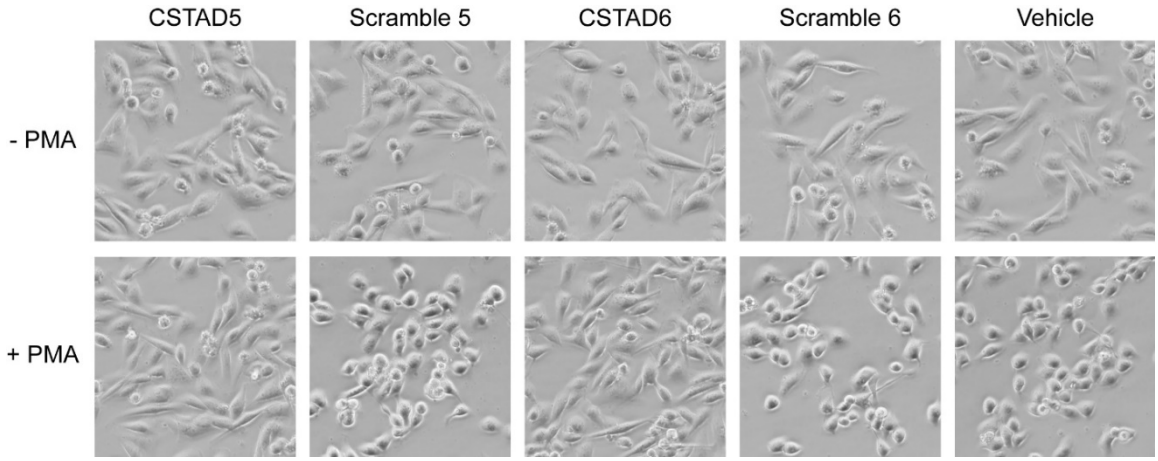

Figure S2.7 Scramble controls do not downregulate PMA-induced cytoskeletal remodeling. Serum starved (24 hours) PC-3 cells were treated with 5 mM CSTAD5, CSTAD6, scramble controls or vehicle (DMSO) for four hours followed by a 45-minute treatment with 500 nM PMA. Phase contrast images pre- and post-PMA stimulation show the preservation of normal cell morphology in CSTAD5- or 6-treated cells as compared to their respective scramble controls or vehicle treated cells.

CHAPTER 3

DISRUPTION OF NASCENT DIMERS BY STAPLED PEPTIDES UPREGULATES PKC MATURATION [3]

[3] Limaye, A. J., Baffi, T. R., Lordén, G., Wozniak, J. M., Feichtner, A., Yeung, W., Kornev, A. P., King, C. C., Del Rio, J. C., Bogomolovas, J., Gould, C. M., Chen, J., Kennedy, E. J., Kannan, N., Gonzalez, D. J., Stefan, E., Taylor, S. S., & Newton, A. C. (2021). mTORC2 controls the activity of PKC and Akt by phosphorylating a conserved TOR interaction motif. Science signaling, 14(678), eabe4509. https://doi.org/10.1126/scisignal.abe4509

Portions of this article (accepted manuscript) are reproduced here with permission of the publisher. © 2021 The Authors, some rights reserved, exclusive licensee American Association for the Advancement of Science.

Baffi, T. R. is the first author, Limaye, A. J.is a co-author.

3.1 Abstract

Similar to all other human protein kinases, PKC requires phosphorylation of the activation loop in order to become catalytically competent. Additionally, as a member of the AGC family of the human kinome, PKC requires phosphorylation at two distinct sites within its C-tail to be fully mature and primed for signaling. These phosphorylation events allow structuring of the different segments of the catalytic domain of PKC allowing it to become catalytic competence and enter autoinhibited state. While PDK1 and mTORC2 have long been established as the regulators of the activation loop and C-tail phosphorylation respectively, the exact biochemical processes behind them have not been well understood. Additionally, the role of mTORC2 in phosphorylating the hydrophobic motif, one of the two phosphorylation sites within PKC C-tail has remained controversial. With recent data suggesting a potential tumor suppressor role for PKC combined with the interest in the development of mTOR inhibitors as potential cancer therapeutics, research has gone into elucidating the mechanisms of how mTORC2 regulates PKC maturation. Recent research revealed a previously undiscovered, unreported homo-dimeric form of nascent PKC, which serves as a rate limiting step in PKC processing by mTORC2. Here we report the development of two cell permeable, all-hydrocarbon stapled peptides modeled after the dimerization interface. Both of these PKC-Dimerization Disruptor (PKC-DD) peptides were able to disrupt nascent PKC dimers and upregulate their processing by mTORC2 and eventual maturation. They serve as proof-of-concept demonstrating that the PKC dimerization interface is actionable and can be targeted to promote PKC maturation.

3.2 Introduction

PKC, similar to majority of the other human protein kinases, requires phosphorylation of the activation loop segment in order to gain catalytic competence. For the AGC family of the human kinome, which PKC belongs to, the activation loop phosphorylation is carried out by PDK1 [165]. Additionally, PKC undergoes phosphorylation at two distinct sites within its C-tail, another characteristic of the AGC family of kinases [85]. The turn motif phosphorylation site within the PKC C-tail has been established to be essential for the stability of the protein and is regulated by mTORC2, one of the two distinct multiprotein complexes formed by mTOR [166]. The second C-tail site, the hydrophobic motif, is essential for the catalytic activity of PKC has been shown to be mTORC2 sensitive [167].

Prior research proposed mTORC2 as the primary regulator of both of the C-tail phosphorylation sites, the turn motif as well as the hydrophobic motif [168-170]. However, multiple reports indicate towards PKC intrinsic mechanisms regulating the phosphorylation of the hydrophobic site, i.e., autophosphorylation [83, 88, 171].

Recent research focused on resolving the mTORC2 regulation of PKC maturation established PDK1 and mTORC2 as the prime regulators of the activation loop and turn motif phosphorylation sites respectively. It also showed the hydrophobic motif phosphorylation to be regulated by PKC intrinsic autophosphorylation. It showed that the hydrophobic motif phosphorylation was dependent on both PDK1 and mTORC2 and required PKC to be catalytically competent. A novel motif within the C-tail was identified dubbed the TOR-interaction motif (TIM) which harbors an additional mTORC2 dependent phosphorylation site which undergoes phosphorylation before the turn motif site. This

research also identified a previously unreported homo-dimeric form of nascent PKC mediated by the TIM. This dimeric, nascent PKC serves as the rate limiting step, where the binding of mTORC2 disrupts TIM dimer interface, followed by the phosphorylation of the novel TIM site. Subsequent phosphorylation of the turn motif site relieves PKC homodimers. This exposes the C-tail, allowing PDK1 recruitment and subsequent phosphorylation of the PKC activation loop. This primes PKC for autophosphorylation of the hydrophobic motif completing its maturation [89].

We hypothesized that extraneous disruption of the nascent PKC dimers may enhance mTORC2's access to the TIM enhancing phosphorylation of the subsequent sites and eventual maturation. With the structural information at hand, combined with synthetic modifications, we developed all-hydrocarbon stapled peptides that were modeled after the PKC homodimer interface. These peptides permeated cells, disrupted nascent PKC dimers, and upregulated PKC maturation as measured by turn motif and hydrophobic motif phosphorylation, demonstrating that the TIM is actionable.

3.3 Results and Discussion

The design process for the PKC dimerization disruptor peptides began with analyzing the only PKCβII catalytic domain crystal structure with the C-tail resolved (PDB ID: 2I0E). Generation of symmetry mates, along with protein-protein docking confirmed TIM as the dimerization interface. Residues 627 through 636 form the TIM helix that makes up the dimerization interface. Phenylalanine (F) residues at positions 629, 632 and 633 are involved in π- π stacking interactions across the dimerization interface and thus are essential for the binding interaction (Fig. 3.1). The native peptide derived from the helix

lacks any positive charge. In order to better optimize the peptide properties, we extended the sequence by three residues towards the N-terminal end. We also placed additional lysine (K) residues at the N- and C-terminal ends of the peptide to improve the overall charge of the peptide as well as its water solubility. We then placed two residues of (S)-2-(4-pentenyl)alanine at *i, i*+4 positions to form a staple across one helical turn. Grubbs 1st generation catalyst was then used to carry out ring closing metathesis and form the all-hydrocarbon staple. Two resultant stapled peptides were named PKC-Dimerization Disruptor Staple 1 (PKC-DD-S1) and PKC-Dimerization Disruptor Staple 2 (PKC-DD-S2). We also synthesized a native version of the peptide dubbed PKC-Dimerization Disruptor Unstapled (PKC-DD-U). [4] (Fig. 3.2A, B)

We first assessed whether the addition of the staple improved the cellular uptake of the PKC-DD peptides. A549 cells were treated with 10 μM 5(6)-carboxyfluorescein (FAM)-labeled PKC-DD-U, S1 and S2 peptides for eight hours. Peptide uptake was then analyzed by fluorescence imaging the fixed cells. Both of the stapled peptides, S1 and S2 showed diffuse, cytoplasmic fluorescence whereas the unstapled peptide showed no noticeable cellular presence (Fig. 3.3A). Quantifications showed that S1 and S2 peptides had ~10 and ~6 fold higher cell uptake respectively as compared to the unstapled version. [4] (Fig. 3.3B)

"Since mTORC2 phosphorylation of the TOR-interaction motif promotes hydrophobic motif phosphorylation and also dissociates PKC dimers, we next addressed whether disrupting PKC dimerization would be sufficient to enhance PKC phosphorylation at the hydrophobic motif. To test this possibility, we designed cell-permeable α-helical

[4] Previously unpublished data

stapled peptides [16, 172] targeting the TOR-interaction motif to relieve dimerization (Fig. 6G). Treatment of cells overexpressing PKCβII with either of two different PKC dimerization disruptor stapled peptides (S1, S2) resulted in increased levels of PKC phosphorylation compared to DMSO-treated controls (Fig. 6H). Thus, peptides targeting the TOR-interaction motif designed to disrupt the dimer interface effectively promoted PKC processing. These data are consistent with a model in which the TOR-interaction motif helix coordinates an immature PKC homodimer, which is dissociated by mTORC2 phosphorylation to promote PKC maturation. Moreover, the TIM dimerization interface, previously identified as a "novel α-helix" in the original crystallization, is therapeutically actionable and can be targeted with stapled peptides in cells to induce PKC processing." [3]

3.4 Conclusion

"Strategies to manipulate hydrophobic motif phosphorylation may be applicable in cancer therapies, where this site is frequently dysregulated. The AGC kinase hydrophobic motif is a hotspot for cancer-associated mutations in sites of post-translational modifications [93]. Additionally, PKC quality control, which involves PHLPP-mediated hydrophobic motif dephosphorylation and degradation, is exploited in cancer to suppress PKC protein levels [173, 174]. Thus, maintaining the integrity of the PKC processing

---

[3] Limaye, A. J., Baffi, T. R., Lordén, G., Wozniak, J. M., Feichtner, A., Yeung, W., Kornev, A. P., King, C. C., Del Rio, J. C., Bogomolovas, J., Gould, C. M., Chen, J., Kennedy, E. J., Kannan, N., Gonzalez, D. J., Stefan, E., Taylor, S. S., & Newton, A. C. (2021). mTORC2 controls the activity of PKC and Akt by phosphorylating a conserved TOR interaction motif. Science signaling, 14(678), eabe4509. https://doi.org/10.1126/scisignal.abe4509

Portions of this article (accepted manuscript) are reproduced here with permission of the publisher. © 2021 The Authors, some rights reserved, exclusive licensee American Association for the Advancement of Science.

Baffi, T. R. is the first author, Limaye, A. J.is a co-author.

machinery that permits hydrophobic motif phosphorylation is critical for PKC's tumor-suppressive function [175, 176]. Akt hydrophobic motif phosphorylation, conversely, generally serves an oncogenic role, and constitutively active or amplified Akt is prevalent in the wide variety of cancers that frequently harbor PI3K pathway alterations [177]. In these cancers, the mTOR kinase is an attractive therapeutic target [92]; however, this strategy should be approached with caution as mTORC1/2 inhibitors would have the unwanted consequence of inhibiting PKC processing, depleting the levels of an important tumor-suppressor. Therefore, utilizing 3rd generation mTOR inhibitors that selectively target mTORC1[178], or exploring methods to promote mTOR-independent PKC processing by targeting PKC dimerization with stapled peptides as we have done here, may potentiate the efficacy of mTOR therapies." [3]

3.5 Materials and Methods

Peptide synthesis

"Peptides used in this study were synthesized using Fmoc (fluorenylmethoxycarbonyl)-protected solid phase peptide synthesis on Rink Amide MBHA resin. Synthesis was performed in NMP (1-methyl-2-pyrrolidinone). Deprotections were performed using 25% v/v solution of piperidine in NMP for30 minutes. Amino acid

---

[3] Limaye, A. J., Baffi, T. R., Lordén, G., Wozniak, J. M., Feichtner, A., Yeung, W., Kornev, A. P., King, C. C., Del Rio, J. C., Bogomolovas, J., Gould, C. M., Chen, J., Kennedy, E. J., Kannan, N., Gonzalez, D. J., Stefan, E., Taylor, S. S., & Newton, A. C. (2021). mTORC2 controls the activity of PKC and Akt by phosphorylating a conserved TOR interaction motif. Science signaling, 14(678), eabe4509. https://doi.org/10.1126/scisignal.abe4509
Portions of this article (accepted manuscript) are reproduced here with permission of the publisher. © 2021 The Authors, some rights reserved, exclusive licensee American Association for the Advancement of Science.
Baffi, T. R. is the first author, Limaye, A. J.is a co-author.

coupling was carried out by adding 10 equivalents of Fmoc-protected amino acid (0.25 M final concentration) along with HCTU [O-(1H-6-Chlorobenzotriazole-1-yl)-1,1,3,3-tetramethyluronium hexafluorophosphate] in NMP (0.24 M final concentration) followed by 8% v/v DIEA (N, N-Diisopropylethylamine) for 45 min. The olefinic amino acid S 5 [Fmoc-(S)-2-(4-pentenyl)alanine] was incorporated as denoted in the sequences below using standard coupling conditions at i, i+4 positions. Ring closing metathesis was carried out on protected and resin bound peptides using 0.4 equivalents of Grubb's 1st Generation catalyst [Benzylidene-bis(tricyclohexylphosphine)dichlororuthenium] in 1,2-dichloroethane for 1 hour. Olefin metathesis was performed twice to ensure completion of staple formation. N-terminal addition of PEG three (Fmoc-11-amino-3,6,9-trioxaundecanoic acid, denoted as asterisks in sequences below) was conducted with 4 molar equivalents under standard coupling conditions. Peptides were biotin labeled at the N-terminus using 10 equivalents of D-biotin, 0.14 M HCTU and 4% v/v DIEA in a 1:1 mixture of DMF and DMSO (dimethyl sulfoxide) overnight at room temperature. Peptides were cleaved from resin using 95% TFA (trifluoroacetic acid), 2.5% water and 2.5% TIS (triisopropylsilane) for 4 h. Products were then precipitated in ice cold MTBE (methyl-tert-butyl ether) and air dried. Crude products were dissolved in methanol and purified using high performance liquid chromatography over a 10-100% acetonitrile gradient. Products were verified by mass spectroscopy and quantified by measuring diminished absorbance

of HABA[2-(4'-hydroxybenzeneazo)benzoic acid]-avidin complex at 500 nm. Molecular weights of the purified products are as follows: S1: Biotin-PEG3-KRNA*NFD*FFTRHK, actual mass 2345.4 (expected mass: 2345.8); and S2: Biotin-PEG3-KRNAENFD*FFT*HK; actual mass 2318.2 (expected mass= 2318.7)." [3]

For fluorescein labeling, deprotected, resin bound peptides were agitated overnight with 2 equivalents of 5(6)-carboxyfluorescein, 0.046 M HCTU and 2% v/v DIEA in DMF (N, N-Dimethylformamide). Fluorescein labeled peptides were quantified by measuring their absorbance at 495 nm. Molecular weights of the purified products are as follows: U: FAM-PEG3-KRNAENFDRFFTRHK, actual mass 2512.6 (expected mass: 2512.7) S1: FAM-PEG3-KRNA*NFD*FFTRHK, actual mass 2477.5 (expected mass: 2477.7); and S2: FAM-PEG3-KRNAENFD*FFT*HK; actual mass 2450.6 (expected mass= 2450.7).

Peptide uptake assay

A549 cells were seeded per chamber on an 8-chamber slide (Nunc Lab-Tek II) and allowed to adhere overnight. Media (RPMI-1640 supplemented with 10% FBS and 1% Penicillin/Streptomycin) containing 10 μM PKC-DD-S1, PKC-DD-S2 or PKC-DD-U was introduced into the chambers. Cells were incubated with the treatments for eight hours followed by three washes with media and one wash with PBS. Cells were then fixed using

---

[3] Limaye, A. J., Baffi, T. R., Lordén, G., Wozniak, J. M., Feichtner, A., Yeung, W., Kornev, A. P., King, C. C., Del Rio, J. C., Bogomolovas, J., Gould, C. M., Chen, J., Kennedy, E. J., Kannan, N., Gonzalez, D. J., Stefan, E., Taylor, S. S., & Newton, A. C. (2021). mTORC2 controls the activity of PKC and Akt by phosphorylating a conserved TOR interaction motif. Science signaling, 14(678), eabe4509. https://doi.org/10.1126/scisignal.abe4509

Portions of this article (accepted manuscript) are reproduced here with permission of the publisher. © 2021 The Authors, some rights reserved, exclusive licensee American Association for the Advancement of Science.

Baffi, T. R. is the first author, Limaye, A. J.is a co-author.

2% paraformaldehyde solution for 10 minutes followed by three brief washes with PBS. Fixed cells were permeabilized using 0.1% Triton X-100 in PBS for 10 minutes. Cells were washed thrice with PBS. Nuclear staining was performed by adding 300 nM DAPI solution to each chamber followed by five minutes of incubation away from light. Cells were washed three times with PBS and slides were air dried. A coverslip was mounted overnight at 4°C using Permafluor aqueous mounting medium. Phase contrast and fluorescence imaging was performed using Olympus IX71 microscope equipped with Exfo X-Cite 120Q light source. ImageJ was used to generate channel overlays for acquired images and calculating corrected total cell fluorescence (CTCF). Data was analyzed in GraphPad Prism. [5]

[5] Previously unpublished data

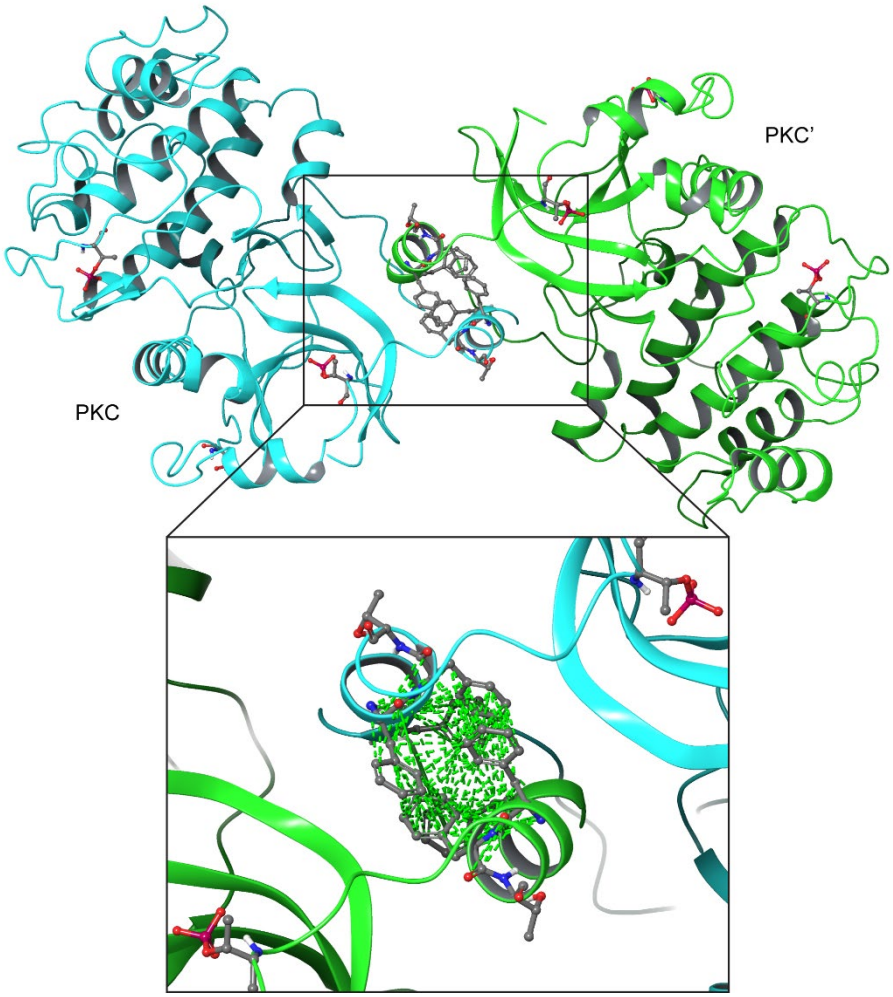

Figure 3.1 TIM mediates dimerization of nascent PKC Crystal structure of PKCβ (PDB ID: 2I0E) demonstrating homodimerization of two nascent PKC catalytic domains (cartoon view, green and cyan) coordinated by the novel TOR-interaction motif or TIM (cartoon representation and sticks). Insert shows the phenylalanine residues on either helix forming hydrophobic interactions which stabilize the homodimer. The novel mTORC2 phosphorylation site, Thr634 in its unphosphorylated form can be seen on the opposite faces of the helices.

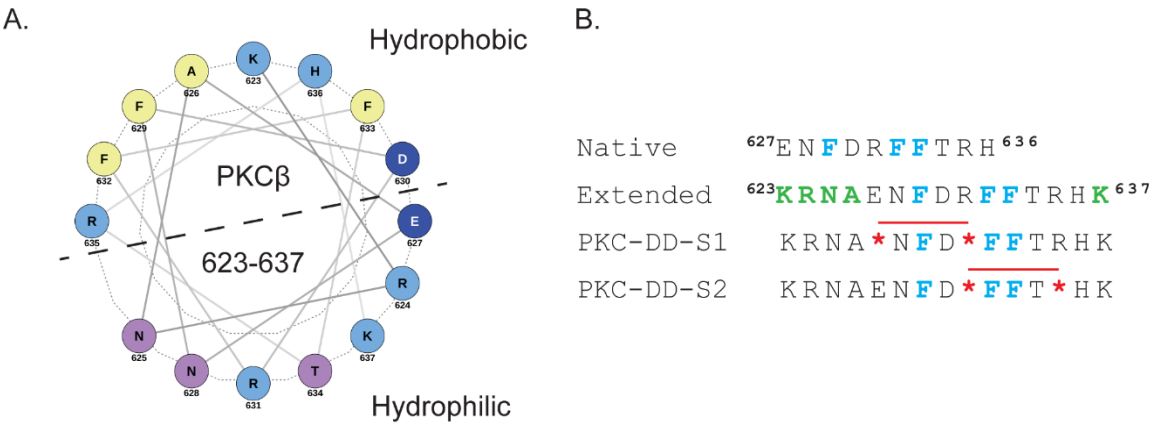

Figure 3.2 Design of the PKC-DD peptides (A) Helical wheel representation of the extended TIM helix (PKCβII residues 623-637) shows its amphipathic nature with basic residues in light blue, acidic residues in deep blue, polar residues in lilac and nonpolar residues in yellow. Helical wheel was generated using NetWheels. (B) Extended TIM helix was used as template for the PKC-DD peptides, extended resides are in green, phenylalanine residues vital for binding are in blue and the synthetic, olefinic amino acid residues are represented by *. Red line represents all-hydrocarbon staple.

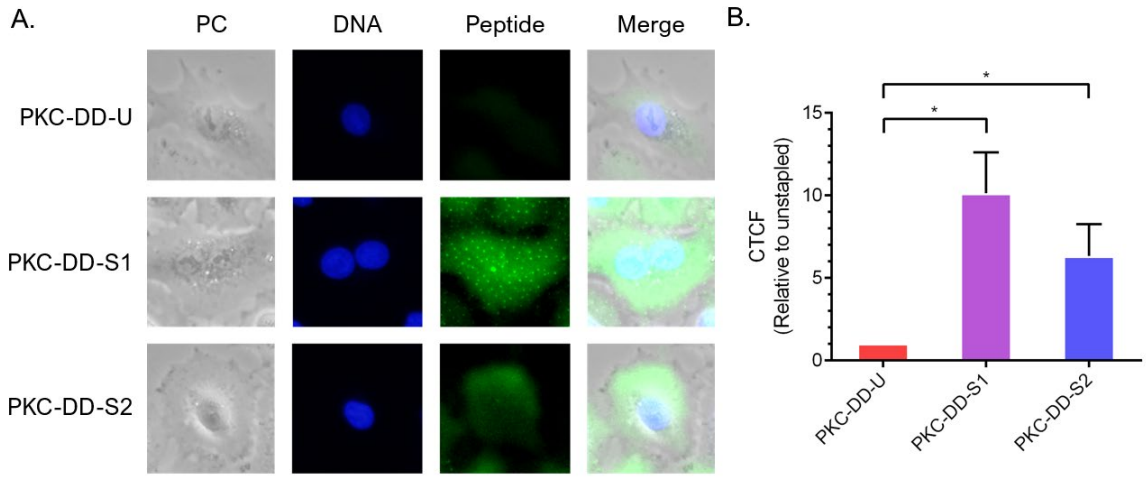

Figure 3.3 Stapled PKC-DD peptides permeate cells (A) Representative images of A549 cells treated with 10 μM PKC-DD peptides for 8 hours. Fluorescence imaging shows cytoplasmic localization of PKC-DD-S1 and PKC-DD-S2 peptides. (B) Quantification of peptide uptake as measured by corrected total cell fluorescence shows that the stapled PKC-DD peptides (S1 and S2) have ~10 and ~6 fold higher cell permeation respectively as compared to the unstapled, native peptide (PKC-DD-U). * $p < 0.05$ by one-way ANOVA and Bonferroni's multiple comparisons test. Error bars represent standard deviation.

CHAPTER 4

IN SILICO OPTIMIZED STAPLED PEPTIDES TARGETING WASF3 IN BREAST CANCER [6]

[6] Limaye, A. J., Bendzunas, G. N., Whittaker, M. K., LeClair, T. J., Helton, L. G., & Kennedy, E. J. (2022). In silico optimized stapled peptides targeting WASF3 in breast cancer. ACS Medicinal Chemistry Letters.
https://doi.org/10.1021/acsmedchemlett.1c00627
Reprinted here with permission of the publisher. ©2022 American Chemical Society

4.1 Abstract

Wiskott-Aldrich Syndrome Protein Family (WASF) members regulate actin cytoskeletal dynamics and WASF3 is directly associated with breast cancer metastasis and invasion. WASF3 forms a hetero-pentameric complex with CYFIP, NCKAP, ABI and BRK1 called the WASF Regulatory Complex (WRC), which cooperatively regulates actin nucleation by WASF3. Since aberrant deployment of the WRC is observed in cancer metastasis and invasion, its disruption provides a novel avenue for targeting motility in breast cancer cells. Here we report the development of a second generation WASF3 mimetic peptide, WAHMIS-2, which was designed using a combination of structure guided design, homology modeling and *in silico* optimization to disrupt binding of WASF3 to the WRC. WAHMIS-2 was found to permeate cells, inhibit cell motility, invasion and MMP9 expression with greater potency than its predecessor, WAHM1. Targeted disruption of WASF3 from the WRC may serve as a useful strategy for suppression of breast cancer metastasis.

4.2 Introduction, Results and Discussion

Cancer metastasis includes the hijacking of intrinsic signaling pathways involved in cell migration that is required for many routine biological processes including embryonic morphogenesis, immune surveillance, tissue repair and regeneration [96]. The aberrant employment of migratory signaling pathways allows cancer cells to invade surrounding tissues and vasculature, which can result in distant metastases [124, 130, 179]. Cell migration and invasion is initiated through the formation of membrane protrusions that are driven by localized polymerization of submembrane actin filaments. To facilitate invasion,

cancer cells use specialized F-actin rich protrusions called invadopodia. Invadopodia secrete matrix metalloproteinases (MMPs) to degrade the surrounding extracellular matrix (ECM) and allow cancer cells to migrate and invade though their microenvironment [97, 98]. Rearrangement of the actin cytoskeleton is critical for the formation of F-actin rich invadopodia. It is mediated by actin related protein 2/3 (Arp2/3) and tightly controlled by its interactions with nucleation factors such as the Wiskott-Aldrich syndrome protein (WASP) family which includes WASP and neuronal-WASP (N-WASP/WASL), WASP family protein members (WASF1/WAVE1/SCAR1, WASF2/WAVE2/SCAR2, WASF3/WAVE3/SCAR3), WASP homolog associated with actin, membranes, and microtubules (WHAMM), WASP and SCAR homolog (WASH/ WASHC1), and junction-mediating regulatory protein (JMY) [100-103]. The WASP family of proteins is responsible for the spatiotemporal control of F-actin assembly in a wide range of cellular processes including polarization, adhesion, vesicle trafficking, migration, and invasion [103].

In resting cells, the three WASF members (WASF1-3) of the WASP family are constitutively sequestered in a hetero-pentametric complex dubbed the WASF regulatory complex (WRC). The WRC is comprised of WASF proteins along with CYFIP, NCKAP, ABI and BRK1 [111, 112]. WASF1-3 all play important, and in some cases, overlapping roles in cell protrusion formation, however, only WASF3 is directly associated with cancer cell invasion and metastasis [128]. The role of WASF3 in breast cancer invasion and metastasis was shown in model organisms [110, 119] and through the clinical observation that high WASF3 expression is associated with more aggressive, high grade cancer subtypes [110, 119, 180]. Additionally, forced re-expression of WASF3 in non-metastatic

breast cancer cells was sufficient to promote the development of an aggressive metastatic phenotype [122].

The pivotal role played by WASF3 in breast cancer invasion and metastasis makes it an attractive target for therapeutic intervention, however, it has not yet been effectively targeted using a small molecule approach. Previously, all-hydrocarbon stapled peptides were designed to disrupt the helical bundle interaction between WASF3 and WRC as a strategy to disrupt protein-protein interactions (PPIs) within the WRC as a strategy to suppress cancer cell invasion and metastasis *in vitro* and *in vivo* [128, 129]. Although important as a proof-of-principle that the complex serves as a viable target for suppression of metastasis, these compounds had several limitations including limited cell permeation and moderate potency with ~50-70% inhibition observed in various assays at 10 μM dosing. In addition, identification of a more potent compound may enhance its translational potential in animal models for metastasis inhibition.

These first-generation stapled peptides targeting the interaction between WASF3 and the WRC, referred to as WASF Helix Mimics (WAHM1/2), were based on the crystal structure (PDB ID: 3P8C) of WASF1 in complex with the WRC [Fig. 4.1A]. This structure revealed a trimeric helical bundle comprised of WASF1-BRK1-ABI2 and a dimer consisting of NCKAP1-CYFIP1. The sequence of WASF1 within the trimeric helical bundle is conserved within the WASF family and is referred to as the WASF homology domain (WHD) [Fig. 4.1A]. In order to design an optimized stapled peptide inhibitor of the WASF3-WRC interaction, a series of homology models were generated using Modeller for WASF3 based on the structure of the WASF1-BRK1-ABI2 helical bundle isolated from the previous WRC crystal structure (PDB ID: 3P8C) [Fig. S4.1] [181]. These models were

then optimized and scored using Rosetta Relax protocol [182]. The optimized homology model containing WASF3 residues 21 to 83 in complex with ABI2 and BRK1 was then used as the input for the Rosetta PeptiDerive protocol [183] to identify a non-modified peptide sequence between 18 and 22 residues, derived from WASF3 that partly overlaps with the WAHM1 sequence but extends beyond the original sequence and was predicted to provide greater energetic contributions than WAHM1 when bound to ABI2 and BRK1.

Using this native sequence, we performed an *in-silico* alanine scanning within Rosetta [184, 185] to identify individual residues that were predicted to energetically contribute to the binding interface [Fig. 4.1B, S4.2, S4.3]. This information, coupled with the structural model, were used to identify positions where the olefinic amino acids could be introduced in positions along the non-binding interface to ultimately form the hydrocarbon staple. We then developed synthetic libraries to experimentally test the compounds where the staple position was varied. The non-natural amino acid (s)-2-(4-pentenyl)alanine (S_5) was incorporated at *i*, *i*+4 positions along the non-binding interface and subsequently cyclized using 1st Generation Grubbs Catalyst to form the hydrocarbon staple to constrain the secondary structure of the peptide. In addition, several residues that were predicted to comprise the solvent-exposed interface of the peptide were substituted to positively charged Lys (K) residues in an effort to enhance water solubility and cellular permeation [Fig. S4.3] [17, 186, 187]. The newly designed stapled peptide library was named WAHM *In-silico*, WAHMIS [Fig. 4.1C].

As a strategy to screen whether the newly designed peptides could effectively disrupt the WASF3-containing WRC, wound healing assays were performed in the triple-negative breast cancer cell line MDA-MB-231 to assess their effect on cell motility [Fig.

4.2A]. WAHMIS-2 was found to cause an overall reduction of ~48% in wound healing as compared to the DMSO control [Fig. 4.2B]. Further, a lower dose of WAHMIS-2 caused a comparable level of inhibition in wound healing as compared to the previously developed inhibitor, WAHM1 (2 μM versus 10 μM), demonstrating increased potency by WAHMIS-2. All other WAHMIS peptides demonstrate minimal inhibitory effects on cell motility when compared to the DMSO control.

To determine whether WAHMIS-2 could inhibit cell motility in a dose-dependent manner, wound healing assays were performed over a concentration gradient of 0.5 -2 μM and compared against its scramble control (2 μM), WAHM1 (10 μM) or vehicle (DMSO) [Fig. 4.3A]. Wound area analysis revealed a dose-dependent reduction in overall cell motility with WAHMIS-2 treatment while the scramble control had no effect on cell motility [Fig. 4.3B]. To verify that the motility effects seen by WAHMIS-2 were not due to cytotoxic effects, MTS and LDH release assays were performed to measure cell viability and membrane lysis. Since Lys residues were substituted in the WAHMIS-2 sequence to improve cell permeability and it has been previously reported that strongly basic peptides can induce cell lysis, we wanted to explore whether they could cause membrane rupture[26]. Cells were treated with either 2 μM WAHMIS-2 or its scramble control. No significant reduction in cell viability or increase in LDH release was detected under all conditions as compared to the DMSO-treated control [Fig. S4.4, S4.5]. Thus, although WAHMIS-2 is not inducing lysis at the concentration tested, it is possible that addition of Lys residues to other peptides in the WAHMIS library may impact their activity.

WAHMIS-2 was chosen to be further characterized for cellular uptake and target binding. Cell permeation was assessed by treating cells with either 2 μM 5(6)-

carboxyfluorescein (FAM)-labeled WAHMIS-2, 10 μM FAM-labeled WAHM1 or vehicle (DMSO) and imaged by fluorescence microscopy. At a four-hour timepoint, a lower dosage of WAHMIS-2 demonstrated cellular uptake that was on par with WAHM1 with fluorescence intensity distributed throughout the cytoplasm [Fig. 4.4A, Fig. S4.6]. Of note, an unstapled control for WAHMIS-2 showed poor cell permeability and was thus not used in subsequent cell-based assays [Fig. S4.7]. To verify that WAHMIS-2 bound to the WRC, pulldowns were then performed using biotin-labeled WAHMIS-2. Cell lysates were treated with 2 μM biotin-labeled WAHMIS-2, its scramble control, 10 μM WAHM1 or vehicle (DMSO) for four hours followed by pulldowns using streptavidin-agarose resin. Pulldowns were analyzed by immunoblotting for ABI2 [Fig. 4.4B, C], a member of the WRC that forms a binding interface with WASF3. ABI2 was found to interact with WAHMIS-2 while the scramble control did not, indicating that WAHMIS-2 binds its intended target in the WRC.

Previous studies utilizing both RNAi as well as stapled peptides have revealed that targeted disruption of individual members of the WRC can lead to a measurable reduction in protein levels for other members of the complex[128, 130, 188]. To measure whether WAHMIS-2-mediated disruption of WASF3 from the WRC would result in altered levels of other members of the WRC, western blots were performed after 72 h peptide treatments [Fig. 4.4D, E]. Both WAHMIS-2 and WAHM1 were found to promote a statistically significant reduction in expression levels of both ABI2 and WASF3. This reduction in the protein levels caused by the peptides could be rescued by MG132 treatment, demonstrating that the proteasomal degradation pathway is somehow linked to this peptide-mediated loss of proteins in the WRC [Fig. S4.8].

Since activation of WRC has been implicated in promoting degradation of the surrounding extracellular matrix and invasion of neighboring tissue in metastasis [128-130], we next sought to evaluate the effects of WAHMIS-2 on cell invasion. The effect of WAHMIS-2 on cell invasion was assessed using transwell migration assays [Fig. 4.5A]. Cells treated with WAHMIS-2 showed a dose-dependent reduction in the number of invading cells. Further, all concentrations tested for WAHMIS-2 showed a statistically significant reduction in the number of invading cells as compared to WAHM1 (10 μM) or the scramble control (2 μM). [Fig. 4.5B], demonstrating that WAHMIS-2 potently inhibits cell migration and invasion.

Additionally, formation of cell protrusions driven by WRC were previously shown to be accompanied by secretion of Matrix Metalloproteinase 9 (MMP9) to facilitate cell invasion [128-130]. Following this line, we next assessed whether WAHMIS-2 could reduce MMP9 expression [Fig. 4.5C]. Cells were treated with WAHMIS-2, WAHM1 or controls for 72 h prior to measuring MMP9 levels by immunoblotting. WAHMIS-2 caused a statistically significant reduction in MMP9 levels (approximately 40%) as compared to the scramble control or vehicle [Fig. 4.5D]. Thus, WAHMIS-2 appears to inhibit MMP9 expression as a consequence of disruption of the WRC.

Since activation of WRC and its regulation of Arp2/3 is essential in maintaining actin cytoskeletal dynamics, extraneous disruption of the WRC results in increased stress fiber formation and decreased cell motility[128]. To determine whether WAHMIS-2 could promote increased actin stress fiber formation due to disruption of the WRC, cells were treated with either WAHMIS-2, its scramble control, WAHM1 or vehicle (DMSO) followed by phalloidin staining to visualize polymeric actin [Fig. 4.6]. Cells treated with

either WAHM1 or WAHMIS-2 showed considerably more intense staining for actin stress fiber bundles as compared to cells treated with either the scramble control or vehicle (DMSO), suggesting that WAHMIS-2 increased stress fiber formation as a consequence of WRC disruption [Fig. 4.6, Fig. S4.9].

In summary, here we report the design and development of a computationally optimized, second generation WASF3 mimetic stapled peptide, WAHMIS-2. WAHMIS-2, like its predecessor, WAHM1, was designed to disrupt binding of WASF3 into the WRC, thereby disrupting and destabilizing formation of the WRC. WAHMIS-2 was found to directly interact with ABI2, one of the primary binding partners of WASF3. In addition to permeating cells, WAHMIS-2 was found to inhibit both cell motility and invasion at comparable levels to WAHM1 but at considerably lower concentrations (5-fold difference). Further, WAHMIS-2 was found to suppress cell motility through increased actin stress fiber formation, reduced MMP9 expression and reduced protein levels for other members that comprise the WRC complex, ABI2 and WASF3.

Complications arising from the distant metastases remains one of the most lethal aspects of breast cancer [189]. Despite the advances in early stage detection and treatment, the 5-year survival rate for metastatic breast cancer remains staggeringly low at 28% compared to over 90% for localized malignancies [190]. This highlights the need for targeted intervention of metastasis in breast cancer and the need for the development of therapeutics aimed at impeding cell migration and invasion. Given that WASF3 expression strongly correlates with a poor prognosis for a variety of diverse cancers [119, 120, 127, 191-193], its targeted disruption from WRC may provide a novel avenue for therapeutic intervention. The development of a more potent inhibitor of the WRC such as WAHMIS-2 may provide

new translational opportunities for potential therapeutic applications in WASF3-driven metastatic cancers.

4.3 Materials and Methods

In Silico Design and Optimization

Crystal structure of WASF1 bound to the WASF regulatory complex (PDB ID: 3P8C) was retrieved from RCSB PDB. The FASTA sequence for WASF3 was retrieved from UNIPROT and Modeller was used to generate a homology model of WASF3 using WASF1 (PDB ID: 3P8C) as a template. This homology model of WASF3 was then aligned with WASF1 within the WRC crystal structure (PDB ID: 3P8C) and the Rosetta Relax protocol used to refine the model. The optimized homology model containing WASF3 residues 21 to 83 in complex with ABI2 and BRK1 was then used as the input for the Rosetta PeptiDerive protocol to determine a linear peptide between 18-22 residues with most significant binding energy compared to the whole interaction. This peptide was then subjected to in silico alanine scanning to determine optimal location for placement of non-natural amino acids which would form the staple and modifications to improve solubility and cell uptake.

Peptide Synthesis

Rink amide MBHA resin, N-α-Fmoc protected amino acids were purchased from Novabiochem (Merck Millipore). (S)-N-Fmoc-2-(4’-pentenyl)alanine and Grubb’s catalyst (1st Generation) were purchased from Sigma-Aldrich. All other reagents and

organic solvents were purchased from Fisher Scientific unless specified otherwise. Solvents used in this synthesis were HPLC grade.

All peptides used in this study were synthesized using standard Fmoc (fluorenylmethoxycarbonyl) protected solid phase peptide synthesis. Rink amide MBHA resin was equilibrated in NMP (1-methyl-2-pyrrolidinone). Fmoc protection group was deprotected using 25% v/v solution of piperidine in NMP for 30 minutes. Deprotection was followed by three washes with NMP. Amino acids were coupled by adding 10 equivalents of Fmoc-protected amino acid (0.25 M final concentration) in NMP to the deprotected resin along with HCTU [O-(1H-6-Chlorobenzotriazole-1-yl)-1,1,3,3-tetramethyluronium hexafluorophosphate] in NMP (0.24 M final concentration) and 8% v/v DIEA (N, N-Diisopropylethylamine). Amino acid coupling was carried out for 45 minutes followed by three washes with NMP. Deprotection and coupling steps were repeated sequentially for the remaining amino acid residues. Two residues of olefinic amino acid 'S5' [Fmoc-(S)-2-(4-pentenyl)alanine] were incorporated during synthesis at predetermined positions using standard coupling conditions. Olefin metathesis/ring closing metathesis was performed on Fmoc-protected, resin bound peptide using 0.4 equivalents of Grubb's first-generation catalyst [Benzylidene-bis(tricyclohexylphosphine)dichlororuthenium] in DCE (1,2-dichloroethane) for 1 hour, performed twice to ensure completion of staple formation. Addition of PEG3 [Fmoc-NH-PEG(3)-COOH] as a flexible N-terminal linker was performed under standard coupling conditions similar to amino acid couplings. Peptides were labeled with fluorescein or biotin at the N-terminal end following PEG3. For fluorescein labeling, deprotected, resin bound peptides were agitated overnight with 2 equivalents of 5(6)-carboxyfluorescein, 0.046 M HCTU and 2% v/v DIEA in DMF (N, N-

Dimethylformamide). Biotin labeling was performed overnight with 10 equivalents of D-biotin, 0.14 M HCTU and 4% v/v DIEA in a 1:1 mixture of DMF and DMSO (dimethyl sulfoxide). Peptides were cleaved from resin in a cleavage cocktail of 95% TFA (trifluoroacetic acid), 2.5% water and 2.5% TIS (triisopropylsilane) for four hours. Products were then precipitated in ice cold MTBE (methyl-tert-butyl ether) and allowed to air dry. Crude products were dissolved in equal parts water and methanol and purified using high performance liquid chromatography. Product peptides were verified with ESI (electrospray ionization) mass spectroscopy. Fluorescein labeled peptides were quantified by measuring their absorbance at 495 nm. Biotin labeled peptides were quantified by measuring diminished absorbance of HABA [2-(4'-hydroxybenzeneazo)benzoic acid]-avidin complex at 500 nm. Purified, dry peptides were dissolved in DMSO to achieve 10 mM stocks. Peptide stocks were stored at 4°C, protected from light.

Peptide Sequences and Molecular Weights

Asterisks (*) represent residues of 2-(4-pentenyl)Alanine (S_5).

Peptides	ESI-MS Expected	ESI-MS Found
WAHMIS-1: (5/6 FAM)-PEG3-*IIR*LSKLSKHAEKIFGELFK 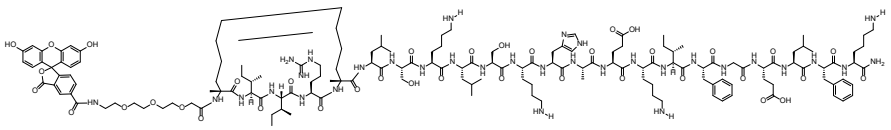	3154.7	3154.4
WAHMIS-2: (5/6 FAM)-PEG3-KIIRKLS*LSK*AEKIFGELFK 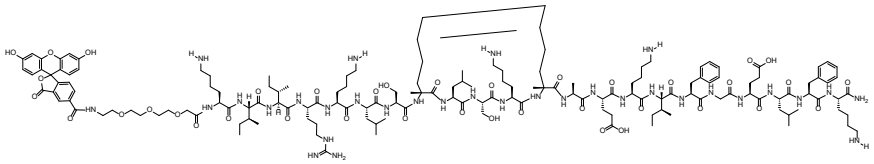	3145.7	3145.5
WAHMIS-2: Biotin-PEG3-KIIRKLS*LSK*AEKIFGELFK 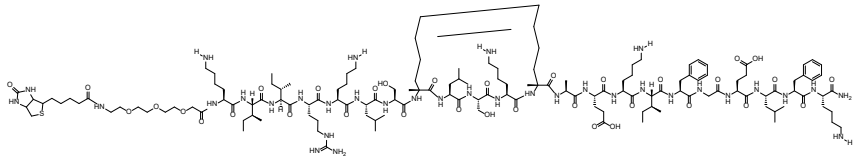	3013.7	3013.6
WAHMIS-2 Scramble: (5/6 FAM)-PEG3-EIKSFFL*AKK*GIRKKSELLI 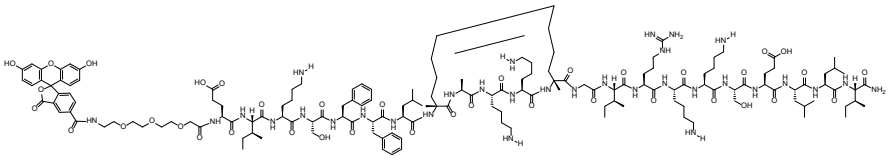	3145.7	3145.4
WAHMIS-2 Scramble: Biotin-PEG3-EIKSFFL*AKK*GIRKKSELLI 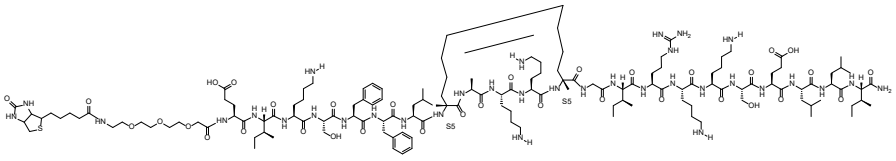	3013.7	3013.5
WAHMIS-2 Unstapled: (5/6 FAM)-PEG3-KIIRKLS*LSK*AEKIFGELFK 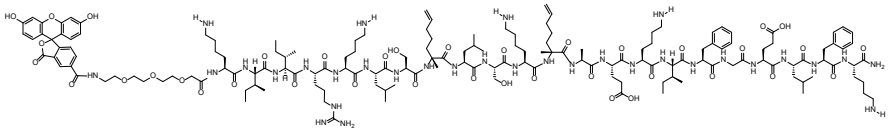	3173.8	3173.2

WAHMIS-3: (5/6 FAM)-PEG3-KII*QLS*LSKHAEKIFGELFK 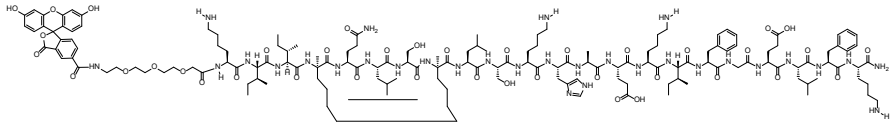	3126.7	3126.6
WAHMIS-4: (5/6 FAM)-PEG3-KIIRQLSKLS*HAE*IFGELFK 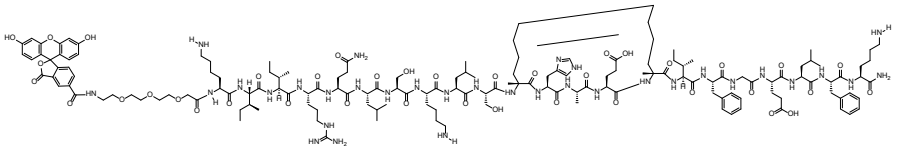	3154.7	3154.5
WAHM1: (5/6 FAM)-PEG3-LEK*TNS*LAKIIRQL 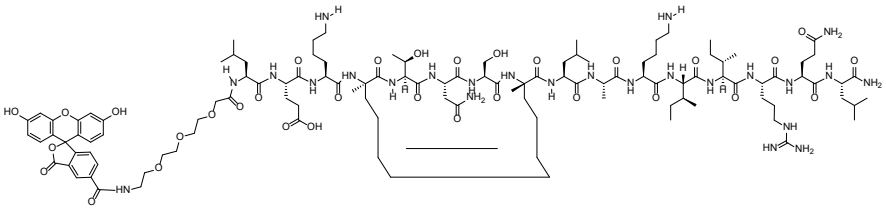	2423.8	2423.7
WAHM1: Biotin-PEG3-LEK*TNS*LAKIIRQL 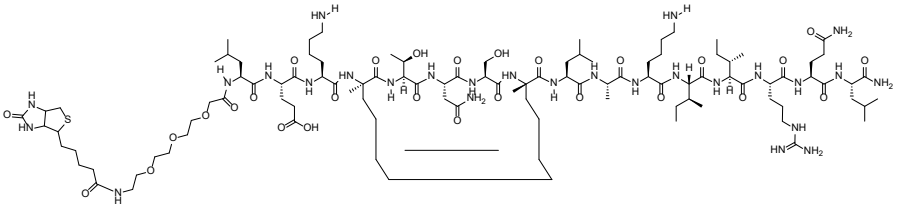	2291.8	2291.6

Cell culture

MDA-MB-231 cells were obtained from ATCC. Cell culture medium, RPMI-1640 and trypsin were purchased from Corning (Cellgro). Fetal bovine serum (FBS) was purchased from HyClone (Cytiva).

Cells were maintained in RPMI-1640 supplemented with 10% FBS and 1% Penicillin-Streptomycin at 37°C with 5% CO_2. Cells were passaged at least twice before being used in any experiment and all experiments were performed in at least triplicate at different passage numbers.

Motility Assay

MDA-MB-231 cells were grown to confluency in 24 well plates and serum starved for 24 hours in 2% FBS RPMI-1640. A wound area was created by dragging a 20-200 μL pipette tip vertically down each well and debris was removed by washing each well three times with serum free RPMI-1640. Following this, initial images were acquired using an Olympus IX71 inverted microscope. Peptides were diluted to desired final concentrations in 5% FBS RPMI-1640 and cells treated for 18 hours or until the control wound area had healed to 95% and above. Wound area prior to and following treatment was measured using the MRI wound healing tool for the ImageJ software suite. Data was analyzed using GraphPad Prism.

Invasion Assay

Matrigel basement membrane coating was applied to Transwell inserts as described in the Corning protocol and allowed to incubate for 30 minutes at 37°C. MDA-MB-231

cells were serum starved in 2% FBS RPMI-1640 for 24 hours and dissociated in 0.25% Trypsin followed by quenching in 10% FBS RPMI-1640. Cells were washed in serum free RPMI-1640 and counted using hemocytometer. ~20,000 cells per chamber were added along with peptide treatment in serum free RPMI-1640 while 10% FBS RPMI-1640 containing peptide treatment was added to the lower chamber as a chemoattractant. Following 24 hours of incubation, inner surfaces of Transwell inserts were swabbed out and fixed in 2% paraformaldehyde in PBS for 10 minutes and stained using 2% crystal violet in methanol for 10 minutes. Inserts were washed by immersing in DI water and imaged using an Olympus IX71 inverted microscope. Invading cells were counted using the ImageJ software suite. Data analysis was carried out in GraphPad Prism.

Phalloidin Quantification and Peptide Uptake

$2x10^4$ cells were seeded per chamber on an 8-chamber slide (Nunc Lab-Tek II) and allowed to adhere overnight. Media containing peptide treatments were introduced and cells were incubated for four hours at 37°C. Cells were then washed 3 times with PBS and fixed using 2% paraformaldehyde solution for 10 minutes followed by three additional washes with PBS. Fixed cells were permeabilized using 0.1% Triton X-100 in PBS for 10 minutes. Following permeabilization, cells were treated with 200 μL of 10 μM Hoechst 33342 nuclear stain and in the case of cells in which F-actin was to be quantified, 1X phalloidin-iFlour 594 in PBS with 10% BSA. Chamber slides were allowed to sit for 30 minutes (or 5 minutes for nuclear staining) protected from light and then washed three times with PBS and air dried. A coverslip was then mounted overnight at 4°C using PermaFluor aqueous mounting medium (Thermo Fisher). Phase contrast and fluorescence

imaging was performed using Olympus IX71 inverted microscope equipped with Exfo X-Cite 120Q light source. ImageJ software suite was used to generate channel overlays for acquired images and calculating corrected total cell fluorescence (CTCF). CTCF was calculated from four separate fields per treatment, across four independent assays. Background fluorescence from each field was accounted for while calculating the CTCF values. Data was analyzed in GraphPad Prism.

Biotin-Streptavidin Pulldown Assay

MDA-MB-231 cells were lysed in ice cold NP-40 lysis buffer (50 mM Tris pH 8.0, 150 mM NaCl, 1% Nonidet P-40 supplemented with 1X Halt Protease Inhibitor Cocktail). Cell lysates were treated with biotin labelled peptides and agitated for four hours at 4°C. 30 µL of Streptavidin-Agarose resin (Millipore) was added to all samples and the samples were agitated overnight at 4°C. Next day, resin was collected by centrifuging the lysate mixtures at 1000G for 5 minutes. Collected resin was washed at least three times with ice cold NP-40 lysis buffer and boiled in Laemmli sample buffer (60 mM Tris-HCl pH 6.8, 2% SDS, 10% glycerol, 5% β-mercaptoethanol, 0.01% bromophenol blue) for 10 minutes at 95°C. SDS-PAGE was performed using 4-20% 4–20% Mini-PROTEAN TGX Precast gels (Biorad) for 1 hour at 100V, followed by standard western blot on to PVDF (Immobilon-FL, Millipore) membranes for 2 hours in an ice bath at 300 mA. Anti-ABI2 antibody (1:1000, Rabbit mAb, Proteintech) was used for primary immunodetection. Secondary antibody (1:15000, Goat anti-Rabbit IRDye 680RD, LI-COR) was used for secondary immunodetection and fluorescence imaging. Membranes were imaged with Odyssey Fc imaging system (LI-COR). Densitometric quantifications were obtained and

statistical analysis was performed using LI-LOR Image Studio and GraphPad Prism respectively.

Protein Levels Assessment

MDA-MB-231 cells were seeded in six well plates and allowed to reach 70% confluency. Cells were then briefly washed with PBS and serum starved for 24 hours in serum free RPMI-1640. Peptide treatments were then introduced, diluted in 5% FBS RPMI-1640. Cells were treated for up to 72 hours with treatments refreshed every 24 hours. 10 μM MG132 was introduced eight hours prior to lysis. 2X Laemmli sample buffer was then used to harvest cells and resulting lysates were boiled for 10 minutes at 95°C. SDS-PAGE was performed using 4-20% 4–20% Mini-PROTEAN TGX Precast gels (Biorad) for 1 hour at 100V, followed by standard western blot on to PVDF (Immobilon-FL, Millipore) membranes for 2 hours in an ice bath at 300 mA. Antibodies used for primary immunodetection were: Anti-ABI2 (1:1000, Rabbit pAb, Proteintech), Anti-WASF3 (1:1000, Rabbit pAb, Thermo Fisher), Anti-MMP9 (1:2000, Rabbit pAb, AbClonal), Anti-Vinculin (1:2000, Rabbit mAb, Cell Signaling Technology), Anti-GAPDH (1:1000, Mouse mAb, Proteintech). Antibodies used for secondary immunodetection: Goat anti-Rabbit IRDye 680RD, Donkey anti-Mouse IRDye 800CW (1:15000 each, LI-COR). Membranes were imaged with Odyssey Fc imaging system (LI-COR). Densitometric quantifications were obtained and statistical analysis was performed using LI-LOR Image Studio and GraphPad Prism respectively.

Cell Viability, Proliferation and LDH Release Assay

$1x10^4$ MDA-MB-231 cells were seeded on 96-well plates and allowed to attach overnight. Cells were then treated with peptides for 48 hours. MTS Assay Kit (Abcam) was used in accordance with the manufacturer's instructions. Absorbance was measured at 490 nm using a BioTek Synergy 2 plate reader and Gen5 software.

Alternatively, MDA-MB-231 cells were seeded on 12-well plates and allowed to attach overnight. Cells were then treated with peptides for up to 24 hours. Supernatant medium from each well was carefully harvested along with the lysis and background control samples. LDH release quantification and assessment was performed according to the instructions provided in the LDH-Cytotoxicity Assay Kit (Fluorometric, Abcam ab197004). BioTek Synergy 2 plate reader and Gen5 software were used to collect fluorometric data. Data analysis was performed using GraphPad Prism.

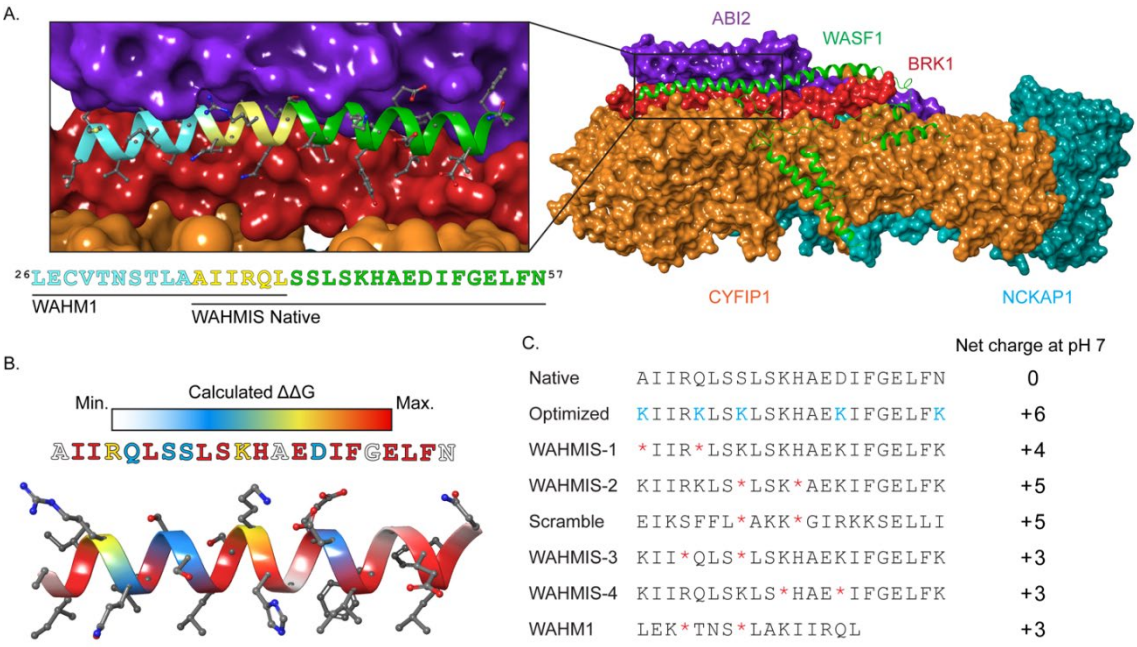

Figure 4.1 Rationale and design of WASF mimetic stapled peptides (A) Crystal structure of the WASF Regulatory Complex (WRC) with CYFIP1 (orange), NCKAP1 (cyan), ABI2 (purple) and BRK1 (red) in surface view and WASF1 (green) in ribbon representation (PDB ID: 3P8C). The insert shows the WASF3 segment corresponding to the prior lead peptide WAHM1 (cyan, yellow) as well as the segment identified by Rosetta PeptiDerive based on its predicted energetic contribution to binding, WAHMIS native (yellow, green). (B) Heatmap displaying the binding energy contribution of individual residues within the WASF3-derived peptide as determined by *in silico* alanine scanning using Rosetta. (C) The information yielded from the structural WASF3 model and *in silico* alanine scan were used to design a library of stapled peptides by placing synthetic olefinic amino acid residues (*) at *i, i+4* positions and lysine substitutions (K) to achieve a net positive charge at positions that were not predicted to contribute to the protein-binding interface. Peptide net charges were calculated using PepCalc.

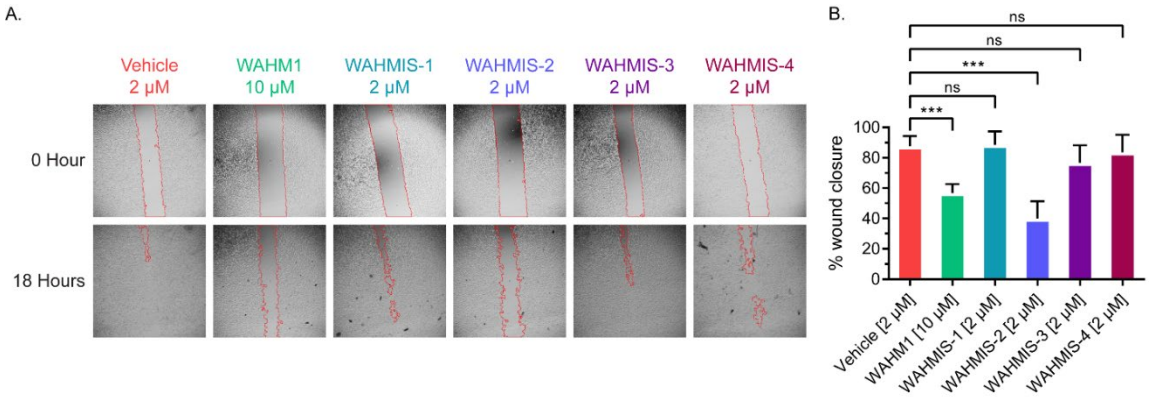

Figure 4.2 WAHMIS-2 reduces cell motility (A) Representative images of wound healing assays (n=3) performed with MDA-MB-231 cells in the presence of WAHMIS1-4, WAHM1 or DMSO. The wound area is marked by red lines generated using the MRI Wound Healing Tool for ImageJ. (B) Quantification of cell motility as measured by percent wound healing over an 18-hour time period across at least three independent wound healing assays. Wound area was calculated using MRI Wound Healing Tool for ImageJ. *** $p < 0.01$; n.s., not significant, as assessed by one-way ANOVA and Bonferroni's multiple comparisons test. Error bars represent standard deviation.

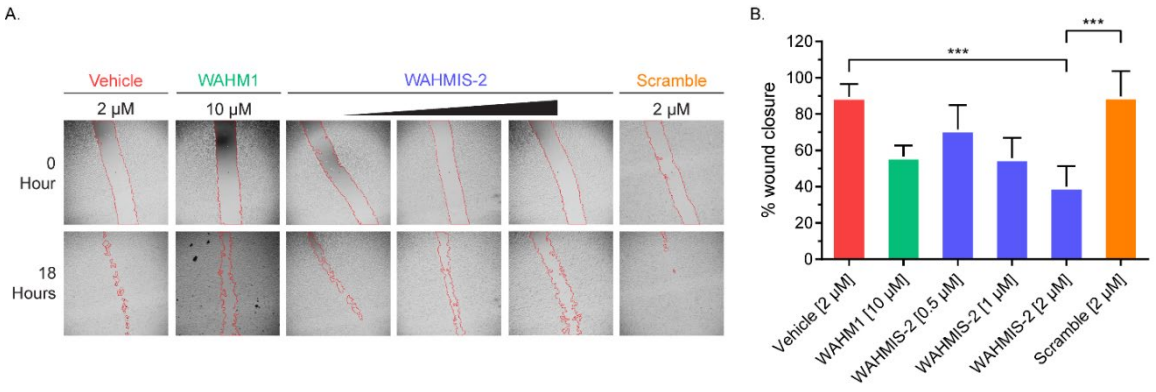

Figure 4.3 WAHMIS-2 reduces cell motility in a dose-dependent manner (A) Representative images of wound healing assays (n=3) performed over a concentration range of WAHMIS-2 (0.5, 1 or 2 µM), its scramble control, WAHM1 or DMSO. The wound area is marked by red lines generated using MRI Wound Healing Tool for ImageJ. (B) Quantification of cell motility as measured by percent wound healing over an 18-hour time period across at least three independent wound healing assays. WAHMIS-2-treated cells show a statistically significant, dose-dependent reduction in wound healing. Wound area was calculated using MRI Wound Healing Tool for ImageJ. *** $p < 0.01$ as assessed by one-way ANOVA and Bonferroni's multiple comparisons test. Error bars represent standard deviation.

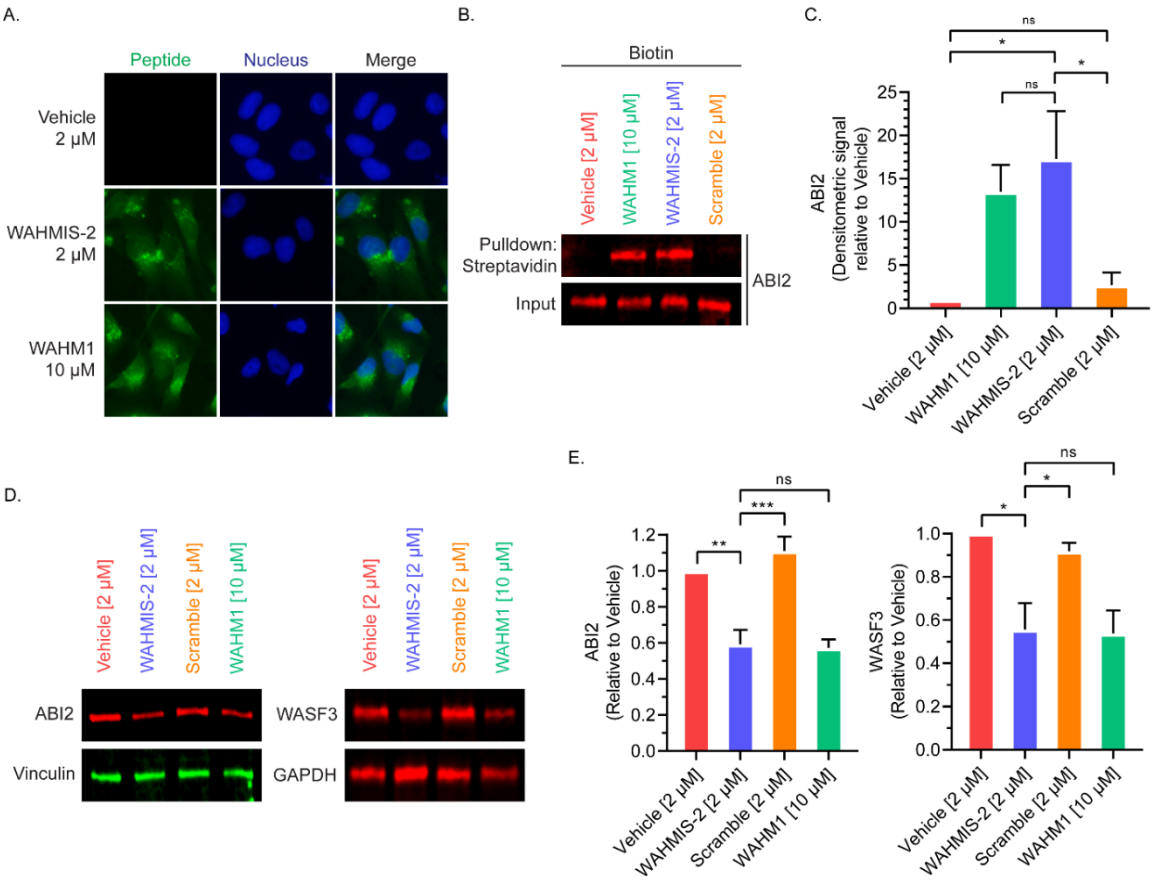

Figure 4.4 WAHMIS-2 permeates cells, binds to ABI2, and reduces WRC protein levels (A) Fluorescence microscopy images of cells treated with fluorescein-labeled version of the indicated peptides for four hours (n=4). WAHMIS-2 demonstrates cytoplasmic fluorescence that is comparable to WAHM1 despite being added to cells at a lower dosage. (B) Representative western blot (n=4) demonstrating that WAHMIS-2, but not the scramble control, binds its target, ABI2. Cell lysates were treated with biotin-labeled peptides for four hours followed by streptavidin pulldowns and detection of ABI2 by immunoblotting. (C) Densitometric quantification of four independent pulldown assays using LI-COR Image Studio showing WAHMIS-2 binds to ABI2 while the scramble control does not. * $p < 0.05$; n.s., not significant, as assessed by one-way ANOVA and Bonferroni's multiple comparisons test. Error bars represent standard deviation. (D) Representative western blot of cells treated with the indicated peptides for 72 hours (n=3). WAHMIS-2- and WAHM1-treated cells show reduced protein levels of ABI2 and WASF3. (E) Densitometric quantification of three independent western blots demonstrate a statistically significant reduction in ABI2 and WASF3 protein levels in WAHMIS-2- and WAHM1-treated cells. Quantification was performed using LI-COR Image Studio. * $p < 0.05$; ** $p < 0.01$; *** $p < 0.001$; ns, not significant as assessed by one-way ANOVA and Bonferroni's multiple comparisons test. Error bars represent standard deviation.

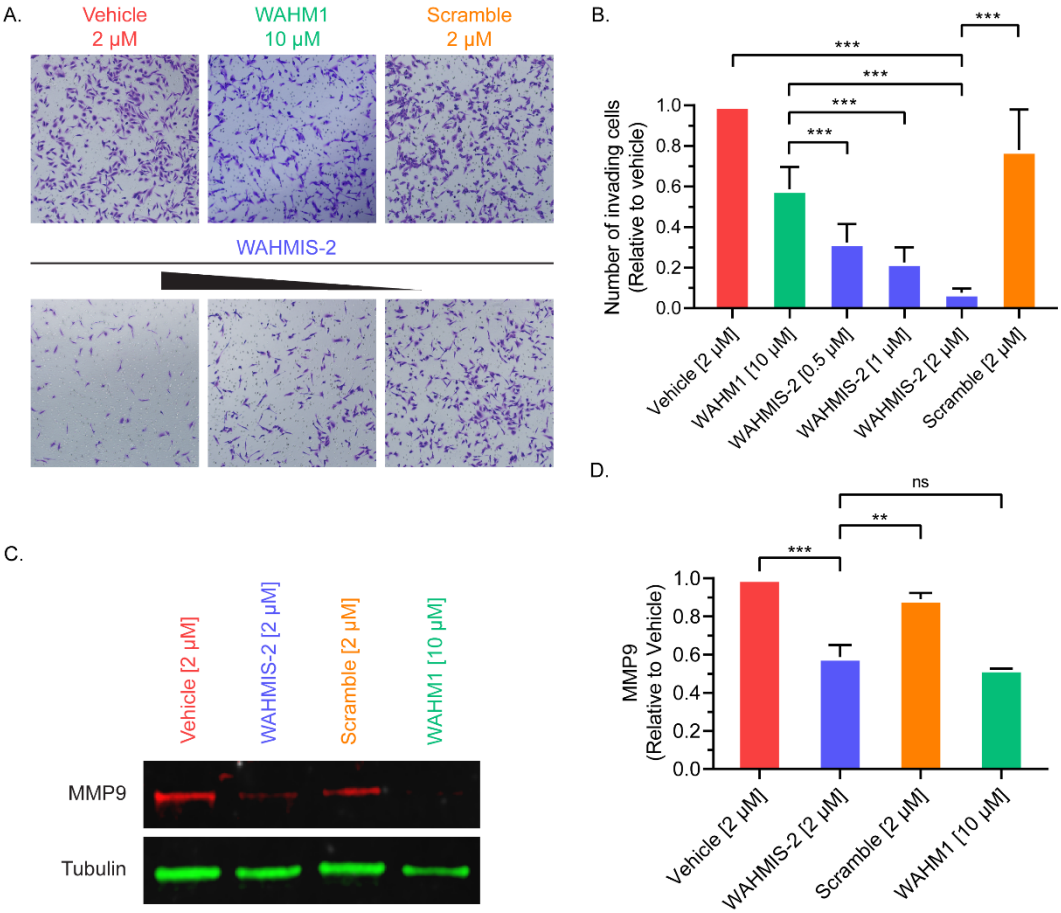

Figure 4.5 WAHMIS-2 suppresses cell invasion in a dose dependent manner and reduces MMP9 expression (A) Representative images from Matrigel invasion assays (n=4) of cells treated with a concentration range of WAHMIS-2 (0.5-2 μM), its scramble control, WAHM1 (10 μM) or DMSO. Invading cells were fixed using paraformaldehyde and stained with crystal violet for imaging and quantification. (B) Invading cells were quantified from at least three independent Matrigel invasion assays as measured using ImageJ. *** $p < 0.01$ as assessed by one-way ANOVA and Bonferroni's multiple comparisons test. Error bars represent standard deviation. (C) Representative western blot from MDA-MB-231 cells treated with indicated peptides for 72 hours (n=3). WAHMIS-2- and WAHM1-treated cells show reduced levels of MMP9 expression. (D) Densitometric quantification of three independent western blots indicated a significant reduction in MMP9 protein levels in WAHMIS-2 and WAHM1 treated cells. Quantification was performed using LI-COR Image Studio. ** $p < 0.01$; *** $p < 0.001$; n.s., not significant, as assessed by one-way ANOVA and Bonferroni's multiple comparisons test. Error bars represent standard deviation.

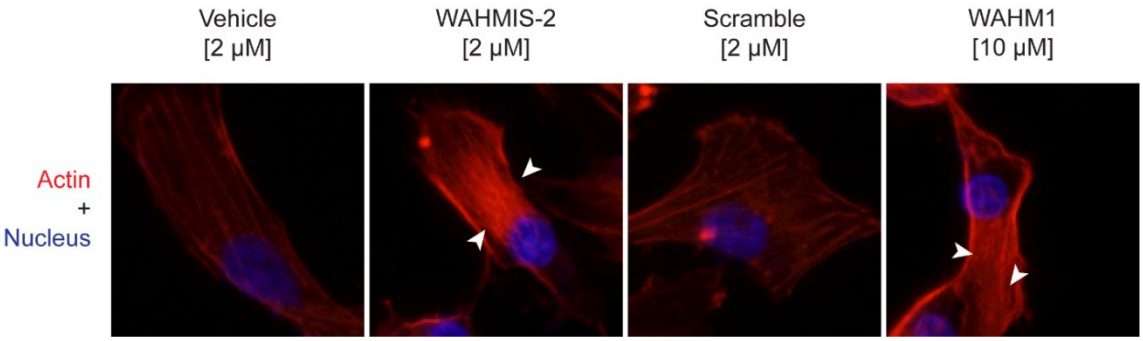

Figure 4.6 WAHMIS-2 treatment increases the density of actin stress fibers Representative fluorescence images of cells treated with indicated biotin labelled peptides for four hours followed by fixation, permeabilization and staining with phalloidin-iFluor 594 (n=4). Cells treated with WAHMIS-2 and WAHM1 display dense bundles of actin stress fibers (white arrows) while vehicle and scramble control do not.

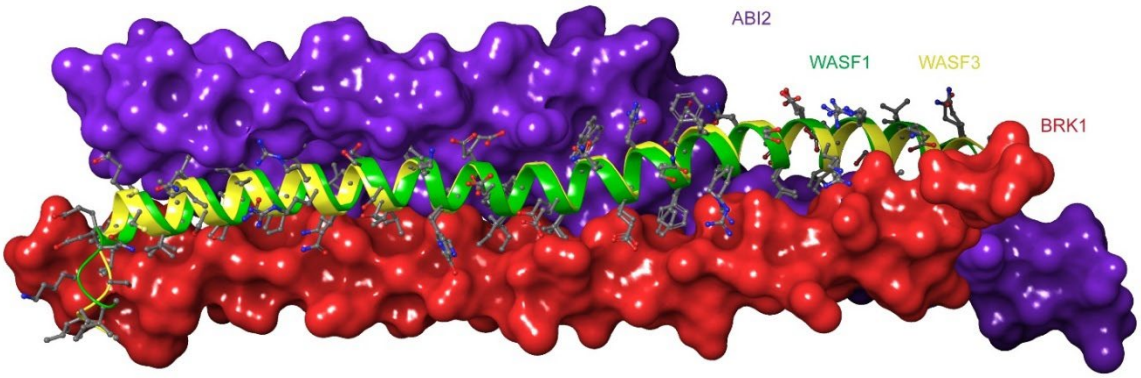

Figure S4.1 Homology model of WASF3 used for peptide design. Representative homology model of WASF3 based on the crystal structure (PDB ID: 3P8C) of WASF1 bound to the WRC. Shown here is the trimeric bundle of WASF1/3-ABI2-BRK1. Helical WASF Homology Domain of WASF3 (yellow) modelled after WASF1 (green) bound to ABI2 (purple, surface view) and BRK1 (red, surface view).

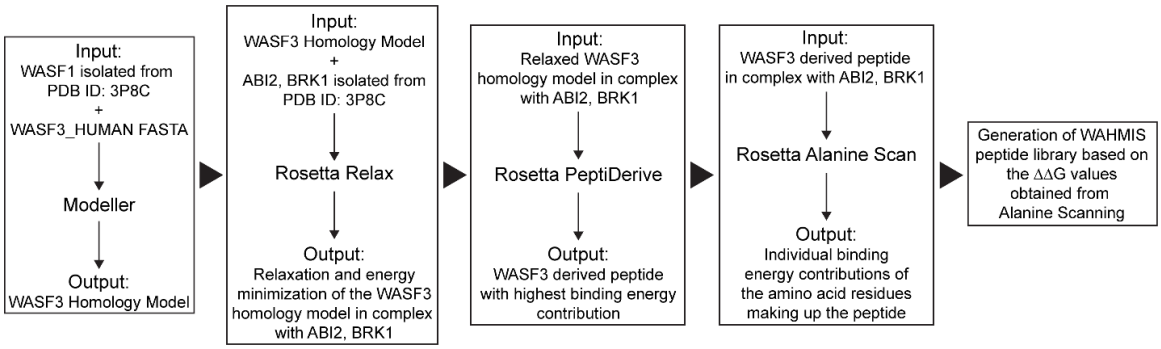

Figure S4.2 Schematic representation of the development of the WAHMIS peptide library. Optimization scheme utilized in the design and development of the WASF3 mimetic, WAHM *In-Silico* (WAHMIS) peptides.

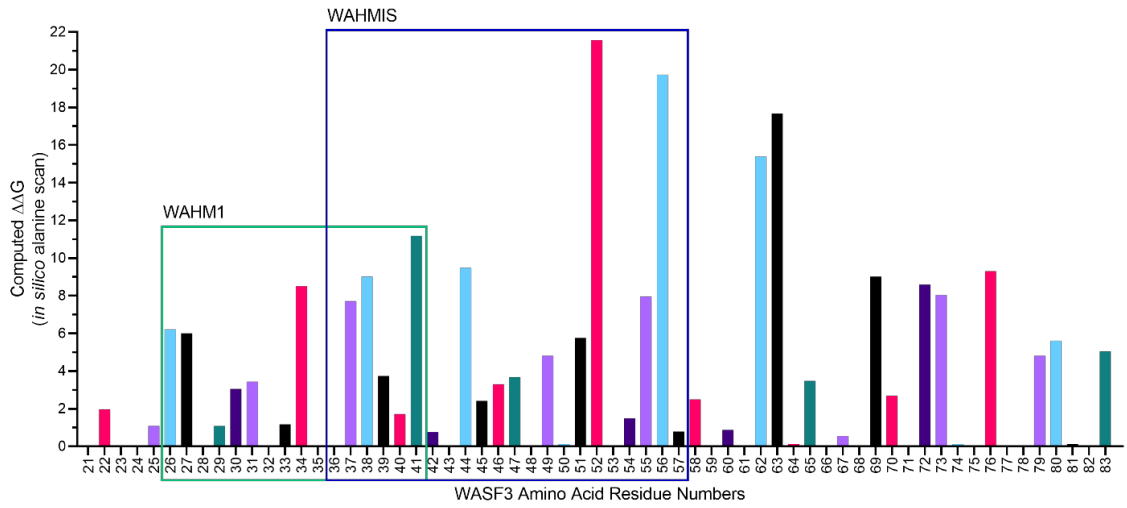

Figure S4.3 Computed ΔΔG values for WASF3 from *in silico* alanine scanning. Graphical representation of computed ΔΔG values for individual amino acid residues on WASF3 obtained via *in silico* alanine scan indicating their binding energy contributions to WASF3-ABI2-BRK1 complex. Green and blue boxes contain the residues making up WAHM1 and WAHMIS peptides respectively.

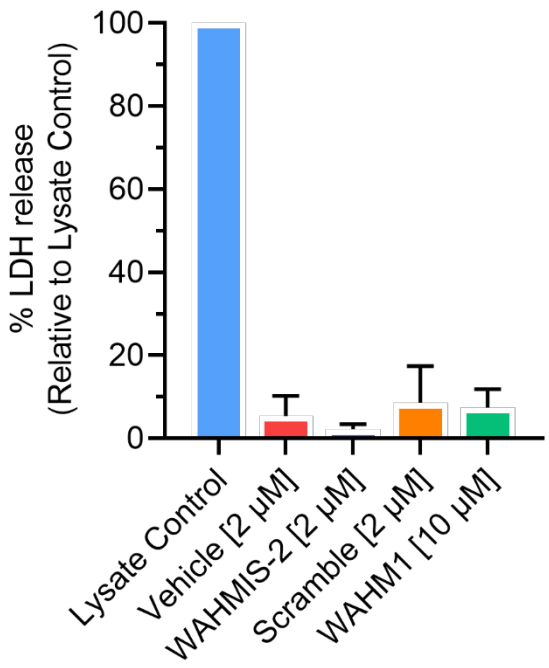

Figure S4.4 Stapled WASF3 mimetic peptides do not cause membrane lysis. MDA-MB-231 cells were treated with 2 µM WAHMIS-2, Scramble, DMSO or 10 µM WAHM1 for 24 hours. LDH release assays (n=3) were carried out to calculate % LDH release in accordance with the kit.

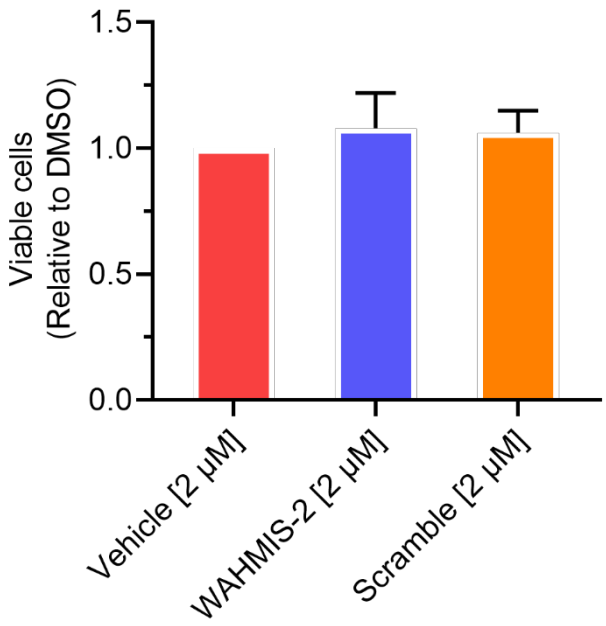

Figure S4.5 WAHMIS-2 does not reduce cell viability and proliferation. MDA-MB-231 cells were treated with 2 µM WAHMIS-2, Scramble or DMSO. Number of viable cells was estimated by measuring the absorbance of MTS tetrazolium compound at 490 nm (n=3).

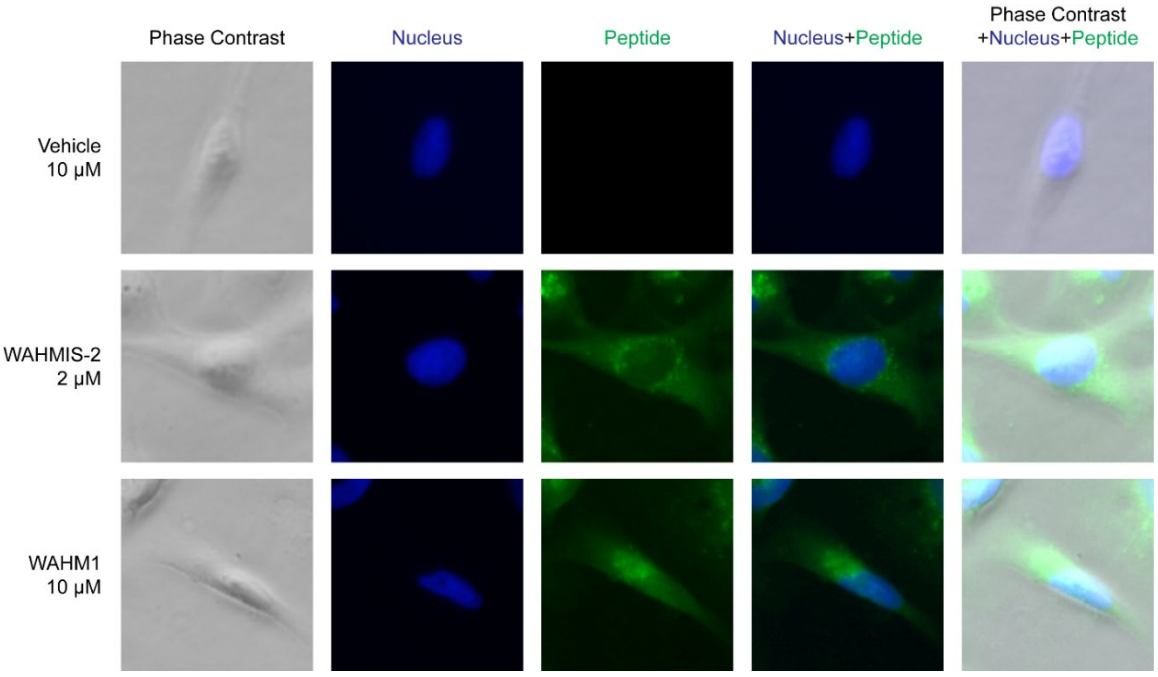

Figure S4.6 WAHMIS-2 permeates cells and is primarily cytosolic. Representative fluorescence microscopy images (n=4) of MDA-MB-231 cells treated with 2 μM WAHMIS-2, 10 μM WAHM1 or vehicle (DMSO) for four hours. Channel overlays demonstrate increased uptake of WAHMIS-2 as compared to WAHM1 and the overall peptide distribution throughout the cytoplasm.

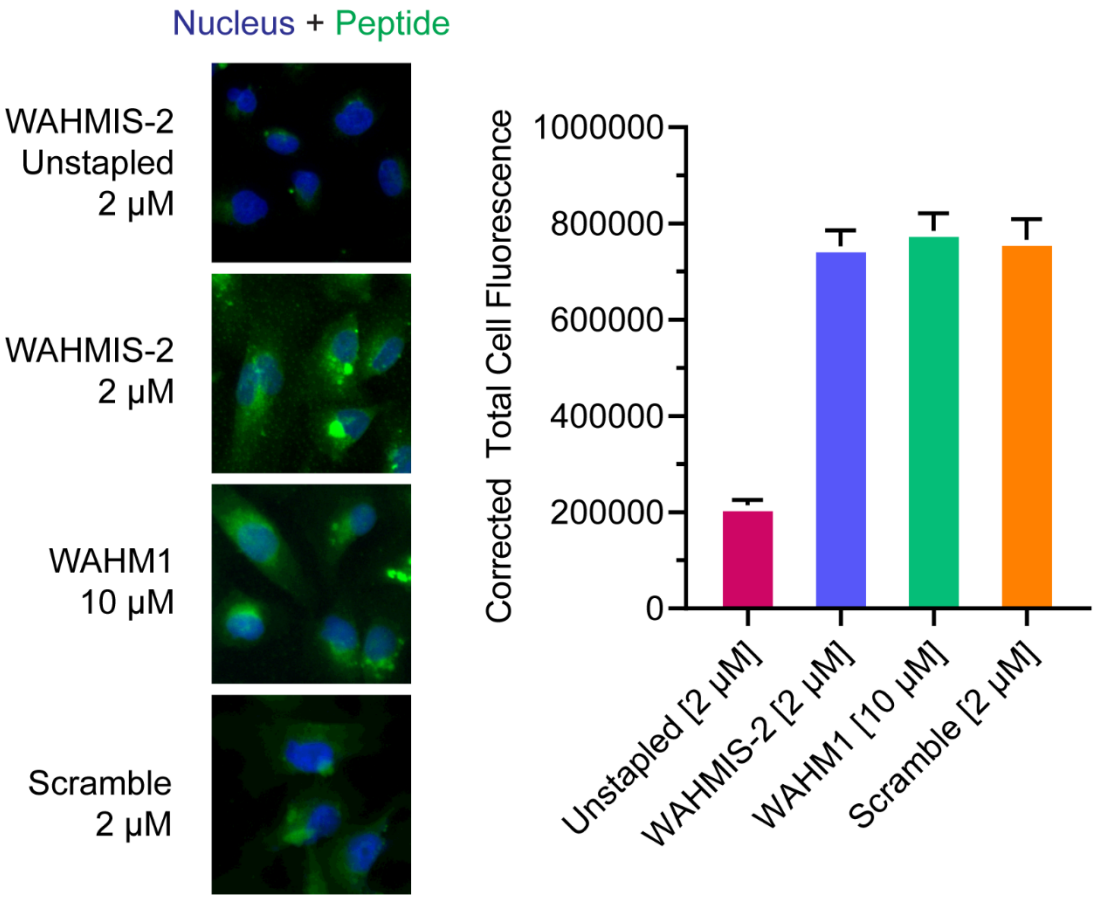

Figure S4.7 Unstapled WAHMIS-2 demonstrates poor cellular uptake. Representative fluorescence microscopy images (n=4) of MDA-MB-231 cells treated with 2 μM unstapled WAHMIS-2, WAHMIS-2, Scramble or 10 μM WAHM1 for four hours. Channel overlays and fluorescence quantification (n=400) show increased uptake of WAHMIS-2 and as compared to its unstapled counterpart and the overall peptide distribution throughout the cytoplasm.

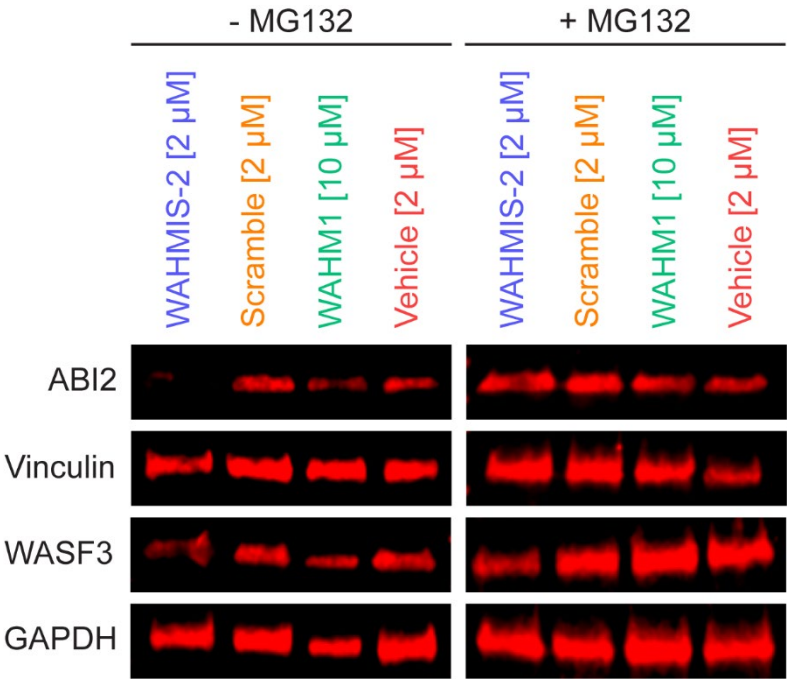

Figure S4.8 MG132 treatment rescues WASF3 and ABI2 degradation. Representative western blot of cells treated with the indicated peptides for 72 hours (n=3). WHAMIS-2- and WAHM1-treated cells show reduced protein levels of ABI2 and WASF3 which is rescued by MG132 treatment for 8 hours prior to lysis.

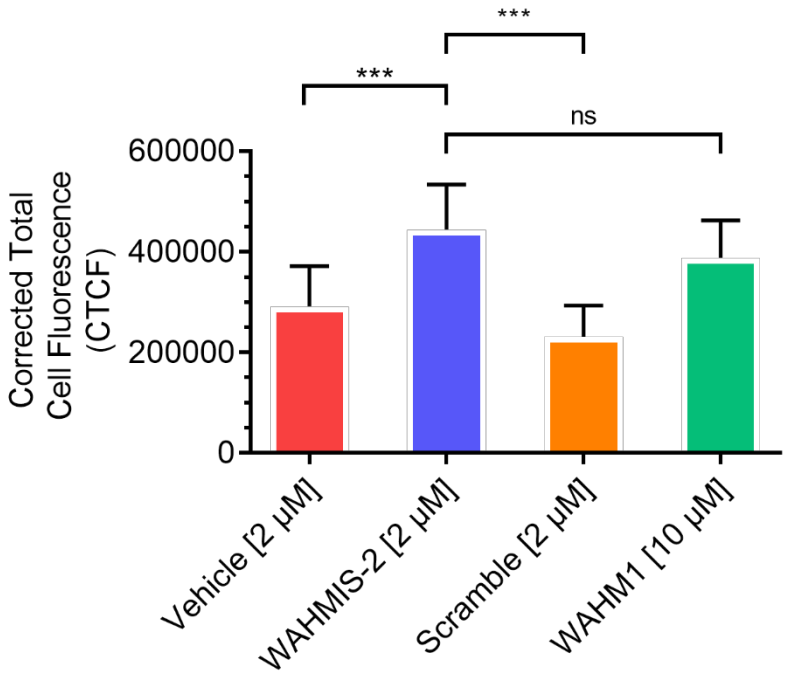

Figure S4.9 WAHMIS-2 treatment leads to increased actin stress fiber formation. Quantification of actin stress fibers in cells treated with 2 µM WAHMIS-2 or scramble control, 10 µM WAHM1 or vehicle (DMSO) for four hours, visualized by phalloidin-iFlour594 staining. Corrected Total Cell Fluorescence (CTCF) measured using ImageJ. *** $p<0.01$ by one-way ANOVA and Bonferroni's multiple comparisons test. Error bars standard deviation.

CHAPTER 5

RATIONALLY DESIGNED BRK1 MIMETIC STAPLED PEPTIDES TO TARGET WASF REGULATORY COMPLEX IN BREAST CANCER[7]

[7] Limaye, Ameya. To be submitted to ACS Chemical Biology, 2023

5.1 Abstract

Distant metastasis remains the most lethal aspect of the majority of cancers. There remains a need for therapies that target pathways involved in driving cancer cell motility, invasiveness, and eventual metastasis. Studies focused on elucidating molecular pathways involved in cancer metastasis have revealed the actin nucleating WASF regulatory complex (WRC) as a driver of malignant cell motility. The WASF regulatory complex is a hetero-pentameric protein complex composed of CYFIP1/2, NCKAP1/1L, WASF1/2/3, ABI1/2/3 and BRK1.

Of the five components, WASF3 expression has been shown to be directly associated with increased invasiveness and metastatic potential in breast cancer cells along with poor patient prognosis. We have previously reported the development of stapled peptides aimed at targeting WASF3. Stapled peptides have also been developed to target CYFIP-NCKAP interaction. Here, we explore the rational design and development of BRK1 mimetic stapled peptides. BRK1 is the smallest, most conserved component of the WRC. It is also, perhaps the most understudied member of the WRC. However, several reports have uncovered a potential role for BRK1 in nucleating the WRC as well as driving cell proliferation, invasiveness, and metastasis. Given the extent of binding interactions BRK1 forms with WASF and ABI as well as its linchpin like positioning within the WRC makes it a tantalizing target.

Through a combination of structure-based design, homology modeling and *in silico* optimization we have identified a region of BRK1 that contributes a significant amount of binding energy to the BRK1-WASF-ABI trimeric bundle. We developed two all-hydrocarbon stapled peptides that are cell permeable and reduce cell motility at low

micromolar concentrations. These peptides further the progress made in terms of targeting the WRC in cancer metastasis using stapled peptides. Given the rather privileged position of BRK1 among the WRC members these peptides may also be used for the development of Proteolysis Targeting Chimeric (PROTAC) compounds for targeted degradation of the WRC members, WASF in particular.

5.2 Introduction, Results and Discussion

BRK1 may be the least characterized member of the WRC. Being rather small, only about 80 amino acid residues in length, it's the only WRC member for which no paralogous genes have been identified and is also the most conserved member of the WRC across all species [188]. Although BRK1 was first identified as Brick1 in maize [194] it is also referred to HSPC300, however, this refers to a specific human cDNA in which the stop codon has been deleted resulting in an elongated protein product [188]. BRK1 is required for cell proliferation, migration, and metastasis of tumor cells [195]. Cellular pools of free BRK1 maintained as homo-trimers are essential precursors for assembly of the WRC [188] as well as the stability of the complex. It is found to be upregulated in NSCLC [196] and associated with metastatic potential of same [197]. Another moniker initially used for human BRK1 was C3orf10 referring to the BRK1 locus on chromosome 3, which is adjacent to the Von Hippel-Lindau (VHL) gene. Loss of VHL gene predisposes patients to tumor formation, however recent correlative studies have shown that patients who lose both VHL and BRK1 gene are in fact protected from these tumors and have better prognosis, thus highlighting the potential role for BRK1 in the development of malignancies [195].

We have previously designed and developed stapled peptides that target various interfaces of the WRC: WASF3 mimetic WAHM and WAHMIS, NCKAP mimetic WANT peptides [128, 130, 198]. Given that BRK1 forms an extensive binding interface with WASF and ABI as well as its conserved nature, we sought to investigate if we could develop BRK1 mimetic stapled peptides to disrupt WRC.

In the previously resolved crystal structure for WRC (PDB ID: 3P8C), BRK1 can be seen to form a biding interface across the entire length of the trimeric helical bundle formed by the WASF Homology Domain of WASF1 and ABI2 (Fig. 5.1A). BRK1 also forms binding interactions with CYFIP1 through residues located at its N- and C-terminal ends. Posterior view of the crystal structure demonstrates the overall buried position of BRK1 within the WRC.

We started the peptide design process by first developing a homology model for BRK1 in complex with WASF3 and ABI1, two members of the WRC that have been shown to drive metastatic potential in breast cancer cells [128, 130, 199-202]. We used BRK1-WASF1-ABI2 trimeric bundle isolated from the PDB file 3P8C as a template along with the FASTA sequences for WASF3 and ABI1 to generate a homology model using SWISS-MODEL [203] (Fig. 5.1B). This homology model was then used as an input for the Bristol University Docking Engine (BUDE) alanine scan web server [204, 205]. With the alanine scanning data, we identified an N-terminal region of BRK1 composed of regularly interspaced hydrophobic residues with substantial $\Delta\Delta G$ values. Structural analysis revealed this region of BRK1 to complementary to the region of WASF3 that served as a template for the original WAHM and WAHMIS peptides. Residues 21-40 of BRK1 were found to be essential for the binding interaction and were used as a template for peptide design. C-

terminal region of BRK1 also contains a stretch of amino acid residues with notable ΔΔG values. Structurally, these residues constitute BRK1's binding interface with WASF3 and ABI1. A stretch of amino acid residues between 46 and 65 of BRK1 was also selected for peptide design (Fig. 5.2A). Through lysine (K) point substitutions to improve the net charge and placement of ((S)-2-(4′-pentenyl)alanine, S5) at *i*, *i*+4 positions, two stapled peptides were generated, dubbed B21S and B46S respectively (Fig. 5.2B).

Both of these BRK derived peptides were screened for their ability to suppress cell motility in wound healing assays with MDA-MB-231 triple negative breast cancer cells. At 10 μM concentration, B46S had no effect on cell motility, whereas B21S showed an average of ~45% reduction when compared to the vehicle (DMSO) control. B21S was on par with the first generation WASF mimetic peptide WAHM1 in terms of overall reduction in wound healing at equal concentrations (Fig. 5.3A). Peptide uptake assays performed with MDA-MB-231 cells demonstrated a significant difference between B21S and B46S. At four-hour time point, cells treated with 10 μM 5(6)-carboxyfluorescein labeled B21S showed diffuse fluorescence throughout the cytoplasm. In contrast, cells treated with B46S showed very low levels of cytoplasmic fluorescence with notable fluorescent puncta (Fig. 5.3B).

With cell motility and uptake data combined, B21S was selected as the lead peptide. Although B21S demonstrated suppression in motility and cellular uptake on par with WAHM1, it lacked water solubility which potentially hindered its uptake and by extension, activity. Thus, we sought to further optimize the B21S peptide for improved solubility and uptake. Through the crystal structure and the homology model we identified two N-terminal and one C-terminal amino acid residues flanking the B21S native sequence. All

three of these residues are on the non-binding, solvent exposed surface of BRK1 and thus could be modified (Fig. 5.4A). Lysine (K) point substitutions were made at positions 20 and 41 to improve the net charge as well as the hydrophilicity of the native sequence. Two residues of ((S)-2-(4′-pentenyl)alanine, S5) were placed at *i*, *i*+4 positions to generate two stapled peptides named BASH1 and BASH2 for BRK1 Analogous Stapled Helix (BASH) [Initially dubbed B19S1 and B19S1 respectively] (Fig. 5.4B).

These newly designed, optimized peptides were screened for activity in wound healing assays using MDA-MB-231 cells. Both, BASH1 and BASH2 at 1 μM concentration demonstrated a significant degree of reduction in wound healing (~50% and ~63% respectively) compared to the vehicle (DMSO) treatment (Fig. 5.5A). Notably, the reduction in cell motility with BASH2 treatment was consistently higher than WAHMIS-2 despite the lower dosage (1 μM vs 2 μM). Next, we tested their cellular uptake using 5(6)-carboxyfluorescein labeled versions of BASH1 and BASH2. At four-hour time point, both BASH1 and BASH2 treated cells demonstrated diffuse fluorescence throughout the cytoplasm with some notable puncta. The overall uptake was found to be on par with the predecessor B21S and WAHMIS-2 despite the ten- and two-fold lower dosage concentration for the BASH peptides (Fig. 5.5B).

To further evaluate the effect of BASH2 treatment on cellular motility, invasiveness, and chemotaxis, we performed transwell invasion assays using MDA-MB-231 cells. Transwell inserts were coated with Matrigel basement membrane and RPMI-1640 cell medium supplemented with 10% fetal bovine serum was used as chemoattractant. Cells were treated with 10 μM WAHM1, 2 μM WAHMIS-2, 0.1-1 μM BASH2, 1 μM BASH2 SCR (BASH2 scramble control) or 10 μM DMSO. After 24 hours of incubation,

the number of invading cells under each treatment was assessed using confocal microscopy following fixation and crystal violet staining (Fig. 5.6A). Quantification revealed a dose dependent reduction in the number of invading cells with BASH2 treatment. Notably, 0.5 μM BASH2 treatment was on par with 10 μM WAHM1 and 2 μM WAHMIS-2 in terms of overall reduction in the number of invading cells relative to DMSO (Fig. 5.6B).

Since non-specific toxicity induced by cell membrane lysis remains a concern with positively charged stapled peptides, we assessed the potential toxicity of BASH2 using LDH release assays. MDA-MB-231 cells were treated with a range of concentrations (0.5, 1, 2, 4 μM) BASH2 along with WAHM1 (10 μM), WAHMIS-2 (2 μM) and vehicle (DMSO, 10 μM) for 24 hours. Supernatants were then analyzed for LDH release using fluorimetry. None of the tested concentrations for all peptides demonstrated a notable increase in normalized LDH to indicate cytotoxicity (Fig. 5.7).

Thus, the design and development of B21S, followed by its optimized versions, BASH1 and BASH2 hints at a potential for BRK1 mimetic stapled peptides as WRC disruptors. The reduction seen in cell motility and invasiveness with the BASH peptides, BASH2 in particular at a low micromolar concentration may be attributed to their enhanced cellular uptake but may also hint at the critical role played by BRK1 in the assembly and stability of the WRC. Further evaluation of these peptides via invasion assays in tandem with MMP9 expression and secretion may provide a more direct measure of their ability to suppress cell invasion and chemotaxis. Additionally, testing their effect on the WRC stability as measured by the degradation of its component proteins may further elucidate how BRK1 contributes towards the stability of the WRC. Measurement of effector proteins such as KISS1, ZEB1 and NFkB downstream of the WRC may also further elucidate the

effects of BASH2 on WRC signaling. The region of BRK1 encompassed by the BASH peptides almost exclusively interacts with WASF homology domain, combined with the fact that there are no known binding partners for BRK1 beyond the WRC component proteins, these BRK1 mimetic peptides could be used as warheads for PROTAC compounds aimed at targeted WASF degradation [206].

5.3 Methods

Homology Modeling, Alanine Scanning

WRC crystal structure (PDB ID: 3P8C) was retrieved from the RCSB Protein Data Bank. FASTA sequences for WASF3 and ABI1 were retrieved from Uniprot. BRK1-WASF1-ABI2 trimeric bundle was isolated from the crystal structure PDB file (3P8C). WASF1 and ABI2 protein chains were then isolated from the previous file and were used as templates along with WASF3 and ABI1 FASTA sequences for homology modeling using SWISS-MODEL. WASF3 and ABI1 homology model chains were then aligned back into the crystal structure with the isolated BRK1-WASF1-ABI2 trimeric bundle. Resulting structure file with BRK1 in complex with WASF3 and ABI1 was then used as an input for the BUDE Alanine Scan webserver. BRK1 was set as the ligand and WASF3, ABI1 were set as receptors. The output of the alanine scanning along with the structural information was then used to determine the placement of lysine (K) substitutions as well as staple placement.

Peptide Synthesis

Rink amide MBHA resin, N-α-Fmoc protected amino acids were purchased from Novabiochem (Merck Millipore). (S)-N-Fmoc-2-(4'-pentenyl)alanine and Grubb's catalyst (1st Generation) were purchased from Sigma-Aldrich. All other reagents and organic solvents were purchased from Fisher Scientific unless specified otherwise. Solvents used in this synthesis were HPLC grade.

All peptides used in this study were synthesized using standard Fmoc (fluorenylmethoxycarbonyl) protected solid phase peptide synthesis. Rink amide MBHA resin was equilibrated in NMP (1-methyl-2-pyrrolidinone). Fmoc protection group was deprotected using 25% v/v solution of piperidine in NMP for 30 minutes. Deprotection was followed by three washes with NMP. Amino acids were coupled by adding 10 equivalents of Fmoc-protected amino acid (0.25 M final concentration) in NMP to the deprotected resin along with HCTU [O-(1H-6-Chlorobenzotriazole-1-yl)-1,1,3,3-tetramethyluronium hexafluorophosphate] in NMP (0.24 M final concentration) and 8% v/v DIEA (N, N-Diisopropylethylamine). Amino acid coupling was carried out for 45 minutes followed by three washes with NMP. Deprotection and coupling steps were repeated sequentially for the remaining amino acid residues. Two residues of olefinic amino acid 'S5' [Fmoc-(S)-2-(4-pentenyl)alanine] were incorporated during synthesis at predetermined positions using standard coupling conditions. Olefin metathesis/ring closing metathesis was performed on Fmoc-protected, resin bound peptide using 0.4 equivalents of Grubb's first-generation catalyst [Benzylidene-bis(tricyclohexylphosphine)dichlororuthenium] in DCE (1,2-dichloroethane) for 1 hour, performed twice to ensure completion of staple formation. Addition of PEG3 [Fmoc-NH-PEG(3)-COOH] as a flexible N-terminal linker was performed under standard coupling conditions similar to amino acid couplings. Peptides

were labeled with fluorescein or biotin at the N-terminal end following PEG3. For fluorescein labeling, deprotected, resin bound peptides were agitated overnight with 2 equivalents of 5(6)-carboxyfluorescein, 0.046 M HCTU and 2% v/v DIEA in DMF (N, N-Dimethylformamide). Biotin labeling was performed overnight with 10 equivalents of D-biotin, 0.14 M HCTU and 4% v/v DIEA in a 1:1 mixture of DMF and DMSO (dimethyl sulfoxide). Peptides were cleaved from resin in a cleavage cocktail of 95% TFA (trifluoroacetic acid), 2.5% water and 2.5% TIS (triisopropylsilane) for four hours. Products were then precipitated in ice cold MTBE (methyl-tert-butyl ether) and allowed to air dry. Crude products were dissolved in equal parts water and methanol and purified using high performance liquid chromatography. Product peptides were verified with ESI (electrospray ionization) mass spectroscopy. Fluorescein labeled peptides were quantified by measuring their absorbance at 495 nm. Biotin labeled peptides were quantified by measuring diminished absorbance of HABA [2-(4'-hydroxybenzeneazo)benzoic acid]-avidin complex at 500 nm. Purified, dry peptides were dissolved in DMSO to achieve 10 mM stocks. Peptide stocks were stored at 4°C, protected from light.

Cell culture

MDA-MB-231 cells were obtained from ATCC. Cell culture medium, RPMI-1640 and trypsin were purchased from Corning (Cellgro). Fetal bovine serum (FBS) was purchased from HyClone (Cytiva).

Cells were maintained in RPMI-1640 supplemented with 10% FBS and 1% Penicillin-Streptomycin at 37°C with 5% CO_2. Cells were passaged at least twice before being used

in any experiment and all experiments were performed in at least triplicate at different passage numbers.

Motility Assay

MDA-MB-231 cells were grown to confluency in 24 well plates and serum starved for 24 hours in 2% FBS RPMI-1640. A wound area was created by dragging a 20-200 μL pipette tip vertically down each well and debris was removed by washing each well three times with serum free RPMI-1640. Following this, initial images were acquired using an Olympus IX71 inverted microscope. Peptides were diluted to desired final concentrations in 5% FBS RPMI-1640 and cells treated for 18 hours or until the control wound area had healed to 95% and above. Wound area prior to and following treatment was measured using the MRI wound healing tool for the ImageJ software suite. Data was analyzed using GraphPad Prism.

Invasion Assay

Matrigel basement membrane coating was applied to Transwell inserts as described in the Corning protocol and allowed to incubate for 30 minutes at 37°C. MDA-MB-231 cells were serum starved in 2% FBS RPMI-1640 for 24 hours and dissociated in 0.25% Trypsin followed by quenching in 10% FBS RPMI-1640. Cells were washed in serum free RPMI-1640 and counted using hemocytometer. ~20,000 cells per chamber were added along with peptide treatment in serum free RPMI-1640 while 10% FBS RPMI-1640 containing peptide treatment was added to the lower chamber as a chemoattractant. Following 24 hours of incubation, inner surfaces of Transwell inserts were swabbed out

and fixed in 2% paraformaldehyde in PBS for 10 minutes and stained using 2% crystal violet in methanol for 10 minutes. Inserts were washed by immersing in DI water and imaged using an Olympus IX71 inverted microscope. Invading cells were counted using the ImageJ software suite. Data analysis was carried out in GraphPad Prism.

LDH Release Assay

MDA-MB-231 cells were seeded on 12-well plates and allowed to attach overnight. Cells were then treated with peptides for up to 24 hours. Supernatant medium from each well was carefully harvested along with the lysis and background control samples. LDH release quantification and assessment was performed according to the instructions provided in the LDH-Cytotoxicity Assay Kit (Fluorometric, Abcam ab197004). BioTek Synergy 2 plate reader and Gen5 software were used to collect fluorometric data. Data analysis was performed using GraphPad Prism.

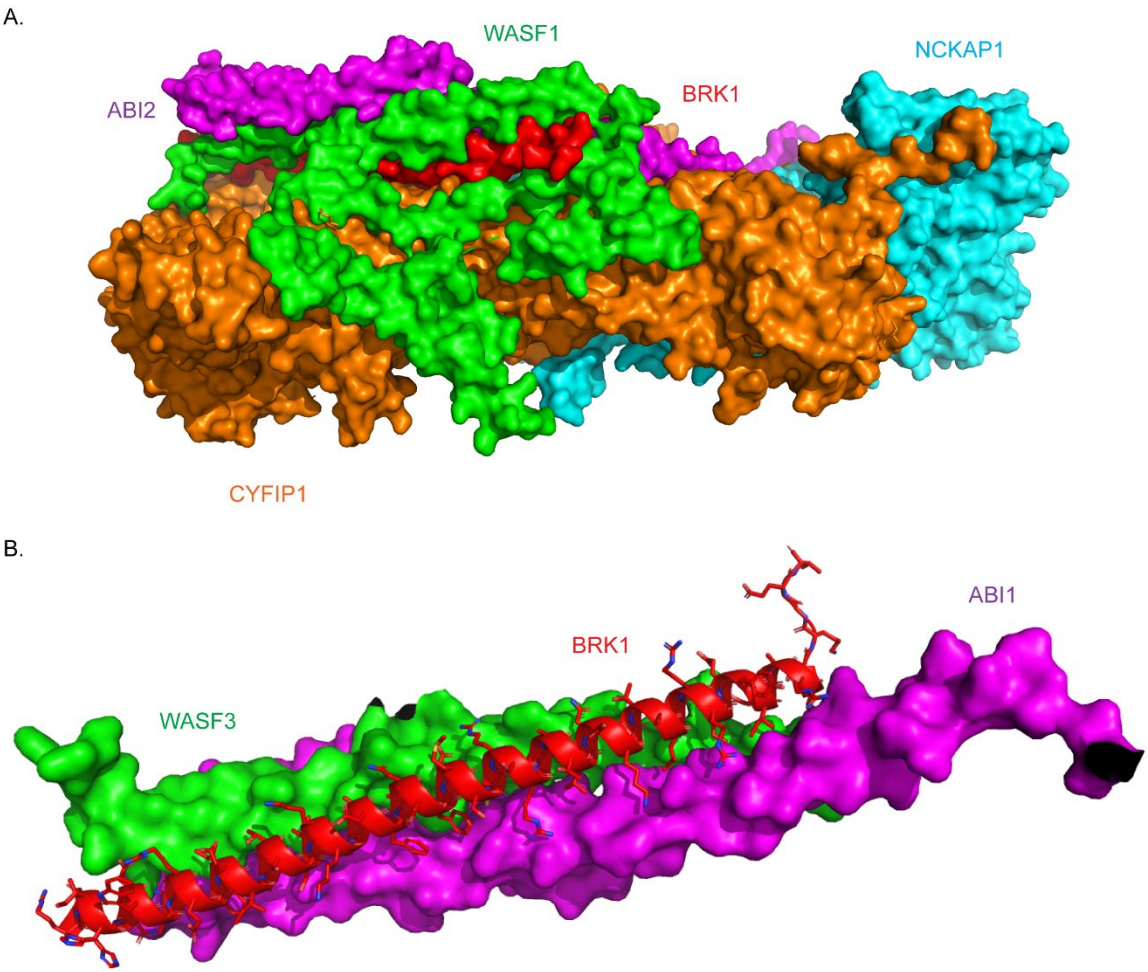

Figure 5.1 BRK1 forms binding interactions with WASF and ABI (A) Crystal structure (PDB ID: 3P8C) of the WASF Regulatory Complex (WRC) shows the deeply buried nature of BRK1 (surface view, red) within the complex. (B) Representative homology model of WASF3 and ABI1 based on the crystal structure (PDB ID: 3P8C) of WASF1 and ABI2 in complex with BRK1. Shown here is the trimeric bundle of WASF3-ABI1-BRK1. Helical WASF Homology Domain of WASF3 (surface view, green) modelled after WASF1 bound to ABI1 (surface view, purple) and BRK1 (surface view, red).

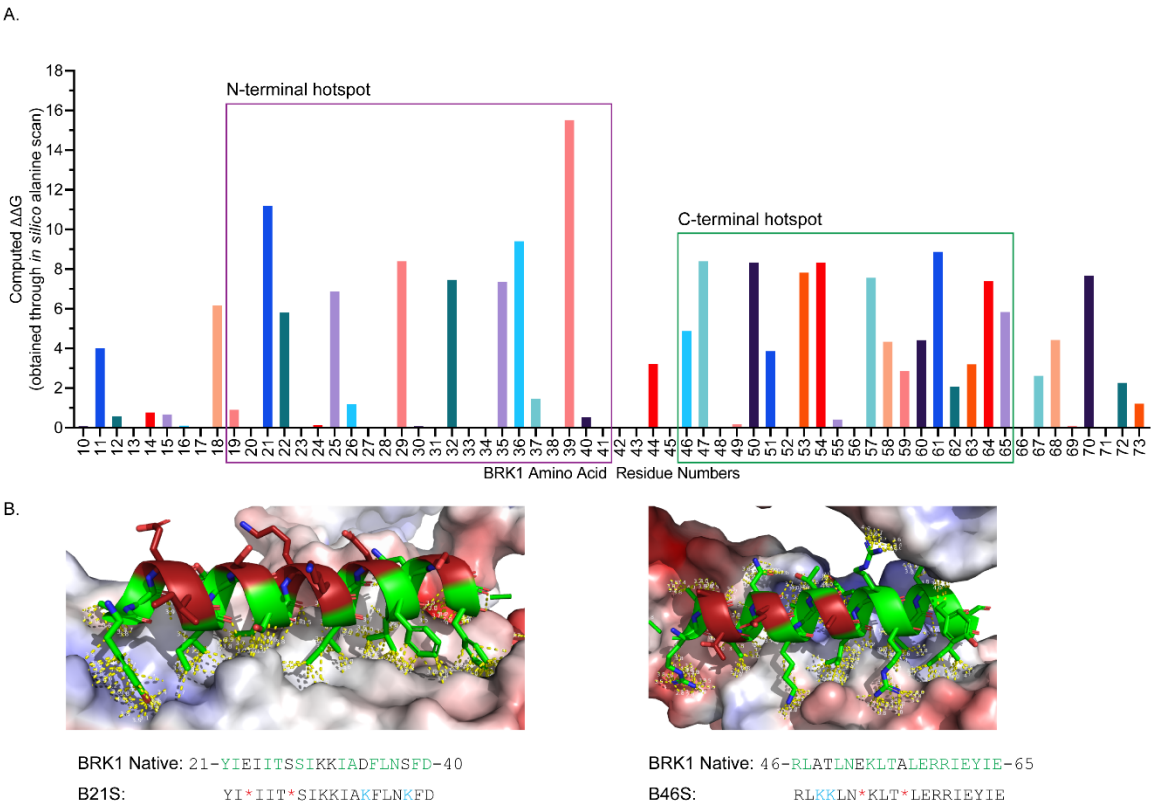

Figure 5.2 Identification of PPI hotspots on BRK1 and design of BRK1 mimetic peptides (A) Graphical representation of computed ΔΔG values for individual amino acid residues on BRK1 obtained via *in silico* alanine scan indicating their binding energy contributions to BRK1-WASF3-ABI1 complex. Purple and green boxes contain the residues making up the N-terminal and C-terminal hotspots. (B) Structural view of regions on BRK1 (cartoon and stick view) making up the N- and C-terminal hotspots (Residues 21-40 and 46-65 respectively). Interaction surface composed of WASF3 and ABI1 (surface view) is shown as electrostatic potential molecular surface (red for negative charge, blue for positive charge, white for uncharged, hydrophobic). Amino acid residues essential for binding are represented in green, lysine substitutions are in blue. * represent synthetic, olefinic amino acid residues.

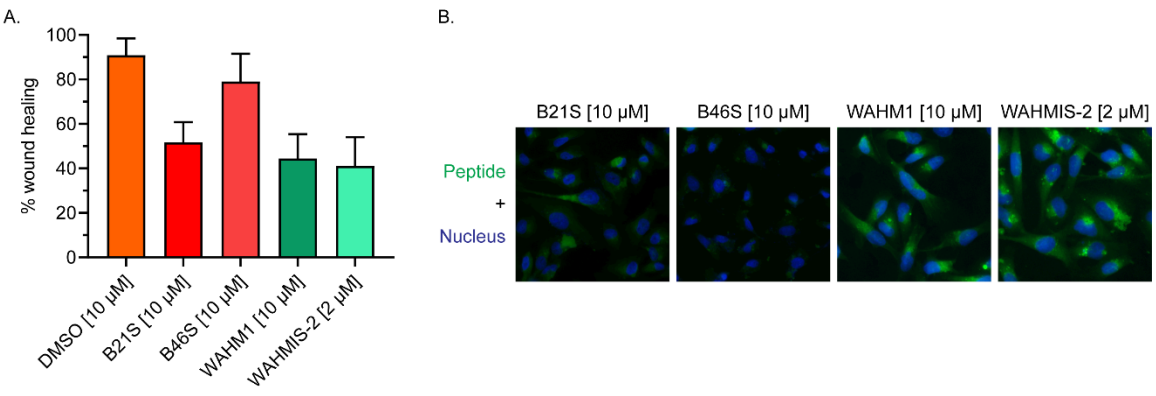

Figure 5.3 BRK1 mimetic stapled peptides suppress cell motility and permeate cells (A) Quantification of wound healing assays (n=3) shown as percent wound healing performed using MDA-MB-231 cells shows reduction in cell motility with B21S treatment that is on par with WAHM1. Wound area was calculated using MRI Wound Healing Tool for ImageJ. (B) Fluorescence microscopy images of MDA-MB-231 cells treated with fluorescein-labeled versions of the indicated peptides for four hours (n=3). Both, B21S and B46S treated cells demonstrate lower fluorescence intensity as compared to WAHM1 and WAHMIS-2 treated cells.

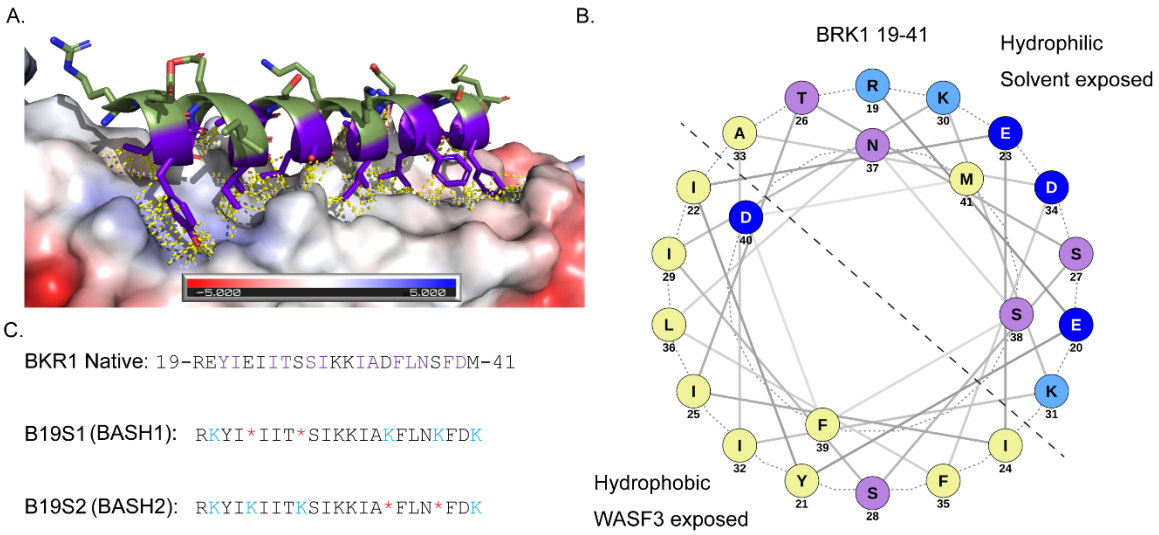

Figure 5.4 Design and development of the extended BRK1 mimetic stapled peptides (A) Structural view of BRK1 residues 19-41 (cartoon and sticks view) in complex with WASF3 (electrostatic gradient, surface view). BRK1 residues involved in the binding interaction are in purple, solvent exposed residues are in forest green. (B) Helical wheel representation of BRK1 19-41 denoting the amphipathic nature of the helix with basic residues in light blue, acidic residues in deep blue, polar residues in lilac and nonpolar residues in yellow. Helical wheel was generated using NetWheels. (C) The extended native BRK1 sequence was used to design two BRK1 mimetic stapled peptides. Amino acid resides essential for binding are shown in purple, lysine substitutions are shown in blue. Synthetic, olefinic amino acid residues are shown as *. These peptides were named BASH1/2 for BRK1 Analogous Stapled Helix, initially dubbed B19S1 and B19S2.

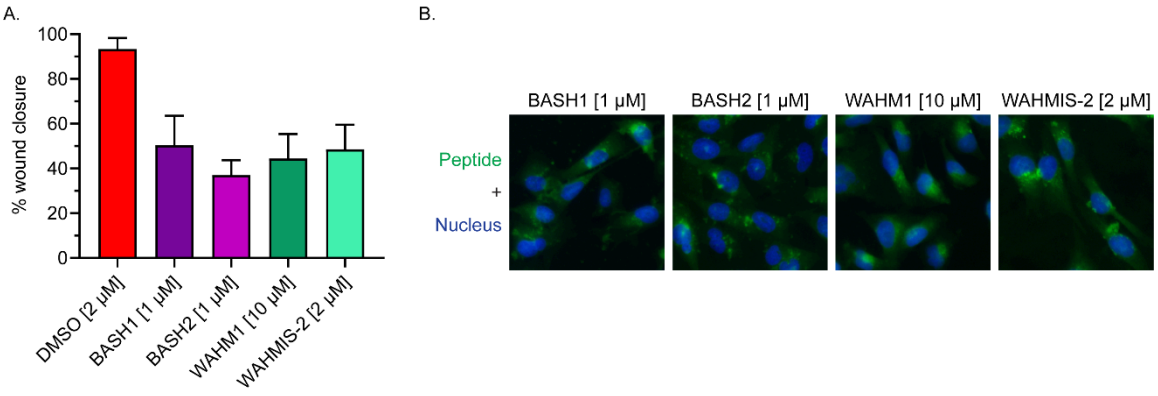

Figure 5.5 Optimized BASH peptides suppress cell motility and permeate cells (A) Quantification of wound healing assays (n=4) shown as percent wound healing performed using MDA-MB-231 cells shows reduction in cell motility with BASH2 treatment that is notably better than both WAHM1 and WAHMIS-2. Wound area was calculated using MRI Wound Healing Tool for ImageJ. (B) Fluorescence microscopy images of MDA-MB-231 cells treated with fluorescein-labeled versions of the indicated peptides for four hours (n=3) demonstrate the uptake of BASH peptides to be on par with WAHM1 and WAHMIS-2 despite significantly lower dosage concentrations.

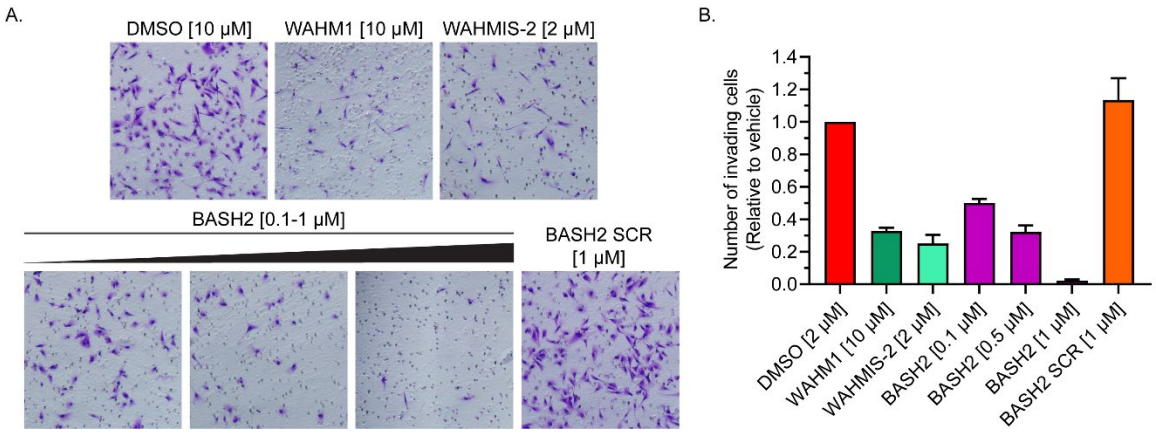

Figure 5.6 BASH2 suppresses cell invasion in a dose dependent manner (A) Representative images from Matrigel invasion assays of MDA-MB-231 cells treated with a concentration range of BASH2 (0.1-1 µM), its scramble control BASH2 SCR, WAHM1, WAHMIS-2 or DMSO. Invading cells were fixed using paraformaldehyde and stained with crystal violet for imaging and quantification. (B) Quantification of invading cells from three independent fields measured using ImageJ.

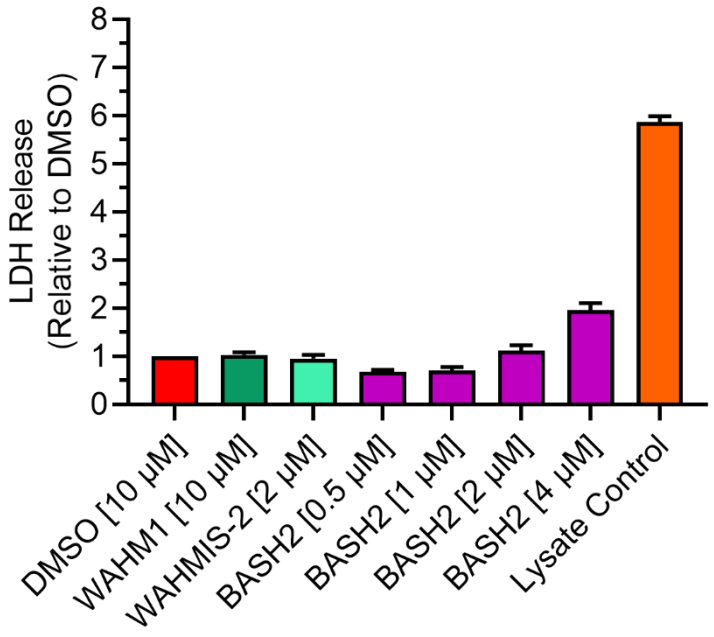

Figure 5.7 BASH2 does not induce membrane lysis and LDH release MDA-MB-231 cells were treated with increasing concentrations of BASH2, its scramble control BASH2 SCR, WAHM1, WAHMIS-2 or DMSO for 24 hours. LDH release assays were carried out to calculate LDH release in accordance with the kit.

CHAPTER 6

CONCLUSIONS

6.1 Summary of Results

In summary, the approach of using all-hydrocarbon stapled peptides to selectively target and modulate specific protein interactions has proven to be highly versatile and adaptable. This work reports the design and development of multiple stapled peptides designed for various purposes such as molecular tools, proof-of-concept probes, and potential therapeutics. Given that α helical interfaces make up for a majority of the PPI interfaces, stapled peptides are uniquely positioned to interrogate them through their synthetic stabilization of the α helical secondary structure [207].

Scaffolding of protein kinases by AKAPs and the formation of multivalent signalosomes has been long known to exert tight control on cellular signaling [208]. Peptides targeting AKAP-PKA scaffolding have previously been developed [162-164]. However, no such peptides had been developed to target AKAP-PKC scaffolding. Given how sensitive PKC signaling is to subcellular localization, we sought to develop stapled peptides and potential molecular tools to target AKAP scaffolding of PKC. These peptides, CSTAD5 and CSTAD6 present novel molecular tools that can be used to interrogate the spatiotemporal dynamics of PKC signaling. Combined with the previously reported AKAP-PKA disruptor STAD peptides, these novel CSTAD peptides can be used to dissect the intricacies of AKAP mediated kinase signaling [209].

The priming and maturation of PKC has long remained an elusive mechanism along with the role of mTORC2 in regulating the phosphorylation of PKC C-tail [167]. Recent collaborative research work established a new dogma for PKC maturation while also identifying a novel PKC dimerization motif that contains a previously unknown mTORC2 phosphorylation site. It also established nascent, dimeric PKC as the rate limiting step for mTORC2 mediated PKC processing. Given the overall interest in the development of mTOR inhibitors for various cancers combined with the emerging role of PKC as potential tumor suppressor, we sought to investigate if the extraneous disruption of nascent PKC dimers could serve to accelerate its maturation [133, 173-176]. Thus, two stapled PKC-DD peptides were designed. Both of the stapled peptides showed improved cell permeation over the native peptide and also upregulated PKC phosphorylation and maturation. These peptides demonstrated that the PKC dimerization interface is actionable and can be potentially targeted to potentiate mTOR inhibition [89].

As metastatic cancer remains a major therapeutic challenge, research has gone into targeting pathways that drive cell motility. The multiprotein WRC regulates actin nucleation and drives mechanistic and molecular pathways that drive metastasis [110, 120, 197, 202, 210]. It has previously been targeted with staple peptides, WAHM1 and WANT3 [128, 130]. These peptides achieved suppression of cell invasion and motility both *in vitro* and *in vivo,* but they required relatively high dosage concentrations. We sought to rationally design an optimized WASF3 mimetic peptide to build upon the success of WAHM1. The resultant lead peptide, WAHMIS-2, designed through a combination of structure-based design and *in silico* optimization improves upon its predecessor WAHM1 in terms of water

solubility, potency, and activity. It also provides a new, more potent tool to understand the intricacies of WASF3 and WRC signaling.

BRK1, the smallest, most conserved member of the WRC has long remained elusive and understudied compared to the other members of the WRC. However, its extensive interactions withing the WRC and high degree of conservation across species makes it a tantalizing target [188, 194, 195]. We iteratively designed BRK1 mimetic all-hydrocarbon stapled peptides as WRC disruptors. Through a combination of homology modeling, structure-guided design and alanine scanning we developed two peptides that demonstrate activity as seen by cell motility assays and cellular uptake at low micromolar dosing. These BASH peptides hold potential to be potent inhibitors of cancer cell motility and invasiveness by targeting the WRC.

Taken together, this work demonstrates the potential of all-hydrocarbon stapled peptides to be made into novel molecular tools and potential therapeutics to target specific PPIs and dissect a wide range of signaling pathways.

6.2 Future Directions

PPIs have long been considered undruggable due to their daunting nature compared to the mechanisms behind small molecule-protein binding and traditional drug design approaches. However, more and more work has gone into developing novel ways to modulate PPIs. Peptides have emerged over the years as an important tool to target PPIs. While native peptides are suitable for *in vitro* assays, they often suffer from drawbacks such as loss of secondary structure, increased entropic penalty, poor target engagement, susceptibility to proteolytic cleavage and impaired cellular uptake [211]. Various strategies

have been developed over the years to address these drawbacks. All d-amino acid, retro-inverso peptides have remarkable stability against proteases and peptidases. Techniques such as macrocyclization and synthetic stabilization of peptide secondary structures have been deployed to improve the "drug-like" properties of peptides. All-hydrocarbon stapling confers and reinforces α helical secondary structure while also imparting cell permeability and proteolytic resistance to peptides. The recent advancement of stapled peptides into clinical trials is a testament to the potential contained by stapled peptides as future therapeutics [212].

CSTAD5 and CSATD6 represent first in class, novel AKAP-PKC scaffolding disruptors. They are cell permeable, PKC specific tools that can be used to interrogate PKC signaling within distinct cellular compartment. Reports have indicated a potential crosstalk between PKA and PKC signaling while docked at certain AKAPs such as gravin. Activation of gravin scaffolded PKC has been shown to affect its subcellular localization along with anchored PKA. This ability of PKC to trigger translocation of gravin represents a higher order of signal organization where a kinase can indirectly affect the activity and substrate orientation of another kinase by altering its localization. Thus, CSTAD peptides can be combined with previously reported PKA-AKAP targeting STAD peptides to further explore the intricacies of AKAP signalosomes. Several other members of the AKAP family apart from gravin and AKAP79 have been known to scaffold PKC. Pericentrin localizes PKC to the centrosome where it regulates microtubule organization, spindle function, and cytokinesis [150]. AKAP9 scaffolding of PKC has been shown to regulate T-cell motility [213]. CSTAD5 and CSTAD6 can be used to disrupt these interactions to further elucidate how AKAPs control the spatiotemporal dynamics of PKC activation and substrate access.

Investigating the specificity of CSTAD5 and CSTAD6 peptides towards various AKAP-PKC scaffolds will be important prior to their deployment in cell-based systems for perturbation of PKC within specific subcellular compartments. Additionally, it may be important to interrogate the potential differences in binding affinities of the CSTAD peptides to various PKC isoforms. The failure of multiple catalytic PKC inhibitors in various clinical trials has highlighted the need for more fine-tuned approaches when therapeutically targeting PKC [60, 61]. Allosteric targeting of PKC activity, altering the "when and where" of PKC activation may serve as the basis for the development of next generation molecular probes and future therapeutics [70].

PKC maturation and priming has long remained elusive, particularly the role of mTORC2 in the same. Recent study laid down new findings that describe the chronology of PKC maturation and its regulation by mTORC2. This study also identified a previously unidentified, homo-dimeric state of nascent PKC. This dimerization is mediated by the TOR-interaction motif and it contains a phosphorylation site regulated by mTORC2. This serves as the rate limiting step in PKC maturation. Extraneous perturbation of the dimeric PKC by PKC-DD stapled peptides accelerates PKC phosphorylation by mTORC2 and subsequent maturation. Several recent studies have identified a potential tumor suppressor role for PKC, where in its dephosphorylation and subsequent inactivation by specific phosphatases such as PHLPP1, PHLPP2 is upregulated in various cancers [173, 174]. Conversely, mTOR is a long sought-after target in several cancers. Deployment of non-specific mTOR inhibitors in certain cancers may lead to the undesired suppression of PKC maturation by mTORC2. In such cases, PKC-DD peptides may be used to upregulate PKC maturation where it functions as a tumor suppressor and synergize with mTOR inhibition.

Such combinatorial approach may also help in overcoming the development of resistance towards mTOR inhibitors [178].

The design and development of WAHMIS-2 and BASH1/2 peptides highlights the importance of structure guided design along with the utility of various computation al tools. Homology modeling has long been used to gain structural clues for proteins with homologs whose crystal structures have been resolved. The advent of artificial intelligence and the development of tools such AlphaFold has furthered the structural insights into the human proteome. These tools can be combined with PeptidDerive and alanine scanning methods to further refine peptide design prior to synthesis and cell-based screening aiding in lead identification [214].

In summary the work presented here demonstrates the value of all-hydrocarbon stapled peptides as PPIs modulators in the context of being novel molecular probes and potential, next generation therapeutics.

REFERENCES

1. Stumpf, M.P., et al., *Estimating the size of the human interactome.* Proc Natl Acad Sci U S A, 2008. **105**(19): p. 6959-64.
2. Ruepp, A., et al., *CORUM: the comprehensive resource of mammalian protein complexes.* Nucleic Acids Res, 2008. **36**(Database issue): p. D646-50.
3. Fischer, G., M. Rossmann, and M. Hyvonen, *Alternative modulation of protein-protein interactions by small molecules.* Curr Opin Biotechnol, 2015. **35**: p. 78-85.
4. Modell, A.E., S.L. Blosser, and P.S. Arora, *Systematic Targeting of Protein-Protein Interactions.* Trends Pharmacol Sci, 2016. **37**(8): p. 702-713.
5. Thompson, A.D., et al., *Fine-tuning multiprotein complexes using small molecules.* ACS Chem Biol, 2012. **7**(8): p. 1311-20.
6. Arkin, M.R., Y. Tang, and J.A. Wells, *Small-molecule inhibitors of protein-protein interactions: progressing toward the reality.* Chem Biol, 2014. **21**(9): p. 1102-14.
7. Fry, D.C. and L.T. Vassilev, *Targeting protein-protein interactions for cancer therapy.* J Mol Med (Berl), 2005. **83**(12): p. 955-63.
8. Loregian, A. and G. Palu, *Disruption of protein-protein interactions: towards new targets for chemotherapy.* J Cell Physiol, 2005. **204**(3): p. 750-62.

9. Petta, I., et al., *Modulation of Protein-Protein Interactions for the Development of Novel Therapeutics.* Mol Ther, 2016. **24**(4): p. 707-18.

10. Hwang, H., et al., *Protein-protein docking benchmark version 4.0.* Proteins, 2010. **78**(15): p. 3111-4.

11. Fuller, J.C., N.J. Burgoyne, and R.M. Jackson, *Predicting druggable binding sites at the protein-protein interface.* Drug Discov Today, 2009. **14**(3-4): p. 155-61.

12. London, N., B. Raveh, and O. Schueler-Furman, *Druggable protein-protein interactions--from hot spots to hot segments.* Curr Opin Chem Biol, 2013. **17**(6): p. 952-9.

13. Calejo, A.I. and K. Tasken, *Targeting protein-protein interactions in complexes organized by A kinase anchoring proteins.* Front Pharmacol, 2015. **6**: p. 192.

14. Pelay-Gimeno, M., et al., *Structure-Based Design of Inhibitors of Protein-Protein Interactions: Mimicking Peptide Binding Epitopes.* Angew Chem Int Ed Engl, 2015. **54**(31): p. 8896-927.

15. Houk, K.N., et al., *Binding affinities of host-guest, protein-ligand, and protein-transition-state complexes.* Angew Chem Int Ed Engl, 2003. **42**(40): p. 4872-97.

16. Verdine, G.L. and G.J. Hilinski, *Stapled peptides for intracellular drug targets.* Methods Enzymol, 2012. **503**: p. 3-33.

17. Limaye, A.J., G.N. Bendzunas, and E.J. Kennedy, *Targeted disruption of PKC from AKAP signaling complexes.* RSC Chem Biol, 2021. **2**(4): p. 1227-1231.

18. Morrison, C., *Constrained peptides' time to shine?* Nat Rev Drug Discov, 2018. **17**(8): p. 531-533.

19. Atangcho, L., T. Navaratna, and G.M. Thurber, *Hitting Undruggable Targets: Viewing Stabilized Peptide Development through the Lens of Quantitative Systems Pharmacology.* Trends Biochem Sci, 2019. **44**(3): p. 241-257.

20. Bullock, B.N., A.L. Jochim, and P.S. Arora, *Assessing helical protein interfaces for inhibitor design.* J Am Chem Soc, 2011. **133**(36): p. 14220-3.

21. Lipinski, C.A., *Rule of five in 2015 and beyond: Target and ligand structural limitations, ligand chemistry structure and drug discovery project decisions.* Adv Drug Deliv Rev, 2016. **101**: p. 34-41.

22. Walensky, L.D. and G.H. Bird, *Hydrocarbon-stapled peptides: principles, practice, and progress.* J Med Chem, 2014. **57**(15): p. 6275-88.

23. Hilinski, G.J., et al., *Stitched alpha-helical peptides via bis ring-closing metathesis.* J Am Chem Soc, 2014. **136**(35): p. 12314-22.

24. Walensky, L.D., et al., *Activation of apoptosis in vivo by a hydrocarbon-stapled BH3 helix.* Science, 2004. **305**(5689): p. 1466-70.

25. Bird, G.H., et al., *Hydrocarbon double-stapling remedies the proteolytic instability of a lengthy peptide therapeutic.* Proc Natl Acad Sci U S A, 2010. **107**(32): p. 14093-8.

26. Bird, G.H., et al., *Biophysical determinants for cellular uptake of hydrocarbon-stapled peptide helices.* Nat Chem Biol, 2016. **12**(10): p. 845-52.

27. Zhang, H., et al., *A cell-penetrating helical peptide as a potential HIV-1 inhibitor.* J Mol Biol, 2008. **378**(3): p. 565-80.

28. Bernal, F., et al., *Reactivation of the p53 tumor suppressor pathway by a stapled p53 peptide.* J Am Chem Soc, 2007. **129**(9): p. 2456-7.

29. Cohen, P., *The role of protein phosphorylation in human health and disease. The Sir Hans Krebs Medal Lecture.* Eur J Biochem, 2001. **268**(19): p. 5001-10.

30. Pawson, T. and J.D. Scott, *Protein phosphorylation in signaling--50 years and counting.* Trends Biochem Sci, 2005. **30**(6): p. 286-90.

31. Manning, G., et al., *The protein kinase complement of the human genome.* Science, 2002. **298**(5600): p. 1912-34.

32. Ardito, F., et al., *The crucial role of protein phosphorylation in cell signaling and its use as targeted therapy (Review).* Int J Mol Med, 2017. **40**(2): p. 271-280.

33. Cohen, P., *Protein kinases--the major drug targets of the twenty-first century?* Nat Rev Drug Discov, 2002. **1**(4): p. 309-15.

34. Roskoski, R., Jr., *Properties of FDA-approved small molecule protein kinase inhibitors: A 2021 update.* Pharmacol Res, 2021. **165**: p. 105463.

35. Bhullar, K.S., et al., *Kinase-targeted cancer therapies: progress, challenges and future directions.* Mol Cancer, 2018. **17**(1): p. 48.

36. Cohen, P., D. Cross, and P.A. Janne, *Kinase drug discovery 20 years after imatinib: progress and future directions.* Nat Rev Drug Discov, 2021. **20**(7): p. 551-569.

37. Zhang, H., et al., *A subcellular map of the human kinome.* Elife, 2021. **10**.

38. Takai, Y., et al., *Calcium-dependent activation of a multifunctional protein kinase by membrane phospholipids.* J Biol Chem, 1979. **254**(10): p. 3692-5.

39. Takai, Y., et al., *Unsaturated diacylglycerol as a possible messenger for the activation of calcium-activated, phospholipid-dependent protein kinase system.* Biochem Biophys Res Commun, 1979. **91**(4): p. 1218-24.

40. Takai, Y., et al., *A role of membranes in the activation of a new multifunctional protein kinase system.* J Biochem, 1979. **86**(2): p. 575-8.

41. Ohno, S., et al., *A novel phorbol ester receptor/protein kinase, nPKC, distantly related to the protein kinase C family.* Cell, 1988. **53**(5): p. 731-41.

42. Nakanishi, H. and J.H. Exton, *Purification and characterization of the zeta isoform of protein kinase C from bovine kidney.* J Biol Chem, 1992. **267**(23): p. 16347-54.

43. Ono, Y., et al., *The structure, expression, and properties of additional members of the protein kinase C family.* J Biol Chem, 1988. **263**(14): p. 6927-32.

44. Nishizuka, Y., *Intracellular signaling by hydrolysis of phospholipids and activation of protein kinase C.* Science, 1992. **258**(5082): p. 607-14.

45. Ono, Y., et al., *Expression and properties of two types of protein kinase C: alternative splicing from a single gene.* Science, 1987. **236**(4805): p. 1116-20.

46. Hernandez, A.I., et al., *Protein kinase M zeta synthesis from a brain mRNA encoding an independent protein kinase C zeta catalytic domain. Implications for the molecular mechanism of memory.* J Biol Chem, 2003. **278**(41): p. 40305-16.

47. Rosse, C., et al., *PKC and the control of localized signal dynamics.* Nat Rev Mol Cell Biol, 2010. **11**(2): p. 103-12.

48. Antal, C.E. and A.C. Newton, *Tuning the signalling output of protein kinase C.* Biochem Soc Trans, 2014. **42**(6): p. 1477-83.

49. Tarafdar, A. and A.M. Michie, *Protein kinase C in cellular transformation: a valid target for therapy?* Biochem Soc Trans, 2014. **42**(6): p. 1556-62.

50. Newton, A.C., *Protein kinase C: perfectly balanced.* Crit Rev Biochem Mol Biol, 2018. **53**(2): p. 208-230.

51. Newton, A.C., *Protein kinase C: poised to signal.* Am J Physiol Endocrinol Metab, 2010. **298**(3): p. E395-402.

52. Mochly-Rosen, D., K. Das, and K.V. Grimes, *Protein kinase C, an elusive therapeutic target?* Nat Rev Drug Discov, 2012. **11**(12): p. 937-57.

53. Toton, E., et al., *Protein kinase Cepsilon as a cancer marker and target for anticancer therapy.* Pharmacol Rep, 2011. **63**(1): p. 19-29.

54. Ishii, H., et al., *Amelioration of vascular dysfunctions in diabetic rats by an oral PKC beta inhibitor.* Science, 1996. **272**(5262): p. 728-31.

55. Simonis, G., et al., *Mechanisms of myocardial remodeling: ramiprilat blocks the expressional upregulation of protein kinase C-epsilon in the surviving myocardium early after infarction.* J Cardiovasc Pharmacol, 2003. **41**(5): p. 780-7.

56. Palaniyandi, S.S., et al., *Protein kinase C in heart failure: a therapeutic target?* Cardiovasc Res, 2009. **82**(2): p. 229-39.

57. Dempsey, E.C., C.D. Cool, and C.M. Littler, *Lung disease and PKCs.* Pharmacol Res, 2007. **55**(6): p. 545-59.

58. Zanin-Zhorov, A., M.L. Dustin, and B.R. Blazar, *PKC-theta function at the immunological synapse: prospects for therapeutic targeting.* Trends Immunol, 2011. **32**(8): p. 358-63.

59. Kawano, T., et al., *Activators and Inhibitors of Protein Kinase C (PKC): Their Applications in Clinical Trials.* Pharmaceutics, 2021. **13**(11).

60. Mackay, H.J. and C.J. Twelves, *Targeting the protein kinase C family: are we there yet?* Nat Rev Cancer, 2007. **7**(7): p. 554-62.

61. Bourhill, T., A. Narendran, and R.N. Johnston, *Enzastaurin: A lesson in drug development.* Crit Rev Oncol Hematol, 2017. **112**: p. 72-79.

62. Perkins, G.A., et al., *PKA, PKC, and AKAP localization in and around the neuromuscular junction.* BMC Neurosci, 2001. **2**: p. 17.

63. Wu-Zhang, A.X. and A.C. Newton, *Protein kinase C pharmacology: refining the toolbox.* Biochem J, 2013. **452**(2): p. 195-209.

64. Wong, W. and J.D. Scott, *AKAP signalling complexes: focal points in space and time.* Nat Rev Mol Cell Biol, 2004. **5**(12): p. 959-70.

65. Scott, J.D., C.W. Dessauer, and K. Tasken, *Creating order from chaos: cellular regulation by kinase anchoring.* Annu Rev Pharmacol Toxicol, 2013. **53**: p. 187-210.

66. Burgers, P.P., et al., *Structure of smAKAP and its regulation by PKA-mediated phosphorylation.* FEBS J, 2016. **283**(11): p. 2132-48.

67. Greenwald, E.C. and J.J. Saucerman, *Bigger, better, faster: principles and models of AKAP anchoring protein signaling.* J Cardiovasc Pharmacol, 2011. **58**(5): p. 462-9.

68. Kapiloff, M.S., M. Rigatti, and K.L. Dodge-Kafka, *Architectural and functional roles of A kinase-anchoring proteins in cAMP microdomains.* J Gen Physiol, 2014. **143**(1): p. 9-15.

69. Carnegie, G.K., C.K. Means, and J.D. Scott, *A-kinase anchoring proteins: from protein complexes to physiology and disease.* IUBMB Life, 2009. **61**(4): p. 394-406.

70. Esseltine, J.L. and J.D. Scott, *AKAP signaling complexes: pointing towards the next generation of therapeutic targets?* Trends Pharmacol Sci, 2013. **34**(12): p. 648-55.

71. Troger, J., et al., *A-kinase anchoring proteins as potential drug targets.* Br J Pharmacol, 2012. **166**(2): p. 420-33.

72. Guo, L.W., et al., *Control of protein kinase C activity, phorbol ester-induced cytoskeletal remodeling, and cell survival signals by the scaffolding protein SSeCKS/GRAVIN/AKAP12.* J Biol Chem, 2011. **286**(44): p. 38356-66.

73. Su, B., et al., *SSeCKS/Gravin/AKAP12 inhibits cancer cell invasiveness and chemotaxis by suppressing a protein kinase C- Raf/MEK/ERK pathway.* J Biol Chem, 2010. **285**(7): p. 4578-86.

74. Gold, M.G., et al., *Architecture and dynamics of an A-kinase anchoring protein 79 (AKAP79) signaling complex.* Proc Natl Acad Sci U S A, 2011. **108**(16): p. 6426-31.

75. Faux, M.C. and J.D. Scott, *Regulation of the AKAP79-protein kinase C interaction by Ca2+/Calmodulin.* J Biol Chem, 1997. **272**(27): p. 17038-44.

76. Mochly-Rosen, D. and A.S. Gordon, *Anchoring proteins for protein kinase C: a means for isozyme selectivity.* FASEB J, 1998. **12**(1): p. 35-42.

77. Souroujon, M.C. and D. Mochly-Rosen, *Peptide modulators of protein-protein interactions in intracellular signaling.* Nat Biotechnol, 1998. **16**(10): p. 919-24.

78. Schechtman, D. and D. Mochly-Rosen, *Adaptor proteins in protein kinase C-mediated signal transduction.* Oncogene, 2001. **20**(44): p. 6339-47.

79. Liron, T., et al., *Rational design of a selective antagonist of epsilon protein kinase C derived from the selective allosteric agonist, pseudo-RACK peptide.* J Mol Cell Cardiol, 2007. **42**(4): p. 835-41.

80. Brandman, R., et al., *Peptides derived from the C2 domain of protein kinase C epsilon (epsilon PKC) modulate epsilon PKC activity and identify potential protein-protein interaction surfaces.* J Biol Chem, 2007. **282**(6): p. 4113-23.

81. Churchill, E.N., N. Qvit, and D. Mochly-Rosen, *Rationally designed peptide regulators of protein kinase C.* Trends in Endocrinology and Metabolism, 2009. **20**(1): p. 25-33.

82. Nolen, B., S. Taylor, and G. Ghosh, *Regulation of protein kinases; controlling activity through activation segment conformation.* Mol Cell, 2004. **15**(5): p. 661-75.

83. Dutil, E.M., A. Toker, and A.C. Newton, *Regulation of conventional protein kinase C isozymes by phosphoinositide-dependent kinase 1 (PDK-1).* Curr Biol, 1998. **8**(25): p. 1366-75.

84. Mora, A., et al., *PDK1, the master regulator of AGC kinase signal transduction.* Semin Cell Dev Biol, 2004. **15**(2): p. 161-70.

85. Keranen, L.M., E.M. Dutil, and A.C. Newton, *Protein kinase C is regulated in vivo by three functionally distinct phosphorylations.* Curr Biol, 1995. **5**(12): p. 1394-1403.

86. Edwards, A.S. and A.C. Newton, *Phosphorylation at conserved carboxyl-terminal hydrophobic motif regulates the catalytic and regulatory domains of protein kinase C.* J Biol Chem, 1997. **272**(29): p. 18382-90.

87. Pearson, R.B., et al., *The principal target of rapamycin-induced p70s6k inactivation is a novel phosphorylation site within a conserved hydrophobic domain.* EMBO J, 1995. **14**(21): p. 5279-87.

88. Ikenoue, T., et al., *Essential function of TORC2 in PKC and Akt turn motif phosphorylation, maturation and signalling.* EMBO J, 2008. **27**(14): p. 1919-31.

89. Baffi, T.R., et al., *mTORC2 controls the activity of PKC and Akt by phosphorylating a conserved TOR interaction motif.* Sci Signal, 2021. **14**(678).

90. Laplante, M. and D.M. Sabatini, *mTOR signaling in growth control and disease.* Cell, 2012. **149**(2): p. 274-93.

91. Forbes, S.A., et al., *COSMIC: mining complete cancer genomes in the Catalogue of Somatic Mutations in Cancer.* Nucleic Acids Res, 2011. **39**(Database issue): p. D945-50.

92. Tian, T., X. Li, and J. Zhang, *mTOR Signaling in Cancer and mTOR Inhibitors in Solid Tumor Targeting Therapy.* Int J Mol Sci, 2019. **20**(3).

93. Huang, L.C., et al., *Integrative annotation and knowledge discovery of kinase post-translational modifications and cancer-associated mutations through federated protein ontologies and resources.* Sci Rep, 2018. **8**(1): p. 6518.

94. Dillekas, H., M.S. Rogers, and O. Straume, *Are 90% of deaths from cancer caused by metastases?* Cancer Med, 2019. **8**(12): p. 5574-5576.

95. Nguyen, D.X. and J. Massague, *Genetic determinants of cancer metastasis.* Nat Rev Genet, 2007. **8**(5): p. 341-52.

96. De Craene, B. and G. Berx, *Regulatory networks defining EMT during cancer initiation and progression.* Nat Rev Cancer, 2013. **13**(2): p. 97-110.

97. Murphy, D.A. and S.A. Courtneidge, *The 'ins' and 'outs' of podosomes and invadopodia: characteristics, formation and function.* Nat Rev Mol Cell Biol, 2011. **12**(7): p. 413-26.

98. Yamaguchi, H., *Pathological roles of invadopodia in cancer invasion and metastasis.* Eur J Cell Biol, 2012. **91**(11-12): p. 902-7.

99. Ogden, A., P.C. Rida, and R. Aneja, *Heading off with the herd: how cancer cells might maneuver supernumerary centrosomes for directional migration.* Cancer Metastasis Rev, 2013. **32**(1-2): p. 269-87.

100. Insall, R.H. and L.M. Machesky, *Actin dynamics at the leading edge: from simple machinery to complex networks.* Dev Cell, 2009. **17**(3): p. 310-22.

101. Yilmaz, M. and G. Christofori, *EMT, the cytoskeleton, and cancer cell invasion.* Cancer Metastasis Rev, 2009. **28**(1-2): p. 15-33.

102. Krause, M. and A. Gautreau, *Steering cell migration: lamellipodium dynamics and the regulation of directional persistence.* Nat Rev Mol Cell Biol, 2014. **15**(9): p. 577-90.

103. Alekhina, O., E. Burstein, and D.D. Billadeau, *Cellular functions of WASP family proteins at a glance.* J Cell Sci, 2017. **130**(14): p. 2235-2241.

104. Stradal, T.E., et al., *Regulation of actin dynamics by WASP and WAVE family proteins.* Trends Cell Biol, 2004. **14**(6): p. 303-11.

105. Millard, T.H., S.J. Sharp, and L.M. Machesky, *Signalling to actin assembly via the WASP (Wiskott-Aldrich syndrome protein)-family proteins and the Arp2/3 complex.* Biochem J, 2004. **380**(Pt 1): p. 1-17.

106. Takenawa, T. and H. Miki, *WASP and WAVE family proteins: key molecules for rapid rearrangement of cortical actin filaments and cell movement.* J Cell Sci, 2001. **114**(Pt 10): p. 1801-9.

107. Burns, S., et al., *Mechanisms of WASp-mediated hematologic and immunologic disease.* Blood, 2004. **104**(12): p. 3454-62.

108. Oda, A., et al., *WAVE/Scars in platelets.* Blood, 2005. **105**(8): p. 3141-8.

109. Eden, S., et al., *Mechanism of regulation of WAVE1-induced actin nucleation by Rac1 and Nck.* Nature, 2002. **418**(6899): p. 790-3.

110. Sossey-Alaoui, K., et al., *Down-regulation of WAVE3, a metastasis promoter gene, inhibits invasion and metastasis of breast cancer cells.* Am J Pathol, 2007. **170**(6): p. 2112-21.

111. Chen, Z., et al., *Structure and control of the actin regulatory WAVE complex.* Nature, 2010. **468**(7323): p. 533-8.

112. Chen, B., et al., *The WAVE regulatory complex links diverse receptors to the actin cytoskeleton.* Cell, 2014. **156**(1-2): p. 195-207.

113. Derivery, E. and A. Gautreau, *Generation of branched actin networks: assembly and regulation of the N-WASP and WAVE molecular machines.* Bioessays, 2010. **32**(2): p. 119-31.

114. Kobayashi, K., et al., *p140Sra-1 (specifically Rac1-associated protein) is a novel specific target for Rac1 small GTPase.* J Biol Chem, 1998. **273**(1): p. 291-5.

115. Oikawa, T., et al., *PtdIns(3,4,5)P3 binding is necessary for WAVE2-induced formation of lamellipodia.* Nat Cell Biol, 2004. **6**(5): p. 420-6.

116. Sossey-Alaoui, K., X. Li, and J.K. Cowell, *c-Abl-mediated phosphorylation of WAVE3 is required for lamellipodia formation and cell migration.* J Biol Chem, 2007. **282**(36): p. 26257-65.

117. Sini, P., et al., *Abl-dependent tyrosine phosphorylation of Sos-1 mediates growth-factor-induced Rac activation.* Nat Cell Biol, 2004. **6**(3): p. 268-74.

118. Sossey-Alaoui, K., et al., *WAVE3-mediated cell migration and lamellipodia formation are regulated downstream of phosphatidylinositol 3-kinase.* J Biol Chem, 2005. **280**(23): p. 21748-55.

119. Teng, Y., et al., *Inactivation of the WASF3 gene in prostate cancer cells leads to suppression of tumorigenicity and metastases.* Br J Cancer, 2010. **103**(7): p. 1066-75.

120. Teng, Y., M. Liu, and J.K. Cowell, *Functional interrelationship between the WASF3 and KISS1 metastasis-associated genes in breast cancer cells.* Int J Cancer, 2011. **129**(12): p. 2825-35.

121. Qin, H., et al., *Wasf3 deficiency reveals involvement in metastasis in a mouse model of breast cancer.* The American journal of pathology, 2019. **189**(12): p. 2450-2458.

122. Teng, Y., et al., *WASF3 regulates miR-200 inactivation by ZEB1 through suppression of KISS1 leading to increased invasiveness in breast cancer cells.* Oncogene, 2014. **33**(2): p. 203-11.

123. Teng, Y., et al., *Critical role of the WASF3 gene in JAK2/STAT3 regulation of cancer cell motility.* Carcinogenesis, 2013. **34**(9): p. 1994-9.

124. Teng, Y., J.L. Ross, and J.K. Cowell, *The involvement of JAK-STAT3 in cell motility, invasion, and metastasis.* JAKSTAT, 2014. **3**(1): p. e28086.

125. Wang, W., et al., *WAVE3 phosphorylation regulates the interplay between PI3K, TGF-beta, and EGF signaling pathways in breast cancer.* Oncogenesis, 2020. **9**(10): p. 87.

126. Taylor, M.A., et al., *Upregulated WAVE3 expression is essential for TGF-beta-mediated EMT and metastasis of triple-negative breast cancer cells.* Breast Cancer Res Treat, 2013. **142**(2): p. 341-53.

127. Wang, G., et al., *miR-218 Inhibits Proliferation, Migration, and EMT of Gastric Cancer Cells by Targeting WASF3.* Oncol Res, 2017. **25**(3): p. 355-364.

128. Teng, Y., et al., *Targeting the WASF3-CYFIP1 Complex Using Stapled Peptides Suppresses Cancer Cell Invasion.* Cancer Res, 2016. **76**(4): p. 965-73.

129. Cowell, J.K., et al., *Suppression of Breast Cancer Metastasis Using Stapled Peptides Targeting the WASF Regulatory Complex.* Cancer Growth Metastasis, 2017. **10**: p. 1179064417713197.

130. Teng, Y., et al., *The WASF3-NCKAP1-CYFIP1 Complex Is Essential for Breast Cancer Metastasis.* Cancer Res, 2016. **76**(17): p. 5133-42.

131. Newton, A.C., C.E. Antal, and S.F. Steinberg, *Protein kinase C mechanisms that contribute to cardiac remodelling.* Clin Sci (Lond), 2016. **130**(17): p. 1499-510.

132. Merida, I., et al., *Diacylglycerol kinase control of protein kinase C.* Biochem J, 2019. **476**(8): p. 1205-1219.

133. Isakov, N., *Protein kinase C (PKC) isoforms in cancer, tumor promotion and tumor suppression.* Semin Cancer Biol, 2018. **48**: p. 36-52.

134. Mukherjee, A., et al., *Spatio-Temporal Regulation of PKC Isoforms Imparts Signaling Specificity.* Front Immunol, 2016. **7**: p. 45.

135. Mackay, K. and D. Mochly-Rosen, *Localization, anchoring, and functions of protein kinase C isozymes in the heart.* J Mol Cell Cardiol, 2001. **33**(7): p. 1301-7.

136. Lanuza, M.A., et al., *Protein kinase C isoforms at the neuromuscular junction: localization and specific roles in neurotransmission and development.* J Anat, 2014. **224**(1): p. 61-73.

137. Burgers, P.P., et al., *A systematic evaluation of protein kinase A-A-kinase anchoring protein interaction motifs.* Biochemistry, 2015. **54**(1): p. 11-21.

138. Kennedy, E.J. and J.D. Scott, *Selective disruption of the AKAP signaling complexes.* Methods Mol Biol, 2015. **1294**: p. 137-50.

139. Helton, L.G., et al., *Novel Stabilized Peptide Inhibitors of Protein Kinases*, in *Next Generation Kinase Inhibitors: Moving Beyond the ATP Binding/Catalytic Sites*, P. Shapiro, Editor. 2020, Springer International Publishing: Cham. p. 141-167.

140. Leah G. Helton, A.J.L., George N. Bendzunas, Eileen J. Kennedy, *Novel Stabilized Peptide Inhibitors of Protein Kinases.*, in *Next Generation Kinase Inhibitors.*, S. P., Editor. 2020, Springer, Cham. p. 141-167.

141. Helton L.G., L.A.J., Bendzunas G.N., Kennedy E.J., *Novel Stabilized Peptide Inhibitors of Protein Kinases.*, in *Next Generation Kinase Inhibitors.*, S. P., Editor. 2020, Springer, Cham. p. 141-167.

142. Pidoux, G. and K. Tasken, *Specificity and spatial dynamics of protein kinase A signaling organized by A-kinase-anchoring proteins.* J Mol Endocrinol, 2010. **44**(5): p. 271-84.

143. Klauck, T.M., et al., *Coordination of three signaling enzymes by AKAP79, a mammalian scaffold protein.* Science, 1996. **271**(5255): p. 1589-92.

144. Nauert, J.B., et al., *Gravin, an autoantigen recognized by serum from myasthenia gravis patients, is a kinase scaffold protein.* Current Biology, 1997. **7**(1): p. 52-62.

145. Takahashi, M., et al., *Association of immature hypophosphorylated protein kinase cepsilon with an anchoring protein CG-NAP.* J Biol Chem, 2000. **275**(44): p. 34592-6.

146. Ng, T., et al., *Ezrin is a downstream effector of trafficking PKC-integrin complexes involved in the control of cell motility.* EMBO J, 2001. **20**(11): p. 2723-41.

147. Carnegie, G.K., et al., *AKAP-Lbc nucleates a protein kinase D activation scaffold.* Mol Cell, 2004. **15**(6): p. 889-99.

148. Kuntziger, T., et al., *Association of PP1 with its regulatory subunit AKAP149 is regulated by serine phosphorylation flanking the RVXF motif of AKAP149.* Biochemistry, 2006. **45**(18): p. 5868-77.

149. Bengrine, A., J. Li, and M.S. Awayda, *The A-kinase anchoring protein 15 regulates feedback inhibition of the epithelial Na+ channel.* FASEB J, 2007. **21**(4): p. 1189-201.

150. Chen, D., et al., *Centrosomal anchoring of protein kinase C betaII by pericentrin controls microtubule organization, spindle function, and cytokinesis.* J Biol Chem, 2004. **279**(6): p. 4829-39.

151. Dempsey, E.C., et al., *Protein kinase C isozymes and the regulation of diverse cell responses.* Am J Physiol Lung Cell Mol Physiol, 2000. **279**(3): p. L429-38.

152. Hoshi, N., et al., *Interaction with AKAP79 modifies the cellular pharmacology of PKC.* Mol Cell, 2010. **37**(4): p. 541-50.

153. Faux, M.C., et al., *Mechanism of A-kinase-anchoring protein 79 (AKAP79) and protein kinase C interaction.* Biochem J, 1999. **343 Pt 2**: p. 443-52.

154. Patel, N., et al., *Molecular basis of AKAP79 regulation by calmodulin.* Nat Commun, 2017. **8**(1): p. 1681.

155. Nygren, P.J., et al., *Intrinsic disorder within AKAP79 fine-tunes anchored phosphatase activity toward substrates and drug sensitivity.* Elife, 2017. **6**.

156. Akakura, S. and I.H. Gelman, *Pivotal Role of AKAP12 in the Regulation of Cellular Adhesion Dynamics: Control of Cytoskeletal Architecture, Cell Migration, and Mitogenic Signaling.* J Signal Transduct, 2012. **2012**: p. 529179.

157. Fan, Q., et al., *Absence of gravin-mediated signaling inhibits development of high-fat diet-induced hyperlipidemia and atherosclerosis.* Am J Physiol Heart Circ Physiol, 2019. **317**(4): p. H793-H810.

158. Gelman, I.H., E. Tombler, and J. Vargas, Jr., *A role for SSeCKS, a major protein kinase C substrate with tumour suppressor activity, in cytoskeletal architecture, formation of migratory processes, and cell migration during embryogenesis.* Histochem J, 2000. **32**(1): p. 13-26.

159. Carr, D.W., et al., *Association of the type II cAMP-dependent protein kinase with a human thyroid RII-anchoring protein. Cloning and characterization of the RII-binding domain.* J Biol Chem, 1992. **267**(19): p. 13376-82.

160. Wang, Y., et al., *Isoform-selective disruption of AKAP-localized PKA using hydrocarbon stapled peptides.* ACS Chem Biol, 2014. **9**(3): p. 635-42.

161. Carlson, C.R., et al., *Delineation of type I protein kinase A-selective signaling events using an RI anchoring disruptor.* J Biol Chem, 2006. **281**(30): p. 21535-45.

162. Wang, Y., et al., *PKA-type I selective constrained peptide disruptors of AKAP complexes.* ACS Chem Biol, 2015. **10**(6): p. 1502-10.

163. Autenrieth, K., et al., *Defining A-Kinase Anchoring Protein (AKAP) Specificity for the Protein Kinase A Subunit RI (PKA-RI).* Chembiochem, 2016. **17**(8): p. 693-697.

164. Bendzunas, N.G., et al., *Investigating PKA-RII specificity using analogs of the PKA:AKAP peptide inhibitor STAD-2.* Bioorg Med Chem, 2018. **26**(6): p. 1174-1178.

165. Le Good, J.A., et al., *Protein kinase C isotypes controlled by phosphoinositide 3-kinase through the protein kinase PDK1.* Science, 1998. **281**(5385): p. 2042-5.

166. Bornancin, F. and P.J. Parker, *Phosphorylation of threonine 638 critically controls the dephosphorylation and inactivation of protein kinase Calpha.* Curr Biol, 1996. **6**(9): p. 1114-23.

167. Facchinetti, V., et al., *The mammalian target of rapamycin complex 2 controls folding and stability of Akt and protein kinase C.* EMBO J, 2008. **27**(14): p. 1932-43.

168. Sarbassov, D.D., et al., *Phosphorylation and regulation of Akt/PKB by the rictor-mTOR complex.* Science, 2005. **307**(5712): p. 1098-101.

169. Alessi, D.R., L.R. Pearce, and J.M. Garcia-Martinez, *New insights into mTOR signaling: mTORC2 and beyond.* Sci Signal, 2009. **2**(67): p. pe27.

170. Su, B. and E. Jacinto, *Mammalian TOR signaling to the AGC kinases.* Crit Rev Biochem Mol Biol, 2011. **46**(6): p. 527-47.

171. Behn-Krappa, A. and A.C. Newton, *The hydrophobic phosphorylation motif of conventional protein kinase C is regulated by autophosphorylation.* Curr Biol, 1999. **9**(14): p. 728-37.

172. Schafmeister, C.E., J. Po, and G.L. Verdine, *An all-hydrocarbon cross-linking system for enhancing the helicity and metabolic stability of peptides.* Journal of the American Chemical Society, 2000. **122**(24): p. 5891-5892.

173. Baffi, T.R., et al., *Protein Kinase C Quality Control by Phosphatase PHLPP1 Unveils Loss-of-Function Mechanism in Cancer.* Mol Cell, 2019. **74**(2): p. 378-392 e5.

174. Baffi, T.R., K. Cohen-Katsenelson, and A.C. Newton, *PHLPPing the Script: Emerging Roles of PHLPP Phosphatases in Cell Signaling.* Annu Rev Pharmacol Toxicol, 2021. **61**: p. 723-743.

175. Antal, C.E., et al., *Cancer-associated protein kinase C mutations reveal kinase's role as tumor suppressor.* Cell, 2015. **160**(3): p. 489-502.

176. Newton, A.C. and J. Brognard, *Reversing the Paradigm: Protein Kinase C as a Tumor Suppressor.* Trends Pharmacol Sci, 2017. **38**(5): p. 438-447.

177. Yuan, T.L. and L.C. Cantley, *PI3K pathway alterations in cancer: variations on a theme.* Oncogene, 2008. **27**(41): p. 5497-510.

178. Rodrik-Outmezguine, V.S., et al., *Overcoming mTOR resistance mutations with a new-generation mTOR inhibitor.* Nature, 2016. **534**(7606): p. 272-6.

179. Mina, L.A. and G.W. Sledge, Jr., *Rethinking the metastatic cascade as a therapeutic target.* Nat Rev Clin Oncol, 2011. **8**(6): p. 325-32.

180. Kulkarni, S., et al., *Increased expression levels of WAVE3 are associated with the progression and metastasis of triple negative breast cancer.* PLoS One, 2012. **7**(8): p. e42895.

181. Webb, B. and A. Sali, *Comparative Protein Structure Modeling Using MODELLER.* Curr Protoc Bioinformatics, 2016. **54**: p. 5 6 1-5 6 37.

182. Rohl, C.A., et al., *Protein structure prediction using Rosetta.* Methods Enzymol, 2004. **383**: p. 66-93.

183. Sedan, Y., et al., *Peptiderive server: derive peptide inhibitors from protein-protein interactions.* Nucleic Acids Res, 2016. **44**(W1): p. W536-41.

184. Kortemme, T., D.E. Kim, and D. Baker, *Computational alanine scanning of protein-protein interfaces.* Sci STKE, 2004. **2004**(219): p. pl2.

185. Kortemme, T. and D. Baker, *A simple physical model for binding energy hot spots in protein-protein complexes.* Proc Natl Acad Sci U S A, 2002. **99**(22): p. 14116-21.

186. Kalafatovic, D. and E. Giralt, *Cell-Penetrating Peptides: Design Strategies beyond Primary Structure and Amphipathicity.* Molecules, 2017. **22**(11).

187. Chu, Q., et al., *Towards understanding cell penetration by stapled peptides.* MedChemComm, 2015. **6**(1): p. 111-119.

188. Derivery, E., et al., *Free Brick1 is a trimeric precursor in the assembly of a functional wave complex.* PLoS One, 2008. **3**(6): p. e2462.

189. Sung, H., et al., *Global cancer statistics 2020: GLOBOCAN estimates of incidence and mortality worldwide for 36 cancers in 185 countries.* CA Cancer J Clin, 2021.

190. Siegel, R.L., et al., *Cancer Statistics, 2021.* CA Cancer J Clin, 2021. **71**(1): p. 7-33.

191. Ghoshal, P., et al., *HIF1A induces expression of the WASF3 metastasis-associated gene under hypoxic conditions.* Int J Cancer, 2012. **131**(6): p. E905-15.

192. Wu, J., et al., *Expression of WASF3 in patients with non-small cell lung cancer: Correlation with clinicopathological features and prognosis.* Oncol Lett, 2014. **8**(3): p. 1169-1174.

193. Shen, L., et al., *MicroRNA-217 regulates WASF3 expression and suppresses tumor growth and metastasis in osteosarcoma.* PLoS One, 2014. **9**(10): p. e109138.

194. Frank, M.J. and L.G. Smith, *A small, novel protein highly conserved in plants and animals promotes the polarized growth and division of maize leaf epidermal cells.* Curr Biol, 2002. **12**(10): p. 849-53.

195. Escobar, B., et al., *Brick1 is an essential regulator of actin cytoskeleton required for embryonic development and cell transformation.* Cancer Res, 2010. **70**(22): p. 9349-59.

196. Liu, Y., et al., *Identification of genes differentially expressed in human primary lung squamous cell carcinoma.* Lung Cancer, 2007. **56**(3): p. 307-17.

197. Cai, X., et al., *Metastatic potential of lung squamous cell carcinoma associated with HSPC300 through its interaction with WAVE2.* Lung Cancer, 2009. **65**(3): p. 299-305.

198. Limaye, A.J., et al., *In Silico Optimized Stapled Peptides Targeting WASF3 in Breast Cancer.* ACS Medicinal Chemistry Letters, 2022.

199. Innocenti, M., et al., *Abi1 is essential for the formation and activation of a WAVE2 signalling complex.* Nat Cell Biol, 2004. **6**(4): p. 319-27.

200. Wang, C., et al., *Expression of Abl interactor 1 and its prognostic significance in breast cancer: a tissue-array-based investigation.* Breast Cancer Res Treat, 2011. **129**(2): p. 373-86.

201. Regua, A., et al., *ABI1-based expression signature predicts breast cancer metastasis and survival.* Mol Oncol, 2021.

202. Wang, C., et al., *Abelson interactor protein-1 positively regulates breast cancer cell proliferation, migration, and invasion.* Mol Cancer Res, 2007. **5**(10): p. 1031-9.

203. Waterhouse, A., et al., *SWISS-MODEL: homology modelling of protein structures and complexes.* Nucleic Acids Res, 2018. **46**(W1): p. W296-W303.

204. Wood, C.W., et al., *BAlaS: fast, interactive and accessible computational alanine-scanning using BudeAlaScan.* Bioinformatics, 2020. **36**(9): p. 2917-2919.

205. Ibarra, A.A., et al., *Predicting and Experimentally Validating Hot-Spot Residues at Protein-Protein Interfaces.* ACS Chem Biol, 2019. **14**(10): p. 2252-2263.

206. Szklarczyk, D., et al., *The STRING database in 2021: customizable protein-protein networks, and functional characterization of user-uploaded gene/measurement sets.* Nucleic Acids Res, 2021. **49**(D1): p. D605-D612.

207. Zhang, S.Q., et al., *The membrane- and soluble-protein helix-helix interactome: similar geometry via different interactions.* Structure, 2015. **23**(3): p. 527-541.

208. Bucko, P.J. and J.D. Scott, *Drugs That Regulate Local Cell Signaling: AKAP Targeting as a Therapeutic Option.* Annu Rev Pharmacol Toxicol, 2021. **61**: p. 361-379.

209. Byrne, D.P., et al., *Biochemical Analysis of AKAP-Anchored PKA Signaling Complexes.* Methods Mol Biol, 2022. **2483**: p. 297-317.

210. Fernando, H.S., et al., *WAVE3 is associated with invasiveness in prostate cancer cells.* Urol Oncol, 2010. **28**(3): p. 320-7.

211. Kannan, S., et al., *Macrocyclization of an all-d linear alpha-helical peptide imparts cellular permeability.* Chem Sci, 2020. **11**(21): p. 5577-5591.

212. Sallman, D.A., et al., *Phase 1/1b Study of the Stapled Peptide ALRN-6924, a Dual Inhibitor of MDMX and MDM2, As Monotherapy or in Combination with Cytarabine for the Treatment of Relapsed/Refractory AML and Advanced MDS with TP53 Wild-Type.* Blood, 2018. **132**(Supplement 1): p. 4066-4066.

213. Verma, N.K., et al., *CG-NAP/Kinase Interactions Fine-Tune T Cell Functions.* Front Immunol, 2019. **10**: p. 2642.

214. Jumper, J., et al., *Highly accurate protein structure prediction with AlphaFold.* Nature, 2021. **596**(7873): p. 583-589.